LES/TPDF investigation of the effects of ambient methanol concentration on pilot fuel ignition characteristics and reaction front structures

Xu, Shijie; Pang, Kar Mun; Li, Yaopeng; Hadadpour, Ahmad; Yu, Senbin; Zhong, Shenghui; Jangi, Mehdi; Bai, Xue song

DOI:
10.1016/j.fuel.2020.119502

Document Version
Peer reviewed version

Citation for published version (Harvard):
Xu, S, Pang, KM, Li, Y, Hadadpour, A, Yu, S, Zhong, S, Jangi, M & Bai, XS 2021, 'LES/TPDF investigation of the effects of ambient methanol concentration on pilot fuel ignition characteristics and reaction front structures', *Fuel*, vol. 287, 119502. https://doi.org/10.1016/j.fuel.2020.119502

Fuel

LES/TPDF investigation of the effects of ambient methanol concentration on pilot fuel ignition characteristics and reaction front structures

--Manuscript Draft--

Manuscript Number:	JFUE-D-20-04960R1
Article Type:	Research Paper
Keywords:	dual-fuel combustion; Auto-ignition; Engine Combustion Network; Large eddy simulation; Eulerian stochastic field
Corresponding Author:	Shijie Xu Lund University Lund, SWEDEN
First Author:	Shijie Xu
Order of Authors:	Shijie Xu
	Kar Mun Pang
	Yaopeng Li
	Ahmad Hadadpour
	Senbin Yu
	Shenghui Zhong
	Mehdi Jangi
	Xue-song Bai
Abstract:	Large-eddy simulations with a transported probability density function model is applied to study the ignition process of an n-heptane spray in a constant volume chamber with a premixed methanol-air atmosphere. Three reacting spray cases with initial methanol-air equivalence ratio ranging from 0 to 0.3 are investigated at an initial temperature of 900 K. The case setup is based on the Engine Combustion Network Spray-H configuration. The effects of the ambient methanol-air equivalence ratio on the ignition characteristics and the reaction front structures in n-heptane/methanol dual-fuel combustion are studied in detail. It is found that the ambient methanol affects the low temperature chemistry of n-heptane, which results in a change of spatial distribution of key species such as heptyl-peroxide. With the presence of methanol in the ambient mixture cool flame is found in the entire fuel-rich region of the n-heptane jet, while when methanol is absent in the ambient mixture, the cool flame is established only around the stoichiometric mixture close to the n-heptane injector nozzle. In general, both low- and high-temperature ignition stages of n-heptane ignition are retarded by the methanol chemistry. An increase in methanol-air equivalence ratio leads to a decrease of the peak heat release rate of the n-heptane first-stage ignition. The chemistry of methanol inhibits the n-heptane ignition by decreasing the overall hydroxyl radicals (OH) formation rate and reducing the OH concentration during the transition period from the first-stage ignition to the second-stage ignition. As a result, the transition time between the two ignition stages is prolonged.

Sep. 26, 2020

Title:	**LES/TPDF investigation of the effects of ambient methanol concentration on pilot fuel ignition characteristics and reaction front structures**
Authors:	Shijie Xu, Kar Mun Pang, Yaopeng Li, Ahmad Hadadpour, Senbin Yu, Shenghui Zhong, Mehdi Jangi, Xue-Song Bai
Journal:	Fuel (Paper No.: JFUE-S-20-06442)

Dear Editor,

Thank you very much for the e-mail of Aug. 28, 2020, regarding the review results of the above paper. The manuscript has been revised in accordance with the referees' and editor's comments and suggestions. We sincerely trust that the revisions made will render the manuscript acceptable to you. Please find enclosed a list of the detailed response to the referees' comments, a "TRACK CHANGE" revision (deleting a text using strike-through mark and rewriting with blue color) and clean version of the revised manuscript.

This article has been neither copyrighted, classified, published, nor is being considered for publication elsewhere. The submission of article is approved by all authors and the responsible authorities where the work was carried out, and if accepted, it will not be published elsewhere in the same form, in English or in any other language, without the written consent of the Publisher.

Thank you very much for your kind consideration and we look forward to your favorable reply.

Sincerely yours,
Shijie Xu

Enclosures

AUTHORS' REPLY TO REVIEWERS' AND EDITOR'S COMMENTS

Title:	**LES/TPDF investigation of the effects of ambient methanol concentration on pilot fuel ignition characteristics and reaction front structures**
Authors:	Shijie Xu, Kar Mun Pang, Yaopeng Li, Ahmad Hadadpour, Senbin Yu, Shenghui Zhong, Mehdi Jangi, Xue-Song Bai
Journal:	Fuel (Paper No.: JFUE-S-20-06442)

We appreciate the valuable comments from the reviewers on our manuscript. According to your advices, we revised the manuscript and the changes are marked with blue color in the revised manuscript. Replies to the reviewers' comments are given below.

The page numbers are numbers in the track-change version.

Reviewer #1's comments

(1) The grammatical errors in the article need to be corrected so that it is easy to be read.

Authors' reply: Thank you for your comments. We have carefully checked and corrected the grammatical errors in the revision. Some sentences are also rephrased. These should collectively improve the overall readability. Kindly refer to the track-change version of the manuscript.

(2) The sentence "To the best of the authors` knowledge, detailed numerical simulations and analyses on methanol based dual fuel combustion are yet to be carried out"is not accurate in the Introduction, page 4. Actually, an article published in Fuel 93(2012)625-613, seeing [45], introduced the similar work.

Authors' reply: Thank you for the suggestion. We rephrase the sentence and more references are reviewered to improve the introduction. This can be found on page 4 in the revised manuscript.

(3) How was methanol ambient formed in the simulation? Did it form in intake stroke or in cylinder?

Authors' reply: In the RCCI engines, the ambient methanol is formed in the intake stroke. In this work, n-heptane is injected into a constant volume combustion chamber, where the gaseous methanol is already premixed with air to form a homogeneous and quiescent primary fuel-air mixture before the n-heptane injection, following the exercise of the previous LES works [1][2][3]. We add the aforementioned description into the 'Case set-up' section. Kindly referred to page 11.

[1] Kahila H, Wehrfritz A, Kaario O, et al. Large-eddy simulation of dual-fuel ignition: Diesel spray injection into a lean methane-air mixture. Combustion and Flame, 2019, 199: 131-151.

[2] Kahila H, Kaario O, Ahmad Z, et al. A large-eddy simulation study on the influence of diesel pilot spray quantity on methane-air flame initiation. Combustion and Flame, 2019, 206: 506-521.

[3] Tekgül B, Kahila H, Kaario O, et al. Large-eddy simulation of dual-fuel spray ignition at different ambient temperatures. Combustion and Flame, 2020, 215: 51-65.

(4) How did the n-heptane penetrate into methanol ambient and diffuse in the ambient?

Authors' reply: The liquid n-heptane is delivered through an injector nozzle. It breaks up and evaporates to gaseous state. The gaseous n-heptane and ambient methanol/air undergo mixing and auto-ignition. The evolution of the n-heptane in single-fuel and dual-fuel cases are discussed in pages 12 and 24 in the revised manuscript.

(5) How did the authors verify their numerical calculation results?

Authors' reply: Thank you for your comments, this is a good point. Akin to the dual-fuel spray LES in Refs. [1][2][3], the validation of the numerical simulation is divided into three parts: A) mechanism validation, B) non-reacting spray, and C) reacting spray flame. A) The performance of the mechanism in predicting the methanol ignition under the spray flame conditions, is first evaluated. The ignition delay times are compared with the shock tube experimental data and methanol detailed mechanisms. Both of them show good aggrement. B) The non-reacting spray involves spray, break-ups, evaporation and mixing. The LES results are compared with the experimental results of 1) liquid penetration length, 2) vapor penetration length, and 3) spatial distribution of mixture fraction. The non-reacting spray experimental data was collected from the ECN Spray-H experiment under similar conditions of the present dual-fuel cases. C) The reacting spray involves auto-ignition and flame stablization. The single-fuel LES (without methanol in the ambient gas) results are validated using the experimental ignition delay times, flame lift-off length and pressure rise under conditions similar to the dual-fuel case. The validated single-fuel setup then serves as the baseline case, which is also used to identify the difference between the single-fuel and dual-fuel combustion.

Reviewer #2's general comments

The Authors have conducted a reacting flow simulation comparing DF and SF sprays in ECN spray setup. The Authors could use the LES data in a much more versatile way.

Authors' reply: Thank you for the kind comments. Following your suggestions, five new figures (Fig. 2, Fig. 3, Fig.6, Fig. 10 and Fig. 11) and a new table (Table 4), together with the associated analysis are added in the revised manuscript. In the following section, we list down the replies to your specific comments and suggestions. The page numbers are numbers in the track-change version.

Reviewer #2's specific comments

(0) Abstract:

a) What does the "Negative correlation ... " sentence mean? I sound like it contradicts the results.

b) It is over interpreting the results if you say that you analyze the reaction front structures, how can you do this at very coarse 250 micron grid where the turbulence resolution is questionable?

Authors' reply: Thank you for your comments.

Reply to comment (a): The original sentence 'negative correlation …' is indeed vague. We clarify this by rephrasing the sentence to 'An increase in Φ_m leads to a decrease of the peak heat release rate of the n-heptane first-stage ignition'. Kindly refer to page 2.

Reply to comment (b): Regarding to the comments on the turbulence resolution, we have examined the reolved turbulent kinetic energy. Figure R1 below shows the ratio of the resolved turbulence kinetic energy, k_{res}, to the total turbulence kinetic energy, k_{tot} at 20, 40 and 60 mm downstream the injection nozzle. The resolved turbulence kinetic energy is estimated from the instantaneous velocity and the time averaged velocity from 1.5 ms to 6.0 ms, when the spray reaches a steady state at 20, 40 and 60 mm. The total turbulence kinetic energy is calculated from the resolved and sub-grid scale kinetic energy k_{sgs}, i.e., $k_{tot} = k_{res} + k_{sgs}$. It is seen that, on average, more than 80% of the turbulence kinetic energy are resolved in most of the flow domain. A similar conclusion was drawn under the same condition and 250 μm grid in our previous LES by Hadadpour et al. [4], where an ensamble average was carried out to calculate the turbulence kinetic energy over 20 LES realizations. Hadadpour et al. [4] concluded that at least 72% of turbulence kinetic energy is resolved, more than 80% of turbulence kinetic energy is resolved on average. According to [5], the turbulence resolution in the present LES is acceptable.

In addition to that, we have also carried out the mesh sensitivity analysis on both non-reacting and reacting spray cases, to show the capability of the current mesh resolution in predicting the spray, ignition and flame stabilization. Detailed discussion on the mesh sensitivity study is given in reply to comment **(10)** below, as well as in Section 3.2 in the revised manuscript.

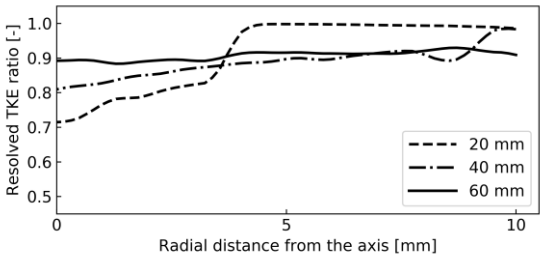

Figure R1. The ratio of the resolved turbulence kinetic energy to the total turbulence kinetic energy (TKE) at 20, 40 and 60 mm downstream the injection nozzle.

[4] Hadadpour A, Jangi M, Bai X S. Jet-jet interaction in multiple injections: A large-eddy simulation study. Fuel, 2018, 234: 286-295.
[5] Pope SB. Ten questions concerning the large-eddy simulation of turbulent flows. New Journal of Physics, 2004, 6(1): 35.

(1) Table 2 -> I don't understand why C and D cases both have 900K or this way: why study 1000K for single fuel but not for df ? Temperature sweep may totally change this picture.
Authors' reply: In this work, effects of ambient methanol concentration on pilot fuel ignition characteristics are invistigated in Cases B, C and D at the ambient temperature of 900 K. The 900K case is selected since the interaction between methanol and n-heptane is stronger than that at higher ambient temperatures. The ignition delay of the methanol at 1000 K condition is comparable to that of n-heptane, i.e. methanol fueled engines under such high temperature become less dependent on the ignition assistance of the pilot fuel. However, the ECN Spray H (with n-heptane only) non-reacting experiment was only performed at 1000 K, this case was therefore used for model validation. To avoid misunderstanding, a discussion on it is provided in the abstract and case setups, on pages 1 and 10 in the revision. This should clarify the ambiguity.

(2) what is effect of temperature or methanol equivalence ratio on chemistry and mixing. This should be looked more carefully, more thorough analysis and new figures are recommended.
Authors' reply: Thank you for your suggestions. In order to clarify the effects of temperature (T) and local equivalence ratio (Φ) on mixing and chemistry, a Φ-T scatter plot is provided (Figure 10 in the revised manuscript) to extract the mixing line prior to the onset of ignition. Based on this, a set of zero-dimentional simulations along the mixing line are conducted and analyzed to discuss the chemistry effect. These can be found on pages 27 and 28 of the revised manuscript.

(3) I don't understand the point of CCM: you say it gives great speedup by factor 10 but then your cases still have extremely long computational time even on a mesh of some million cells. More work would be required to convince the benefit of the approach.
Authors' reply: The benefit of the CCM can be viewed in two different aspects: A) a speedup for the finite-rate chemistry method, and B) a further speedup for the Eulerian stochastic field (ESF) based transported probability density function (TPDF) model. The long computational time needed in the present study is due to the use of relatively comprehensive chemical

kinetic mechanism with 68 species. Without CCM, the computational time is prohibitively long (2 to 5 times longer) for LES.

A) In the finite-rate chemistry method, chemistry integration and species transportation are the most time-consuming processes. The CCM speedup factor of 10 is for the chemistry integration, while the species transport (by convection and diffusion) is not accelerated. Therefore, an overall 2 to 5 times reduction of the clock time [6,7] is achieved for the finite-rate chemistry method. Moreover, as aforementioned, the mechanism used in the current LES is the Lu-68 mechanism [8], which is a relatively comprehensive and stiff mechanism consisting of 68 species and 283 reactions, which requires a high computational cost on both chemistry integration and species transport.

B) The ESF based TPDF model is an expensive turbulence chemistry interaction model in terms of computational cost. To illustrate the benefit of the CCM in ESF, we ran three reacting spray cases with well-stired reactor (WSR), partially-stired reactor (PaSR) and ESF. It is worth mentioning that all of the cases are performed with CCM. The CPU hours using 144 processors in parallel until the same time (1.0 ms) after the start of injection, are 18024, 19352 and 85149 hours for WSR, PaSR and ESF, respectively. In theory, ESF has a computational cost proportional to the number of stochastic fields, N_{sf}. The N_{sf} used in this study is 8, which means that the computational cost is 8 times higher than the WSR and PaSR combustion models. However, the CPU hours of the ESF is only 5 times of the WSR or PaSR model by using CCM. This indicates that the combination of ESF and CCM has a further speedup. More discussion on CPU hours can be found in the reply to comment **(5) below**.

Following your suggestion, we rephased the CCM description in the revision to clarify its necessities and applicability. Kindly refer to page 8.

[6] Gong C, Jangi M, Bai X S. Large eddy simulation of n-dodecane spray combustion in a high pressure combustion vessel. Applied energy, 2014, 136: 373-381.
[7] Jangi M, Zhao X, Haworth D C, et al. Stabilization and liftoff length of a non-premixed methane/air jet flame discharging into a high-temperature environment: An accelerated transported PDF method. Combustion and Flame, 2015, 162(2): 408-419.
[8] Lu T, Law C K, Yoo C S, et al. Dynamic stiffness removal for direct numerical simulations. Combustion and Flame, 2009, 156(8): 1542-1551.

(4) "sake of" -> rephrase.
Authors' reply: The sentence has been rephrased to 'It is worth mentioning that the "air" is not the atmosphere air but resembles those of the ECN experiment to mimic the in-cylinder mixture of engines'.

(5) description of CPU hours is not convincing. You say that it took 100000 CPU hours to run on 144 processors one of the cases. This seems to translate a clock time which makes little sense. So my concern is that there is some problem with the code.
Authors' reply: Indeed, OpenFOAM recorded two times: ExecutionTime and ClockTime.

The ExecutionTime is the time spent by the processor and the ClockTime is the wall clock time. The ClockTime is always longer than ExecutionTime, in this simulation, ClockTime ~ 102% ExecutionTime. In the manuscript, 100000 CPU hours approximately equal to 144 processors * 24 hours/day * 28 days ClockTime. The code has been validated in our previous studies and has been used to study different spray combustion processes [6, 7, 9].

[9] Pang K M, Jangi M, Bai X S, et al. Modelling of diesel spray flames under engine-like conditions using an accelerated Eulerian Stochastic Field method. Combustion and Flame, 2018, 193: 363-383.

(6) Please analyse more carefully the heat release rate and present pictures.
Authors' reply: Following your suggestion, a new figure (Fig. 6 in the revision) is presented to analyze the evolution of the maximum heat release rate. The associated discussion can also be found on pages 19 to 21 of the revised manuscript.

(7) I am confused about the chosen temperature 900 K. Methanol is known to pose peculiar autoignition features and the temperature sensitivity would be needed to assess by 0d studies along the mixing line. Please present this analysis.
Authors' reply: This is a very good suggestion. In the revision, discussion on the 0D studies along the mixing line are presented. Kindly refer to pages 27 and 28.

(8) Motivation on chosen phi values is required. Are those even practically feasible, seems very lean i.e. would that allow flame propagation and what would be S_L in those conditions ?
Authors' reply:
We fully agree that the laminar flame speed (S_L) at Φ_m of 0.3 is low while Φ_m = 0.1 lies outside the methanol burning range [10]. Experimental measurements of S_L at high pressure is unfortunately not available, but S_L in general reduces with the increase of pressure. However, the main objective of this LES is to investigate the effects of ambient methanol concentration on pilot fuel ignition characteristics. The Φ_m of 0.3 is chosen based on the engine conditions defined in Ref. [11]. It is an averaged global equivalence ratio under the medium-load condition of the diesel/methanol RCCI engine. On the other hand, the selection of Φ_m of 0.1 is based on the experiment in Ref. [10]. It is found in Ref. [10] that under very lean condition, the associated low amount of ambient methanol concentration is sufficient to retard the ignition delay of the pilot fuel. In practice, the methanol equivalence ratio distribution is not 100% homogeneous in the engines [12]. There may exist local lean mixture even at the high-load engine conditions. It is important to know how the ignition and combustion processes evolve when the pilot fuel is injected into these very lean mixture. Hence, we selected Φ_m = 0.1 and 0.3 to analyse the effects of the methanol concentrations on n-heptane ignition. In the revised manuscript, these discussions are added on pages 3 and 11 to highlight the motivation behind the selected lean conditions.

[10] Yin Z, Yao C, Geng P, et al. Visualization of combustion characteristic of diesel in premixed methanol–air mixture atmosphere of different ambient temperature in a constant volume chamber. Fuel, 2016, 174: 242-250.

[11] Dempsey A B, Walker N R, Reitz R. Effect of piston bowl geometry on dual fuel reactivity controlled compression ignition (RCCI) in a light-duty engine operated with gasoline/diesel and methanol/diesel. SAE International Journal of Engines, 2013, 6(1): 78-100.
[12] Chen Z, Yao C, Yao A, et al. The impact of methanol injecting position on cylinder-to-cylinder variation in a diesel methanol dual fuel engine. Fuel, 2017, 191: 150-163.

(9) More quantitative results need to be expressed. E.g. τ_1 and τ_2 values are not reported and they should in a table . That kind of table could also take 0D and 3D ign.del. times into account (both must be reported).
Authors' reply: Thank you for your comments. Both two stage ignition delay times τ_1 and τ_2 in 0D and 3D simulations are listed in Table 4 as suggested. Kindly refer to page 29 in the revision.

(10) All in all, the paper suffers from incomplete analysis of the data. I am also quite concerned about the 250 micron grid. Is there something that could be done with this regard ? Is the reason for coarse grid that actually the chemistry method is quite laborious? It is simply that if you go for LES you would need to resolve the flow and we see from your literature table that this resolution is very coarse. How does the single fuel ign.delay time compare to ECN data ? This should be reported.
Authors' reply: Following your suggestions, more results (Fig. 2, Fig. 3, Fig.6, Fig. 10 and Fig. 11), a new table (Table 4) and more in-depth analysis are added in the revised manuscript to enrich the paper.

a) As seen in Table 1, the LES with the finest mesh are based on n-dodecane fueled spray flame (Spray-A), which has a higher ambient pressure thus requiring a finer mesh. For the n-heptane fueled spray flame (Spray-H, the condition we studied in this paper), 250 μm grid is acceptable. The resolved turbulence kinetic energy in Figure R1 also supports this argument.

b) The use of an advanced turbulence chemistry interaction model (ESF) allows us to use the current mesh resolution since the sub-grid scale turbulence-chemistry interaction was taken into consideration [9]. Recently, for example, W. Jones et. al. [13] simulated ECN Spray-H spray flame and achieved reasonably good result using ESF with a 500 μm grid. To the best of the authors' knowledge, this is the first LES/ESF study based on the ECN Spray-H conditions using the grid as fine as 250 μm mesh resolution. With this grid, a good agreement between the LES prediction and the ECN experiments, in terms of the liquid and vapor penetrations, mixture fraction distribution, ignition delay time and flame lift-off length, is achieved.

To investigate the impact of this mesh resolution, a mesh sensitive analysis (125, 250 and 500 μm grid) is performed on both non-reacting and reacting spray. Figure R2 shows the evolution of liquid and vapor penetrations (LPL and VPL). It is seen in Fig. R2a and R2b, the 500 μm mesh is not able to correctly replicate the experimental LPL and VPL. Using the 250 μm

mesh yields similar LPL and VPL results using 125 μm mesh. As compared with measurements, the maximum error of VPL is only 2% when the 250 μm mesh is used. Therefore, for the non-reacting spray, using the 250 μm mesh shows a reasonable resolution in terms of the liquid and vapor penetration prediction.

Figure R3 shows the evolution of the pressure rise and lift-off length (LOL) in reacting spray with three mesh resolutions. As recommended in ECN [14], LOL is defined as the distance from the fuel nozzle to the farthest location where Favre average OH mass fraction reaches 2% of its maximum in the domain after a stable flame is established. As seen in Fig. R3a, the mean pressure rise profiles are found to be insensitive to the mesh resolution. In terms of the LOL, the LOL in 500 μm mesh is underestimated while 250 μm mesh show good agreement with both the 125 μm mesh results and the measurements. Therefore, the 250 μm mesh provides reasonable accuracy in prediction of non-reacting and reacting spray at an affordable computational cost.

c) The ignition delay time of the single fuel case in the current LES is 0.80 ms, which is 0.79 ms in the ECN experiment [14]. The definition and comparison of the ignition delay time is explained in the revision. These can be found on page 18.

The above remarks are added to Sections 3.2 and 3.3 in the revision of the manuscript. These can be found on pages 14 to 18.

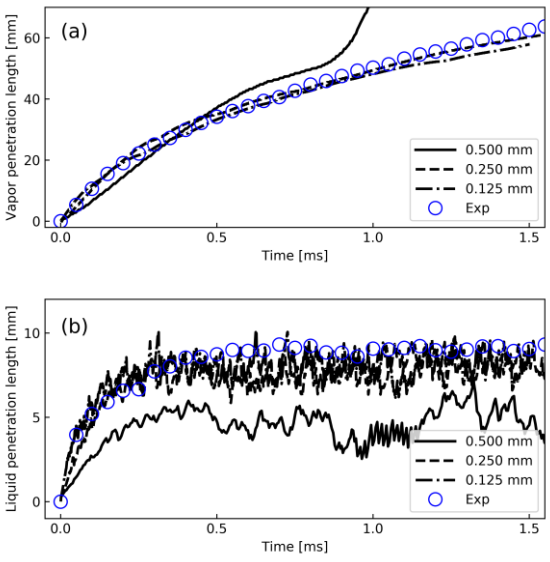

Figure R2. Temporal evolution of (a) the vapor penetration length (VPL), and (b) liquid penetration length (LPL) from experiments [14] and LES with mesh size of 125, 250 and 500 μm.

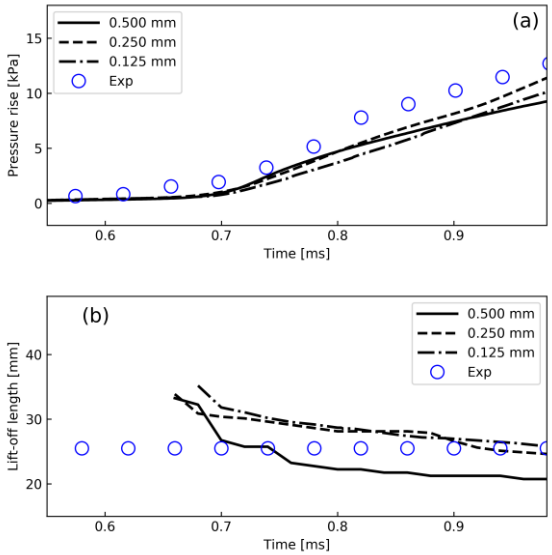

Figure R3. (a) The experimental and LES predicted pressure rise with mesh size of 125, 250 and 500 μm. (b) The predicted flame lift-off length (LOL). The evolution of the experimental LOL is not available. The horizontal dashed line is the measured steady state LOL, 25.5 mm [14].

[13] Gallot-Lavallée S, Jones W P. Large eddy simulation of spray auto-ignition under EGR conditions. Flow, Turbulence and Combustion, 2016, 96(2): 513-534.
[14] Engine combustion network, https://ecn.sandia.gov, Accessed Sep., 2020.

Highlights

- LES with state-of-the-art approach (TPDF) is used to study a dual-fuel spray flame;
- A negative correlation between Φ_m and the value of the first stage HRR is observed;
- It is found that ambient methanol affects the n-heptane LTC and cool flame structure.

LES/TPDF investigation of the effects of ambient methanol concentration on pilot fuel ignition characteristics and reaction front structures

Shijie Xu[a,*], Kar Mun Pang[b], Yaopeng Li[a,c], Ahmad Hadadpour[a], Senbin Yu[a], Shenghui Zhong[a,d], Mehdi Jangi[e], Xue-song Bai[a]

[a]*Department of Energy Sciences, Lund University, 22100 Lund, Sweden*
[b]*MAN Energy Solutions, Teglholmsgade 41, 2450 Copenhagen SV, Denmark*
[c]*Key Laboratory of Ocean Energy Utilization and Energy Conservation of Ministry of Education, Dalian University of Technology, 116024 Dalian, P.R. China*
[d]*State Key Laboratory of Engines, Tianjin University, 135 Yaguan Rd, 300350 Tianjin, P.R. China*
[e]*School of Mechanical Engineering, University of Birmingham, Edgbaston, Birmingham B15 2TT, UK*

Abstract

Large-eddy simulations with a transported probability density function model coupled with a finite-rate chemistry is applied to study the ignition process of an n-heptane spray in a constant volume chamber with a premixed methanol-air atmosphere under conditions relevant to reactivity controlled compression ignition (RCCI) engines. A non-reacting spray and three reacting spray cases with initial methanol-air equivalence ratio (ϕ_m) ranging from 0 to 0.3 are investigated under initial temperatures of 900 K and 1000 K. The case setup is based on the Engine Combustion Network Spray-H configuration, where n-heptane fuel is used. The effects of the ambient methanol-air equivalence ratio on the ignition characteristics and the reaction front structures in n-heptane/methanol RCCI combustion are studied in detail. It is found that ambient methanol affects the low temperature

*Corresponding author.
E-mail address: shijie.xu@energy.lth.se

chemistry of n-heptane, which results in a change of spatial distribution of key species such as heptyl-peroxide, and therefore the cool flame structure. With methanol in the ambient gas cool flame is found in the entire fuel-rich region of the n-heptane jet, whereas without methanol cool flame is established only around the stoichiometric mixture close to the n-heptane injector nozzle. In general, both low- and high-temperature ignition stages of n-heptane ignition are retarded by the methanol chemistry. A negative correlation between ϕ_m and the value of the first stage heat release rate is observed. The chemistry of methanol inhibits the n-heptane ignition by decreasing the overall hydroxyl radicals (OH) formation rate and reducing the OH concentration during the transition period from the first stage ignition to the second stage ignition. As a result, the transition time between the two ignition stages is prolonged. Under the present lean methanol/air ambient mixture conditions, the impact of methanol on n-heptane ignition has a tendency of reducing the high temperature fuel-rich region, which is in favor of soot reduction.
Keywords: Dual-fuel combustion, Auto-ignition, Engine Combustion Network, Large eddy simulation, Eulerian stochastic field

1. Introduction

Methanol is a promising alternative fuel to fossil fuels. Compared with natural gas and hydrogen, methanol is easier to store, transport, distribute, and use since methanol is liquid at room temperature. Methanol can be produced from a wealth of sources, such as coal, natural gas, biomass and municipal waste. One challenge in utilizing methanol in conventional compression-ignition (CI) engines is the difficulty in igniting the fuel due to its high latent heat of evaporation and long ignition-delay time (IDT). This issue becomes more severe in the condition of a

cold start or at low engine loads [1, 2]. As a result, novel combustion strategies, e.g., dual-fuel combustion, are developed to improve the ignition process in methanol fueled CI engines. One of the dual-fuel combustion strategies is the reactivity controlled compression ignition (RCCI) concept. In an RCCI engine, a low-reactivity fuel (primary fuel) is injected into the cylinder during the intake stroke to form a premixed fuel-air mixture. The mixture is then ignited by injecting a high-reactivity fuel (pilot fuel) during the compression stroke. Due to the lean premixed combustion in RCCI, high-temperature and rich-fuel regions can be avoided in the cylinder, leading to reduced soot and NOx emissions [3–6]. An engineering challenge in the RCCI engine is the control of ignition time and heat release rate (HRR) [7]. Unlike the ignition of a conventional diesel engine, the auto-ignition mechanism in a dual-fuel engine is not well understood [8].

Yin *et al.* [9] performed experiments on diesel/methanol dual-fuel combustion in a constant volume combustion chamber under a range of ambient temperatures (840-960 K) with methanol-air equivalence ratio (ϕ_m) of 0.1. The results showed that when the temperature is below 920K, the IDT of diesel in the methanol-air atmosphere is longer than that in the pure air atmosphere. However, no detailed analysis of the ignition phenomenon, including complex two-stage ignitions, was available due to the lack of intermediate species in the measurements. Srna *et al.* [10] reported optical diagnosis experiments of n-dodecane spray combustion in a methane-air atmosphere in a rapid compression-expansion machine (RCEM). It was found that the ambient methane could affect the onset of the first stage ignition (the cool flame) but the temporal separation of the first stage ignition and second stage ignition was shown to be independent of the methane concentration in the ambient methane-air mixture. Kahila *et al.* [8] conducted a large eddy simulation

(LES) of an n-dodecane/methane-air dual-fuel combustion in the Engine Combustion Network (ECN) [11] constant volume configuration. It was found that the low-temperature reactions of the pilot fuel (n-dodecane) provided intermediate species and heat, which played an important role in the primary fuel (methane) oxidation. In turn, both the first and the second ignition stages of the pilot fuel were retarded in methane-air atmosphere, mainly due to the consumption of OH in ambient methane oxidation. To the best of the authors' knowledge, detailed numerical simulations and analyses on methanol based dual-fuel combustion are yet to be carried out. This has motivated the present study.

The recent LES study of dual-fuel combustion [8, 23, 24] have used a well-stired reactor (WSR) assumption, in which turbulence-chemistry interaction (TCI) in the sub-grid scale (SGS) has been neglected. They used very fine spatial resolution to compensate the neglected TCI effect. However, Varna *et al.* [26] pointed out that TCI is important for the spray flame in engine-like conditions, especially for the low temperature case with long IDT. Since the IDT is typically longer in dual-fuel combustion, it is desirable to incorporate a TCI model in dual-fuel ignition simulations. The commonly used TCI models are the Conditional Moment-Closure (CMC) [21], the probability density function (PDF) model [14], the linear eddy model (LEM) [16, 25], and the Flamelet Generation Manifold (FGM) [19]. Table 1 shows a list of recent LES studies of the ECN spray combustion cases. A summary of the unsteady Reynolds-averaged Navier–Stokes (URANS) simulations is available in Ref. [27].

Set against these backgrounds, LES which is known to have better capability in predicting flow structure and mixing, is carried out to study n-heptane/methanol dual-fuel combustion in a constant volume combustion chamber. In addition to

Table 1: Recent LES studies of ECN spray flames.

Fuel	Species number	Mesh size [μ m]	Combustion model	Turbulence model	Code	Ref.
n-Heptane	42, 68	250	WSR	Smagorinsky	Converge	[12]
n-Heptane	44	200	FMDF [1]	-	In-house	[13]
n-Heptane	22	500	ESF	Dynamic Smagorinsky	In-house	[14]
n-Heptane	140	250, 125, 62.5	WSR	Smagorinsky, dynamic structure	ANSYS	[15]
n-Heptane/ methane	44	-	LEM	-	KIVA	[16]
n-Dodecane	103	250	WSR	One-equation eddy	OpenFOAM	[17]
n-Dodecane	103	62.5	WSR	Dynamic structure	Converge	[18]
n-Dodecane	257, 103	62.5	FGM	-	OpenFOAM	[19]
n-Dodecane	103	62.5	TFM [2]	Dynamic structure	Converge	[20]
n-Dodecane	54	125	CMC	$k-\ell$ two-equations	Star-CD	[21]
n-Dodecane	54	240	PaSR [3]	One-equation eddy	OpenFOAM	[22]
n-Dodecane/ methane	54, 96	160, 80, 62.5	WSR	Implicit LES	OpenFOAM	[8, 23, 24]
n-Dodecane	54	-	LEM	-	KIVA	[25]

[1] Compressible filtered mass density function (FMDF).

[2] Tabulated Flamelet Model (TFM).

[3] Partially stirred reactor (PaSR) model.

this, an Eulerian stochastic field (ESF) transported probability density function (TPDF) model is employed to account for the SGS TCI effects. The baseline case uses the ECN Spray-H (n-heptane fueled) conditions. The associated experimental data is used for the validation of the current LES-TPDF model under both non-reacting spray and reacting spray conditions. A series of methanol-air equivalence ratios are selected to investigate the ignition process under conditions relevant to low and moderate engine loads [28]. The main purpose of this work is to elucidate the effects of ambient methanol concentration on the ignition process of an n-heptane spray under conditions relevant to RCCI engines.

2. Methodology

2.1. Eulerian-Lagrangian approach

In order to describe the two-phase flow in spray combustion, the Lagrangian particle tracking approach is applied. In the LES framework, the gas phase is governed by spatially filtered Navier-Stokes equations, while the Lagrangian liquid phase is described and tracked using a large number of parcels. The interaction between the gas and liquid phases is considered via the source terms in the mass conservation, momentum, species and energy transport equations. Details of the LES spray model are referred to Ref. [29, 30]. A one-equation SGS kinetic energy model (k-equation model) is used to model the SGS viscosity. The ambient methanol-air mixture is assumed to be in a quiescent gas phase, following the previous LES [8, 23, 24] studies. The n-heptane fuel is injected as liquid droplets, with the initial droplet size following the Rosin-Rammler distribution. The mean diameter of droplets is set as half the injector nozzle diameter, $d_n/2$. The maximum size is set to the diameter of the injector nozzle, d_n, where $d_n = 0.1mm$. The

evaporation rate is modelled using the Spalding formula. The Ranz-Marshall correlation is used to model heat transfer between the liquid and gas phases. The current numerical configurations will be validated against experimental data as discussed in Section 3.2.

A finite-rate chemistry is considered in the present study. Several n-heptane mechanisms [31–34] are evaluated for modeling of the ignition process of n-heptane/methanol-air mixture under a range of equivalence ratios, temperatures, and pressure conditions relevant to the present dual-fuel combustion cases. The n-heptane mechanism of Lu *et al.* (hereinafter denoted as Lu-68) with 68 species and 283 reactions [31] has shown the best trade-off between computational efficiency and model accuracy in terms of the prediction of IDT. In addition, this mechanism has been applied in both ECN spray cases [12] and the direct numerical simulation (DNS) study of n-heptane/methanol dual-fuel combustion [35]. To speed up the integration of the chemical reaction rates, a chemistry coordinate mapping (CCM) method is employed. In the CCM approach, the integration of the stiff chemical reaction rates is performed in a low-dimensional chemical phase space, and the results are mapped back to the mesh points in the physical space. In the present study, the phase space coordinates include the mixture fraction, temperature, scalar dissipation rate, and the mass fraction of n-heptane. This approach can speed up the time-consuming integration of the chemical reaction rates by a factor of 10 [36]. Details of the CCM method and its application to the simulation of spray combustion can be found in Refs. [30, 36].

The OpenFOAM code [37] is used in this study. The solver is based on the finite volume method, with a second order backward Euler scheme for temporal integration and the second order normalised variable diagram (NVD) scheme

named Gamma [38] for convective fluxes discretization.

2.2. *Eulerian stochastic field method*

As aforementioned in the introduction, the TCI effects are important particularly in cases with long ignition delay. To accommodate the TCI in spray combustion, a TPDF approach is employed based on the ESF method [39]. In this method, the one-point one-time joint PDF is expressed as an ensemble of a series of stochastic fields, where the PDF is written as,

$$P\left(\psi;\mathbf{x},t\right)=\frac{1}{N_F}\sum_{n=1}^{N_F}\prod_{\alpha=1}^{N_s}\delta(\psi_\alpha-\xi_\alpha^n) \tag{1}$$

Here, δ represents the Dirac delta function, while N_F and N_s are the number of stochastic fields and the number of scalars, respectively. The scalars include the mass fractions of species and the enthalpy. ξ_α^n denotes the α-th scalar in the n-th stochastic field.

The ESF equation in its discrete form is given in Eq. (2), describing the evolution of each stochastic field,

$$\begin{aligned}\overline{\rho}d\xi_\alpha^n=&-\overline{\rho}\tilde{\mathbf{U}}\nabla\xi_\alpha^n+\nabla\left(\Gamma_t\nabla\xi_\alpha^n\right)dt+\overline{\rho}\sqrt{2\frac{\Gamma_t}{\overline{\rho}}}\nabla\xi_\alpha^n d\mathbf{W}^n\\&-\frac{\overline{\rho}C_\phi}{2\tau_{sgs}}(\xi_\alpha^n-\tilde{\phi}_\alpha)dt+\overline{\rho}\dot{\omega}_\alpha(\underline{\xi}^n)dt.\end{aligned} \tag{2}$$

Here, $d\mathbf{W}^n$ represents the increment of a vector Wiener process to take the random process into consideration, which is spatially uniform but varying in different fields. Γ_t denotes the total diffusion coefficient, accounting for both the laminar and SGS diffusion. In addition, $\tilde{\phi}_\alpha$ represents the mean scalar field, τ_{sgs} is the SGS mixing time scale, and $C_\phi=2$ is a model constant for micro-mixing. The same model constants as in Ref. [27] are used, where more details about these constants can

be found. The number of stochastic fields is set to 12, following the suggestion of a previous study [40].

2.3. Case set-up

Table 2: Setup of the computational cases.

	Single-fuel		Dual-fuel	
	Case A	Case B	Case C	Case D
T [K]	1000	900	900	900
O_2 [vol. %]	0	0.21	0.21	0.21
ϕ_m [-]	0	0	0.1	0.3

Table 2 shows the four computational cases in this study. Cases A and B are the single-fuel cases, which have been studied in the ECN Spray-H experiments [11]. They are selected for validations of current LES models under non-reacting (Case A) and reacting spray (Case B) conditions, respectively. In addition, Case B serves as a baseline reference condition for the evaluation of the effects of the ambient mixture equivalence ratio on the dual-fuel combustion process. Cases C and D are the dual-fuel cases, with different methanol concentration in the ambient mixture. In the dual-fuel configuration, the n-heptane fuel serves as the pilot fuel which ignites the main fuel (methanol) in dual-fuel engines. The ambient methanol cocentration is parameterized using equivalence ratios (ϕ_m) according to the diesel/methanol RCCI engine of Dempsey *et al.* [28]. Case C (ϕ_m = 0.1) is representative of a low-load engine operating condition, while Case D (ϕ_m = 0.3) is for a medium-load condition [28]. The equivalence ratio ϕ_m is defined as the ratio of the actual methanol-"air" ratio to the stoichiometric methanol-"air"

ratio. It is worth mentioning that the "air" is not the atmosphere air. For the sake of validation, it is set as ECN experiments with a gas density of 14.8 kg/m^3 and a mole concentration of O_2 21%, N_2 69.33%, CO_2 6.11%, H_2O 3.56% [11]. According to the ideal gas equation of state, the pressure is calculated from the gas density, ambient temperature and the mixture average molar mass. Details of the ambient mixture initial conditions can be found in Table 3.

Table 3: Initial conditions of the ambient mixture.

Case	Density [kg/m^3]	Pressure [MPa]	Ambient methanol/air mass fraction composition				
			CH_3OH	O_2	N_2	CO_2	H_2O
A	14.8	4.2906	0	0	0.8763	0.1001	0.0237
B	14.8	3.7577	0	0.2280	0.6590	0.0913	0.0218
C	14.8	3.7532	0.0150	0.2246[1]	0.6491	0.0899	0.0214
D	14.8	3.7445	0.0437	0.2180[1]	0.6302	0.0873	0.0208

[1] The ambient oxidizer gas in Cases B, C and D is a mixture of air and CO_2 and H_2O (with the same composition as that specified in Case B). The addition of methanol reduces the oxygen mass fraction.

In all four cases, liquid n-heptane is injected into a constant volume chamber at an injection pressure of 150 MPa. The chamber configuration is the same as that in the ECN Spray-H experiments, which is a cube with a side length of 108 mm. The injection duration of n-heptane is 6.6 ms with a total mass of 17.5 mg, the injection mass flow rate is calculated using an injection model described in Ref. [41]. A locally refined grid system is used, with the finest cell size of 0.25 mm. The maximum Courant–Friedrichs–Lewy number adopted in the simulation is 0.1, which gives a typical time step of the temporal integration of 50 ns. The

mesh size and time step are adopted from our previous works [29, 30], in which a grid sensitivity study was carried out. As will be shown later, the present grid and time step showed an adequate resolution of the spray, evaporation and flame dynamics. The present grid resolution is similar to most LES studies reported recently [12, 13, 15, 17, 22], cf. Table 1. In particular, the LES study of Gallot-Lavallée *et al.* based on a coarse mesh (with a mesh size of 0.5 mm, which is coarser than the present 0.25 mm mesh) with the presently used ESF-TPDF model showed a fairly good prediction of IDT and flame lift-off length [14]. The LES studies of Kahila *et al.* used a finer mesh (with a mesh size of 0.16, 0.08 and 0.0625 mm) but without a TCI model [8]. In terms of the computation cost, it varied with the simulation time. The simulation times in Case B, C and D were 1.5, 2.5 and 3.0 ms, respectively. It took 100,000 CPU hours for Case B to run up to 1.5 ms with 144 processors in parallel.

3. Results and discussion

3.1. The performance of the chemical mechanism

An evaluation of the methanol sub-mechanism in the current Lu-68 n-heptane mechanism is conducted to investigate the accuracy of this mechanism in prediction of the ignition process in the ambient methanol/air mixture. Figure 1 shows the IDT of stoichiometric and lean methanol/air mixture (equivalence ratio of 0.5) predicted by Lu-68 mechanism and two detailed methanol mechanisms, as well as the corresponding high-pressure shock-tube experiments at National University of Ireland (NUI) Galway [42]. The initial pressure is chosen as 50 bar, which is similar to current spray flames. The two detailed methanol mechanisms considered are the Aramco 2.0 mechanism [43] and the Konnov mechanism [44]. It is shown that

the IDTs predicted using the Lu-68 mechanism are comparable to those calculated using the detailed mechanisms and the shock tube data.

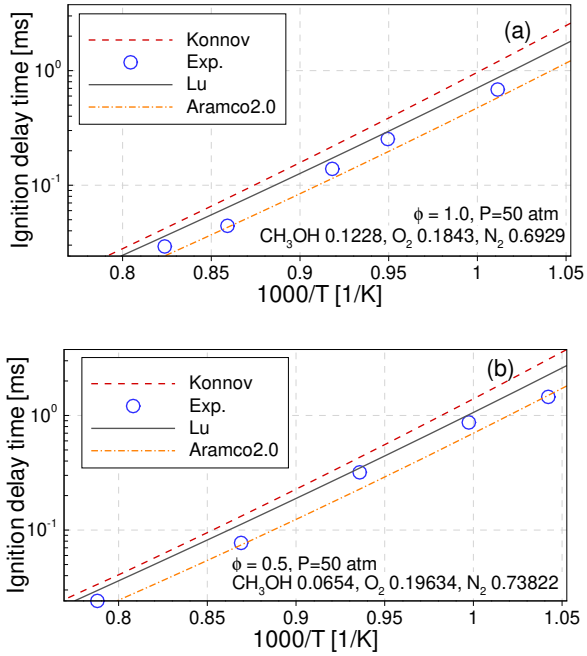

Figure 1: IDT predicted using different mechanism for a) stoichiometric and b) lean methanol/air mixture with equivalence ratio of 0.5 at different initial temperatures and a pressure of 50 bar. The symbols represent the the high-pressure shock-tube experimental data from National University of Ireland (NUI) Galway [42].

3.2. Validation of the LES spray combustion model

Figure 2a shows the liquid and vapor penetration lengths in the non-reacting case (Case A) from the present LES and the corresponding ECN Spray-H experiments, under the condition of 1000K and oxygen-free environment. The horizontal axis represents the time after the start of injection (ASI), whereas the the vertical axis shows the liquid and the vapor penetration lengths. The experimental data were obtained using Schlieren imaging and Mie-scattering [11]. The liquid penetration length from LES is defined as the distance from the injector nozzle to

the downstream position where the liquid fuel mass within this region accounts for 95% of the un-evaporated liquid mass in the domain. In addition, as recommended in ECN [11], the vapor penetration length is defined as the maximum distance from the nozzle outlet to the location with the fuel mass fraction reaching 0.1%. Figure 2b shows the spatial distribution of the mean mixture fraction from LES and experiments. The error bar indicates the uncertainty in experimental data obtained from the Rayleigh scattering [11]. The current LES model setup and grid resolution yield in good agreement with the measurements.

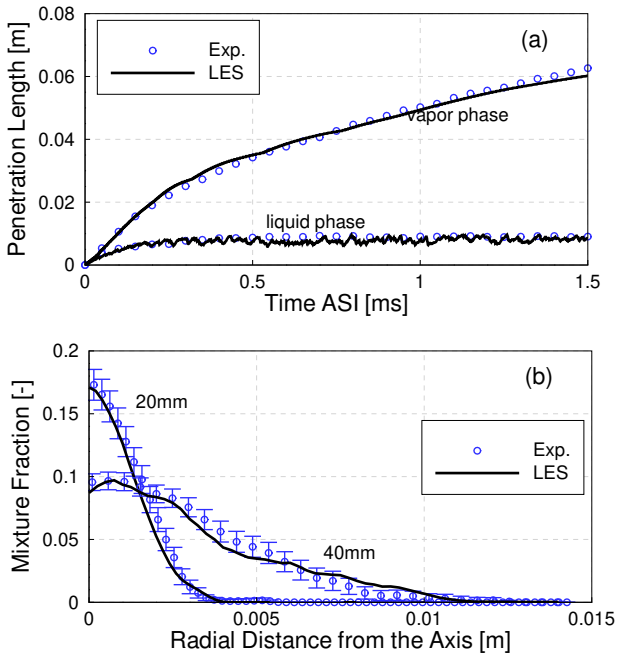

Figure 2: Liquid and vapor penetration lengths from LES and experiments (a), and mean mixture fraction from LES (time averaged) and experiments (ensemble averaged) at two axial positions (20 mm and 40 mm) downstream the nozzle (b). The results are for the evaporating spray case, case A.

For the reacting spray case (case B), the IDT and lift-off length (LOL) from

LES and experiments are compared. The IDT from LES is defined based on the time at which the maximal time derivative of temperature is reached. LOL is defined as the distance from the fuel nozzle to the farthest location where Favre-average OH mass fraction reaches 2% of its maximum in the domain after a stable flame is established, following the ECN suggestion [11]. The IDT and LOL predicted in the current LES are 0.80 ms and 25 mm, respectively. These agree with the experimental IDT of 0.79 ms and LOL of 25.5 mm [11] reasonably well, where the relative differences remain below 2%. Moreover, the LES replicates the experimental pressure profile (shown in the next section). In summary, the present LES spray combustion model is capable of simulating the spray vaporization and vapor mixing processes, the ignition timing and the flame stabilization. In the following, the LES model is applied to predict and analyze the spray combustion process for both the single- and dual-fuel cases.

3.3. Effects of ambient methanol on pressure rise and heat-release rate

Figure 3 shows the temporal evolution of pressure rise (the difference between the chamber pressure and its initial pressure) and net HRR, which is the heat release rate term integrated over the entire chamber, for cases B, C, and D (with ambient methanol equivalence ratio varying from 0 to 0.3). Before the onset of ignition, the chamber pressure decreases due to the endothermic evaporation process during n-heptane injection. After a short while, a pressure rise is observed, along with noticeable HRR, indicating the onset of ignition. Both the initial HRR and the pressure-rise rate are rather low; this stage of ignition is known as the first stage ignition or low temperature ignition. Thereafter, around 0.6 ms ASI, HRR increases rapidly to a substantially high value, along with a rapid increase of chamber pressure. The start of the high HRR indicates the onset of second

stage ignition, also known as the high temperature ignition stage. This two-stage ignition process is observed for the n-heptane fuel, while methanol ignition undergoes only the high temperature stage [45]. As shown in the inset of Fig. 3, where the first stage HRR is displayed, the onset of first stage ignition is retarded in the dual-fuel cases ($\phi_m = 0.1$ and $\phi_m = 0.3$). This is consistent with the observation in methane-based dual-fuel experiments [10] and LES [8] studies. Moreover, the higher methanol-air equivalence ratio in the ambient mixture, the longer retardation time of the first stage ignition, and the lower the peak HRR from the first stage ignition. Furthermore, the ambient methanol also retards the second stage ignition, evident by the time difference between the second stage ignition and the first stage ignition, which increases with the increase of ϕ_m in the ambient mixture.

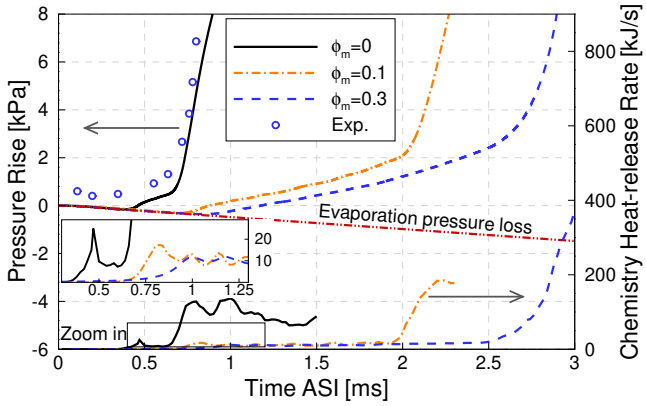

Figure 3: Effect of ambient methanol concentration on pressure rise and total heat-release rate for cases B, C, and D. The experimental pressure rise is shown using symbols.

3.4. Effects of ambient methanol concentration on the ignition process

In order to track the ignition event, the most reactive local mixture is defined. The HRR of the local mixture (in each computational cell) is compared and the

one with the highest HRR is defined as the most reactive local mixture. The spatial location of the most reactive local mixture changes with time. The most reactive local mixture is tracked in order to investigate how it evolves and where it is located. The temporal evolution of heptyl-peroxide (RO_2) and OH mass fractions in the most reactive local mixture is shown in Figure 4. To illustrate the wide range, mass fractions in vertical coordinates are shown in log-scale. RO_2 has been recommended by ECN [11] as the marker of the first stage ignition: the first stage IDT is suggested to be at the time of RO_2 mass fraction reaching 20% of its maximum, denoted as τ_1 in Fig. 4a with the vertical dashed lines. On the other hand, OH is used as the indicator for the second stage ignition , denoted as τ_2 in Fig. 4b. It is seen that the mass fractions of RO_2 and OH of the most reactive mixture increases (approximately) exponentially with time (ASI) until it reaches a plateau shortly after τ_1, and the mass fraction of OH reaches a second plateau after τ_2. In the second stage ignition, the maximum OH mass fraction is independent of ϕ_m, while during the transition period from the first stage ignition to the second stage ignition, it decreases with ϕ_m in the ambient mixture. The transition time from the onset of first stage ignition to the second stage ignition is 0.23 ms, 1.17 ms, and 1.52 ms for cases B, C, and D, respectively, showing an increasing retardation effect of methanol on the n-heptane ignition process with ϕ_m. Similar retardation effect has been reported for n-dodecane/methane-air dual-fuel combustion [10].

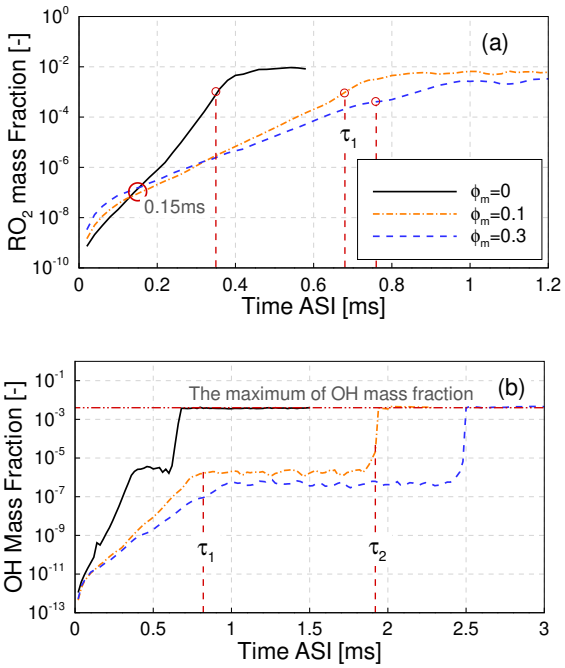

Figure 4: Temporal evolution of mass fraction of RO_2, Y_{RO_2} (a), and OH, Y_{OH} (b), in the most reactive local mixture for cases B, C, and D (with ϕ_m varying from 0 to 0.3), respectively. The vertical dashed lines indicate the time of first stage ignition (τ_1, a) and the first and second stage ignition (τ_1 and τ_2, b). The two plateaus in the OH profiles indicate the transition period from the onset of the first stage ignition to the onset of the second stage ignition, and the period after the onset of the second stage ignition.

The maximal mass fraction of RO_2 in the most reactive mixture is higher initially (before 0.15 ms ASI) in the cases with higher methanol concentration in the ambient mixture. This indicates that the ambient methanol enhances the production of RO_2. However, shortly after 0.15 ms ASI, the suppression effect of methanol on RO_2 is evident. The underlying mechanism behind this is investigated in Section 3.6.

3.5. *Effects of methanol on the structure of the spray flame*

In a three-dimensional n-heptane/methanol dual-fuel spray flame, during the liquid n-heptane injection, the ignition reactions in the methanol-air mixture take place, but not to the critical point of auto-ignition. This period of time is referred to as the ignition induction time. This implies that in the present n-heptane/methanol dual-fuel combustion process, the effects of methanol chemistry on the n-heptane ignition is different at different spatial locations of the spray jet due to the discrepancy in the induction time.

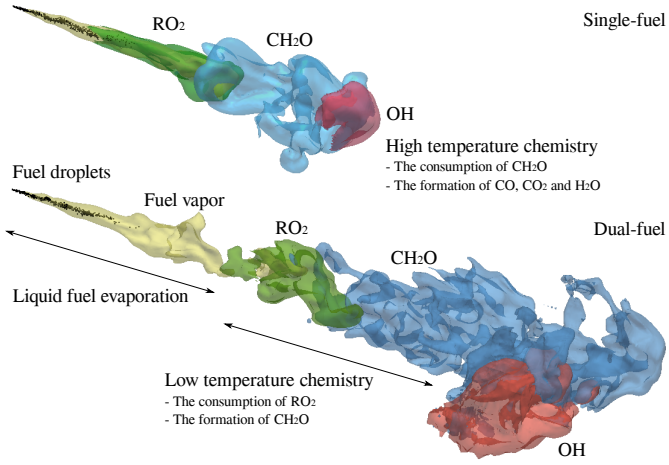

Figure 5: Three-dimensional flame structure at the instance of second stage ignition for the single-fuel Case B (upper) and dual-fuel Case D (bottom). Black dots indicate the fuel droplets.

Figure 5 shows the three-dimensional flame structure of single-fuel (Case B) and dual-fuel combustion (Case D) at the instance of second stage ignition. The liquid n-heptane is injected and evaporated to fuel vapor in the immediate downstream of the fuel jet. The intermediate species, such as RO_2 and CH_2O, are produced in the low-temperature ignition region. The high-temperature ignition takes place in downstream regions of the spray, where the intermediate species are

oxidized to CO_2 and H_2O with the participation of radicals such as OH.

The fuel vapor is enveloped by the RO_2 in the single-fuel case, while the RO_2 region in the dual-fuel case is in the downstream of the fuel vapor region. The ambient methanol/air mixture retards the onset of the first stage ignition, affects the cool flame structure, and postpones the onset of second stage ignition kernel at further downstream. The postponed high temperature ignition extends the mixing time before the start of high-temperature combustion, which reduces the high-temperature and rich-fuel regions forming soot. This result is consistent with the soot reduction in dual-fuel engines reported in the literature [3, 46, 47].

To investigate the first stage ignition kernel structure of the present spray flames in more detail, the spatial and temporal distributions of RO_2, HO_2, CH_2OH, and OH mass fractions before the onset of the first stage ignition in a cross plane along the spray axis, are plotted in Fig. 6. The mass fractions are normalized by its maximal value in the domain for the given case at the given instance of times.

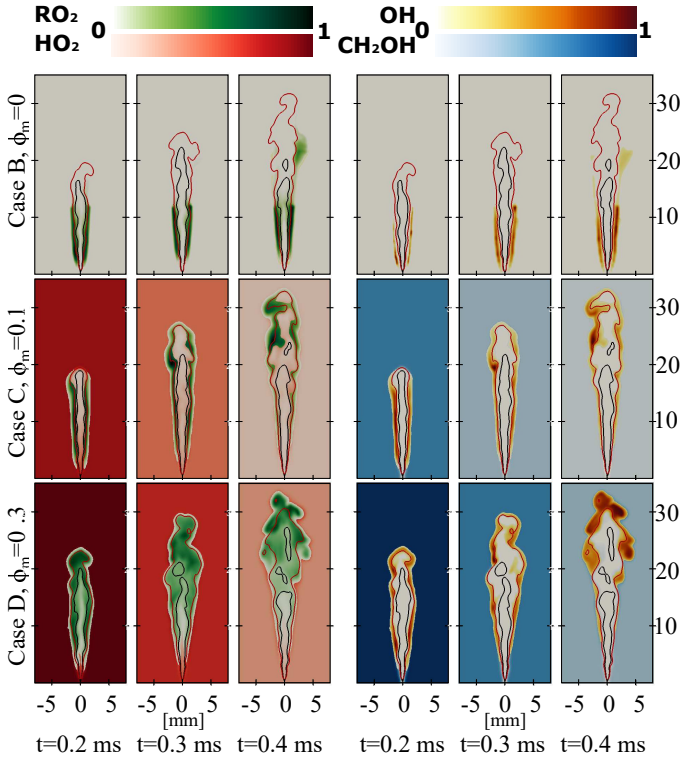

Figure 6: Distributions of RO_2 and HO_2 (left hand side), OH and CH_2OH (right hand side) prior to the onset of first stage ignition in a cross section along the spray axis. The red line denotes the iso-line of stoichiometric mixture fraction, and the black line is the iso-line of temperature of 700 K.

For Case B ($\phi_m = 0$), the formation of RO_2 starts in the upstream region of the spray jet, around the iso-surface of the stoichiometric mixture fraction. As time goes on, the fuel vapor continues to penetrate downstream but most of the RO_2 still concentrates upstream, until a new reactive region appearing at 0.4 ms in the downstream around stoichiometric contour line. At this stage, $t \leq 0.4$ ms, the concentration of HO_2 is rather low. CH_2OH is negligible in Case B.

In contrast, the flame structure in the dual-fuel cases is significantly different. Due to the presence of methanol in the ambient gas, ignition reactions take place in

the ambient mixture giving rise to the formation of HO_2 and CH_2OH, among other species. This affects the formation of RO_2 and OH radicals. In Case C, with the methanol-air equivalence ratio of $\phi_m = 0.1$, the RO_2 is formed not only in the near nozzle region but also downstream, around the iso-surface of the stoichiometric mixture fraction. In Case D, with a higher methanol-air equivalence ratio of $\phi_m = 0.3$, the RO_2 fills up the entire fuel-rich region of the jet.

As a key species generated in the methanol ignition reactions, HO_2 is essential for n-heptane ignition since it participates in the reaction forming heptyl radicals, $C_7H_{16} + HO_2 = C_7H_{15} + H_2O_2$, which leads further to the formation of RO_2. This explains the enhanced formation of RO_2 in the cool flame downstream region of spray jet, and the elevated mass fraction of RO_2 in the early first stage ignition, i.e., $t < 0.15$ ms, Fig. 4a. However, as shown in Fig. 4b, the presence of methanol in the ambient gas has, in general, a suppression effect on the ignition of n-heptane, due to the non-linear interaction among the different elementary reactions involved. This will be next examined using the reaction pathways.

3.6. Analysis of the dual-fuel reaction pathways

Zero-dimensional homogeneous reactor simulations are conducted to identify the reaction path and to explain the effects of methanol on the ignition of n-heptane. The rates of reactions are compared to identify the relative importance of OH and HO_2 consumption rates in different reactions. Three cases are investigated according to the composition of the stoichiometric mixture in the spray cases B, C and D. A conversion ratio of species i in reaction j (β_{ij}) is defined as, $\beta_{ij} = I_{ij}/I_i$, where i represents either OH or HO_2. I_{ij} is the integration of the consumption rate of species i in reaction j, within the induction time before the onset of the second stage ignition. I_i is the sum of I_{ij} over all reactions. The conversion ratios for OH

and HO_2 in key reactions are listed in Table 4.

Table 4: Conversion ratios of OH and HO_2 in key reactions.

Key reactions \ ϕ_m [-]	0	0.1	0.3
$CH_3OH + OH = CH_2OH + H_2O$ (R1)	0	9.45%	32.28%
$CH_2O + OH = HCO + H_2O$ (R3)	40.01%	39.13%	38.02%
$C_7H_{16} + HO_2 = C_7H_{15} + H_2O_2$ (R4)	2.10%	2.64%	2.96%
$C_7H_{16} + OH = C_7H_{15} + H_2O$ (R5)	16.16%	11.71%	6.71%

The ambient methanol contributes to the consumption of OH through $CH_3OH + OH = CH_2OH + H_2O$ reaction (denoted as R1). As seen in Table 4, the percentage of OH consumption in reaction R1 increases with the increase of the ambient methanol-air equivalence ratio, ϕ_m. About 32% of OH is consumed by CH_3OH in R1 in the $\phi_m = 0.3$ case. This reduces the OH accumulation rate, prolonging the first stage ignition delay times, τ_1. Meanwhile, the intermediate product, CH_2OH, is formed in the ambient methanol-air mixture. The oxidation of CH_2OH, in reaction $CH_2OH + O_2 = CH_2O + HO_2$ (denoted as R2), generates HO_2. Even though HO_2 will be converted to H_2O_2 and supply OH through reaction $H_2O_2 + M = OH + OH + M$, this reaction has a high activation energy, thus, the formation of OH from methanol-air mixture is limited before the temperature increases up to 1000 K [45]. OH is therefore consumed by reacting with methanol via R1 (but cannot be replenished) in the low temperature ignition stage. As such, the maximum OH mass fraction in the dual-fuel spray cases is lower than that in the single-fuel case during the transition induction period, $\tau_1 < t < \tau_2$. Thereafter, the high temperature reaction condition is met, OH is consumed in

a series of high temperature reactions. One of the important reactions is the oxidation of formaldehyde (CH_2O), $CH_2O + OH = HCO + H_2O$ (denoted as R3). The existence of CH_3OH has a rather minor effect on the OH consumption in R3, as shown in Table 4. This explains the nearly constant maximal value of OH mass fractions for different ambient methanol concentrations after the onset of second ignition, $t > \tau_2$, as illustrated earlier in Fig. 4b.

The formation of HO_2 from the ambient methanol in reaction R2 contributes to the consumption of C_7H_{16} through the reaction $C_7H_{16} + HO_2 = C_7H_{15} + H_2O_2$ (denoted as R4). This leads to the elevated production of RO_2 during the early stages of the first stage ignition, shown in Fig. 4a, and the change of the cool flame structure in Fig. 6. On the other hand, the reaction $C_7H_{16} + OH = C_7H_{15} + H_2O$ (denoted as R5) is slowed down, with the OH conversion ratio decreasing from 16% ($\phi_m = 0$) to 7% ($\phi_m = 0.3$). The suppression of reaction R5 by methanol is the reason for the retardation of the first stage ignition and the transition from τ_1 to τ_2, shown in Fig. 4.

4. Conclusion

LES with a transported probability density function (TPDF) model is performed to investigate the effects of the ambient methanol-air equivalence ratio (ϕ_m from 0 to 0.3) on the n-heptane spray combustion under reactivity controlled compression ignition (RCCI) engine-like conditions. The baseline case is chosen from ECN n-heptane spray experiments. The LES models are validated against experiments. A good agreement between the LES prediction and the ECN experiments, in terms of the liquid length, vapor penetration length, mixture fraction, ignition delay time and lift-off length, is achieved. The dual-fuel combustion results gener-

ated using the LES-TPDF model are analyzed to elucidate the effects of methanol chemistry on the ignition of the n-heptane spray. The following conclusions are drawn.

(1) Ambient methanol has a general effect of suppressing the ignition of n-heptane. Both the first stage and second stage ignitions of n-heptane are retarded by ambient methanol. A longer transition time between the two ignition stages and a lower first local peak value of the heat release rate are observed when increasing ambient methanol concentration (i.e. ϕ_m). The reason behind the suppression of ignition is that the concentration of radicals (e.g. OH) is reduced by reaction with ambient methanol, e.g., through elementary reaction $CH_3OH + OH = CH_2OH + H_2O$. The OH consumption rate increases with the increase of ϕ_m.

(2) In the earlier induction period before the onset of first stage ignition, ambient methanol has an effect of enhancing the formation of heptyl-peroxide (RO_2) that has been considered as the marker of the first stage ignition. Chemical pathway analysis shows that HO_2 generated in the ambient methanol promotes the formation heptyl radicals, via $C_7H_{16} + HO_2 = C_7H_{15} + H_2O_2$, this subsequently enhancing the formation of RO_2. However, the consumption of OH through reaction $CH_3OH + OH = CH_2OH + H_2O$ suppresses the reaction $C_7H_{16} + OH = C_7H_{15} + H_2O$, which retards eventually the onset of both the first stage and the second stage ignition of n-heptane.

(3) Under the lean ambient mixture conditions studied in the present work, ambient methanol affects the n-heptane spray flame structures in both the ignition stage and in the steady spray flame stage. In the single-fuel methanol-free case, the low temperature ignition and cool flame marker, RO_2, is shown to distribute around the stoichiometric mixture in the proxmity of the fuel nozzle, with the

cool flame enveloping the fuel rich region. In the dual-fuel RCCI cases, RO_2 is found in the entire fuel-rich region farther downstream. The onset of second stage ignition kernel is postponed at further downstream, this resulting a longer liftoff length in the methanol/n-heptane dual-fuel cases than that of single fuel n-heptane spray flame. The postponed ignition and the longer liftoff length extend the mixing time before the start of high-temperature combustion, this reducing the high-temperature and rich-fuel regions in the dual-fuel cases, which explains the reduced soot emission in dual-fuel engines reported in the literature.

Acknowledgments

This work is sponsored by Swedish Research Council (VR). Shijie Xu and Shenghui Zhong are sponsored by China Scholarship Council. We thank Rui Li for the assistance on chemical analysis. The simulations are performed on resources provided by the Swedish National Infrastructure for Computing (SNIC) at HPC2N and PDC.

References

[1] Y. Li, M. Jia, Y. Liu, M. Xie, Numerical study on the combustion and emission characteristics of a methanol/diesel reactivity controlled compression ignition (RCCI) engine, Applied energy 106 (2013) 184–197.

[2] B. Ma, A. Yao, C. Yao, T. Wu, B. Wang, J. Gao, C. Chen, Exergy loss analysis on diesel methanol dual fuel engine under different operating parameters, Applied Energy 261 (2020) 114483.

[3] D. Splitter, R. Hanson, S. Kokjohn, R. D. Reitz, Reactivity controlled compression ignition (RCCI) heavy-duty engine operation at mid-and high-loads

with conventional and alternative fuels, Tech. Rep., SAE Technical Paper, 2011.

[4] X. Kan, L. Wei, X. Li, H. Li, D. Zhou, W. Yang, C.-H. Wang, Effects of the three dual-fuel strategies on performance and emissions of a biodiesel engine, Applied Energy 262 (2020) 114542.

[5] D. Zhou, W. Yang, H. An, J. Li, Application of CFD-chemical kinetics approach in detecting RCCI engine knocking fuelled with biodiesel/methanol, Applied Energy 145 (2015) 255–264.

[6] J. Liu, F. Yang, H. Wang, M. Ouyang, S. Hao, Effects of pilot fuel quantity on the emissions characteristics of a CNG/diesel dual fuel engine with optimized pilot injection timing, Applied Energy 110 (2013) 201–206.

[7] K. Ryu, Effects of pilot injection timing on the combustion and emissions characteristics in a diesel engine using biodiesel–CNG dual fuel, Applied Energy 111 (2013) 721–730.

[8] H. Kahila, A. Wehrfritz, O. Kaario, V. Vuorinen, Large-eddy simulation of dual-fuel ignition: Diesel spray injection into a lean methane-air mixture, Combustion and Flame 199 (2019) 131–151.

[9] Z. Yin, C. Yao, P. Geng, J. Hu, Visualization of combustion characteristic of diesel in premixed methanol–air mixture atmosphere of different ambient temperature in a constant volume chamber, Fuel 174 (2016) 242–250.

[10] A. Srna, M. Bolla, Y. M. Wright, K. Herrmann, R. Bombach, S. S. Pandurangi, K. Boulouchos, G. Bruneaux, Effect of methane on pilot-fuel auto-

ignition in dual-fuel engines, Proceedings of the Combustion Institute 37 (4) (2019) 4741–4749.

[11] Engine combustion network, https://ecn.sandia.gov, Accessed Jan., 2020.

[12] S. Som, D. E. Longman, Z. Luo, M. Plomer, T. Lu, P. K. Senecal, E. Pomraning, Simulating flame lift-off characteristics of diesel and biodiesel fuels using detailed chemical-kinetic mechanisms and large eddy simulation turbulence model, Journal of Energy Resources Technology 134 (3) (2012) 032204.

[13] A. Irannejad, A. Banaeizadeh, F. Jaberi, Large eddy simulation of turbulent spray combustion, Combustion and Flame 162 (2) (2015) 431–450.

[14] S. Gallot-Lavallée, W. Jones, Large eddy simulation of spray auto-ignition under EGR conditions, Flow, Turbulence and Combustion 96 (2) (2016) 513–534.

[15] C.-W. Tsang, Y. Wang, C. Wang, A. Shelburn, L. Liang, K. Puduppakkam, A. Modak, C. Naik, E. Meeks, C. Rutland, Evaluation and Validation of Large-Eddy-Simulation (LES) for Gas Jet and Sprays, Tech. Rep., SAE Technical Paper, 2017.

[16] H. Wei, W. Zhao, J. Qi, Z. Liu, L. Zhou, Effect of injection timing on the ignition process of n-heptane spray flame in a methane/air environment, Fuel 245 (2019) 345–359.

[17] C. Gong, M. Jangi, X.-S. Bai, Large eddy simulation of n-dodecane spray

combustion in a high pressure combustion vessel, Applied Energy 136 (2014) 373–381.

[18] Y. Pei, S. Som, E. Pomraning, P. K. Senecal, S. A. Skeen, J. Manin, L. M. Pickett, Large eddy simulation of a reacting spray flame with multiple realizations under compression ignition engine conditions, Combustion and Flame 162 (12) (2015) 4442–4455.

[19] A. Wehrfritz, O. Kaario, V. Vuorinen, B. Somers, Large eddy simulation of n-dodecane spray flames using flamelet generated manifolds, Combustion and Flame 167 (2016) 113–131.

[20] P. Kundu, M. M. Ameen, S. Som, Importance of turbulence-chemistry interactions at low temperature engine conditions, Combustion and Flame 183 (2017) 283–298.

[21] C. K. Blomberg, L. Zeugin, S. S. Pandurangi, M. Bolla, K. Boulouchos, Y. M. Wright, Modeling split injections of ECN "Spray A" using a conditional moment closure combustion model with RANS and LES, SAE International Journal of Engines 9 (4) (2016) 2107–2119.

[22] A. Hadadpour, M. Jangi, K. M. Pang, X. S. Bai, The role of a split injection strategy in the mixture formation and combustion of diesel spray: A large-eddy simulation, Proceedings of the Combustion Institute 37 (4) (2019) 4709–4716.

[23] H. Kahila, O. Kaario, Z. Ahmad, M. G. Masouleh, B. Tekgül, M. Larmi, V. Vuorinen, A large-eddy simulation study on the influence of diesel pilot

spray quantity on methane-air flame initiation, Combustion and Flame 206 (2019) 506–521.

[24] B. Tekgül, H. Kahila, O. Kaario, V. Vuorinen, Large-eddy simulation of dual-fuel spray ignition at different ambient temperatures, Combustion and Flame 215 (2020) 51–65.

[25] W. Zhao, H. Wei, M. Jia, Z. Lu, K. H. Luo, R. Chen, L. Zhou, Flame–spray interaction and combustion features in split-injection spray flames under diesel engine-like conditions, Combustion and Flame 210 (2019) 204–221.

[26] A. Varna, A. Wehrfritz, E. R. Hawkes, M. J. Cleary, T. Lucchini, G. D'Errico, S. Kook, Q. N. Chan, Application of a multiple mapping conditioning mixing model to ECN Spray A, Proceedings of the Combustion Institute 37 (3) (2019) 3263–3270.

[27] K. M. Pang, M. Jangi, X.-S. Bai, J. Schramm, J. H. Walther, Modelling of diesel spray flames under engine-like conditions using an accelerated Eulerian Stochastic Field method, Combustion and Flame 193 (2018) 363–383.

[28] A. B. Dempsey, N. R. Walker, R. Reitz, Effect of piston bowl geometry on dual fuel reactivity controlled compression ignition (RCCI) in a light-duty engine operated with gasoline/diesel and methanol/diesel, SAE International Journal of Engines 6 (1) (2013) 78–100.

[29] M. Jangi, R. Solsjo, B. Johansson, X.-S. Bai, On large eddy simulation of diesel spray for internal combustion engines, International Journal of Heat and Fluid Flow 53 (2015) 68–80.

[30] C. Gong, M. Jangi, X.-S. Bai, Large eddy simulation of n-dodecane spray combustion in a high pressure combustion vessel, Applied Energy 136 (2014) 373–381.

[31] T. Lu, C. K. Law, C. S. Yoo, J. H. Chen, Dynamic stiffness removal for direct numerical simulations, Combustion and Flame 156 (8) (2009) 1542–1551.

[32] R. Li, S. Li, F. Wang, X. Li, Sensitivity analysis based on intersection approach for mechanism reduction of cyclohexane, Combustion and Flame 166 (2016) 55–65.

[33] S. Liu, J. C. Hewson, J. H. Chen, H. Pitsch, Effects of strain rate on high-pressure nonpremixed n-heptane autoignition in counterflow, Combustion and flame 137 (3) (2004) 320–339.

[34] K. M. Pang, N. Karvounis, J. H. Walther, J. Schramm, Numerical investigation of soot formation and oxidation processes under large two-stroke marine diesel engine-like conditions using integrated CFD-chemical kinetics, Applied energy 169 (2016) 874–887.

[35] S. Hu, C. Gong, X.-S. Bai, Dual Fuel Combustion of N-heptane/methanol-air-EGR Mixtures, Energy Procedia 105 (2017) 4943–4948.

[36] M. Jangi, X. Zhao, D. C. Haworth, X.-S. Bai, Stabilization and liftoff length of a non-premixed methane/air jet flame discharging into a high-temperature environment: An accelerated transported PDF method, Combustion and Flame 162 (2) (2015) 408–419.

[37] The OpenFOAM Foundation, https://www.openfoam.gov, Accessed Jan., 2020.

[38] H. Jasak, H. G. Weller, A. D. Gosman, High resolution NVD differencing scheme for arbitrarily unstructured meshes, International Journal for Numerical Methods in Fluids 31 (2) (1999) 431–449, ISSN 0271-2091.

[39] L. Valiño, A field Monte Carlo formulation for calculating the probability density function of a single scalar in a turbulent flow, Flow, turbulence and combustion 60 (2) (1998) 157–172.

[40] M. Jangi, M. Altarawneh, B. Z. Dlugogorski, Large-eddy simulation of methanol pool fires using an accelerated stochastic fields method, Combustion and Flame 173 (2016) 89–98.

[41] L. Xu, X.-S. Bai, M. Jia, Y. Qian, X. Qiao, X. Lu, Experimental and modeling study of liquid fuel injection and combustion in diesel engines with a common rail injection system, Applied Energy 230 (2018) 287–304.

[42] U. Burke, W. K. Metcalfe, S. M. Burke, K. A. Heufer, P. Dagaut, H. J. Curran, A detailed chemical kinetic modeling, ignition delay time and jet-stirred reactor study of methanol oxidation, Combustion and Flame 165 (2016) 125–136.

[43] National University of Ireland Galway, http://c3.nuigalway.ie/combustionchemistrycentre/mechanismdownloads, Accessed Jan., 2020.

[44] M. Christensen, E. Nilsson, A. Konnov, A systematically updated detailed kinetic model for CH2O and CH3OH combustion, Energy & Fuels 30 (8) (2016) 6709–6726.

[45] H. Xu, C. Yao, G. Xu, Chemical kinetic mechanism and a skeletal model for oxidation of n-heptane/methanol fuel blends, Fuel 93 (2012) 625–631.

[46] Q. Tang, H. Liu, X. Ran, M. Li, M. Yao, Effects of direct-injection fuel types and proportion on late-injection reactivity controlled compression ignition, Combustion and Flame 211 (2020) 445–455.

[47] Q. Tang, X. Liu, H. Liu, H. Wang, M. Yao, Investigation on the dual-fuel active-thermal atmosphere combustion strategy based on optical diagnostics and numerical simulations, Fuel 276 (2020) 118023.

LES/TPDF investigation of the effects of ambient methanol concentration on pilot fuel ignition characteristics and reaction front structures

Shijie Xu[a,*], Kar Mun Pang[b], Yaopeng Li[a,c], Ahmad Hadadpour[a], Senbin Yu[a], Shenghui Zhong[a,d], Mehdi Jangi[e], Xue-song Bai[a]

[a]*Department of Energy Sciences, Lund University, 22100 Lund, Sweden*
[b]*MAN Energy Solutions, Teglholmsgade 41, 2450 Copenhagen SV, Denmark*
[c]*Key Laboratory of Ocean Energy Utilization and Energy Conservation of Ministry of Education, Dalian University of Technology, 116024 Dalian, P.R. China*
[d]*State Key Laboratory of Engines, Tianjin University, 135 Yaguan Rd, 300350 Tianjin, P.R. China*
[e]*School of Mechanical Engineering, University of Birmingham, Edgbaston, Birmingham B15 2TT, UK*

Abstract

Large-eddy simulations with a transported probability density function model coupled with a finite-rate chemistry is applied to study the ignition process of an n-heptane spray in a constant volume chamber with a premixed methanol-air atmosphere under conditions relevant to reactivity controlled compression ignition (RCCI) engines. Three reacting spray cases with initial methanol-air equivalence ratio (ϕ_m) ranging from 0 to 0.3 are investigated at an initial temperature of 900 K. The case setup is based on the Engine Combustion Network Spray-H configuration, where n-heptane fuel is used. The effects of the ambient methanol-air equivalence ratio on the ignition characteristics and the reaction front structures in n-heptane/methanol RCCI combustion are studied in detail. It is found that the ambient methanol affects the low temperature chemistry of n-heptane, which

*Corresponding author.
E-mail address: shijie.xu@energy.lth.se

results in a change of spatial distribution of key species such as heptyl-peroxide, and therefore the cool flame structure. With the presence of methanol in the ambient mixture cool flame is found in the entire fuel-rich region of the n-heptane jet, while when methanol is absent in the ambient mixture, the cool flame is established only around the stoichiometric mixture close to the n-heptane injector nozzle. In general, both low- and high-temperature ignition stages of n-heptane ignition are retarded by the methanol chemistry. An increase in ϕ_m leads to a decrease of the peak heat release rate of the n-heptane first-stage ignition. The chemistry of methanol inhibits the n-heptane ignition by decreasing the overall hydroxyl radicals (OH) formation rate and reducing the OH concentration during the transition period from the first-stage ignition to the second-stage ignition. As a result, the transition time between the two ignition stages is prolonged. Under the present lean methanol/air ambient mixture conditions, the impact of methanol on n-heptane ignition has a tendency of reducing the high-temperature, fuel-rich region, which is in favor of soot reduction.

Keywords: Dual-fuel combustion, Auto-ignition, Engine Combustion Network, Large eddy simulation, Eulerian stochastic field

---

1. Introduction

Methanol is a promising alternative fuel to fossil fuels. As compared with natural gas and hydrogen, methanol is easier to store, transport, distribute, and use since methanol is in liquid form at room temperature. Methanol can be produced from a wealth of sources, such as coal, natural gas, biomass and municipal waste. One of the main challenges in utilizing methanol in conventional compression-ignition (CI) engines is the difficulty in igniting the fuel due to its high latent

heat of evaporation and long ignition-delay time (IDT). This issue becomes more severe in the condition of a cold start or at low engine loads [1, 2]. As a result, novel combustion strategies, e.g., dual-fuel combustion, are developed to improve the ignition process in methanol fueled CI engines. The engines using dual-fuel combustion strategies are known as dual-fuel engines. One of the dual-fuel engines is the reactivity controlled compression ignition (RCCI) engine. In the RCCI engine, a low-reactivity fuel (primary fuel) is delivered into the cylinder during the intake stroke to form a premixed fuel-air mixture. The mixture is then ignited by injecting a high-reactivity fuel (pilot fuel) during the compression stroke. Due to the lean premixed combustion in RCCI, high-temperature and rich-fuel regions can be avoided in the cylinder, leading to reduced soot and NOx emissions [3–6]. An engineering challenge in the dual-fuel engine is the control of ignition time and heat release rate (HRR) [7]. Unlike the ignition of a conventional diesel engine, the auto-ignition mechanism in a dual-fuel engine is not well understood [8]. In practice, the equivalence ratio distribution of the primary fuel/air mixture may not be perfectly homogenous in the dual-fuel engines [9]. When the pilot fuel is introduced, the associated ignition characteristics vary due to the local condition [9]. This further complicates the auto-ignition mechanism in dual-fuel engines.

Several experimental and numerical studies were carried out to improve the understandings of pilot fuel ignition in the ambient primary fuel/air mixture. Yin *et al.* [10] performed experiments on diesel/methanol dual-fuel combustion in a constant volume combustion chamber under a range of ambient temperatures (840–960 K) with methanol-air equivalence ratio (ϕ_m) of 0.1. The results showed that when the temperature is below 920 K, the IDT of diesel in the methanol-air atmosphere is longer than that in the pure air atmosphere. However, detailed

analysis of the ignition phenomenon, such as complex two-stage ignitions, was not provided, due to the lack of intermediate species in the measurements. Srna *et al.* [11] reported optical diagnosis experiments of n-dodecane spray combustion in a methane-air atmosphere in a rapid compression-expansion machine (RCEM). It was found that the ambient methane could affect the onset of the first-stage ignition (the cool flame) but the temporal separation of the first-stage ignition and the second-stage ignition was shown to be independent of the methane concentration in the ambient methane-air mixture. Xu *et al.* [12] studied the reaction paths of the n-heptane/methanol blends. The results showed that radical pool was a bridge connecting methanol and n-heptane in oxidation, where the methanol concentration was important. Kahila *et al.* [8] conducted a large eddy simulation (LES) of an n-dodecane/methane-air dual-fuel combustion in the Engine Combustion Network (ECN) [13] constant volume configuration. It was found that the low-temperature reactions of the pilot fuel (n-dodecane) provided intermediate species and heat, which played an important role in the primary fuel (methane) oxidation. In turn, both the first and the second ignition stages of the pilot fuel were retarded in the methane-air atmosphere, mainly due to the consumption of OH in the ambient methane oxidation. The same group also investigated different aspects of n-dodencane/methane dual-fuel combustion using their LES models [8, 14, 15]. Yet, LES on methanol based dual-fuel combustion have been rare. This motivates the present study which aims to investigate the effects of ambient methanol concentration on pilot fuel ignition.

It may also be worth mentioning that the recent LES studies [8, 14, 15] of dual-fuel combustion used a well-stired reactor (WSR) assumption, in which turbulence-chemistry interaction (TCI) in the sub-grid scale (SGS) has been neglected. They

Table 1: Recent LES studies of ECN spray flames.

Fuel	Species number	Mesh size [μm]	Combustion model	Turbulence model	Code	Ref.
n-Heptane	42, 68	250	WSR	Smagorinsky	Converge	[16]
n-Heptane	44	200	FMDF [1]	-	In-house	[17]
n-Heptane	22	500	ESF	Dynamic Smagorinsky	In-house	[18]
n-Heptane	140	250, 125, 62.5	WSR	Smagorinsky, dynamic structure	ANSYS	[19]
n-Heptane/ methane	44	-	LEM	-	KIVA	[20]
n-Dodecane	103	250	WSR	One-equation eddy	OpenFOAM	[21]
n-Dodecane	103	62.5	WSR	Dynamic structure	Converge	[22]
n-Dodecane	257, 103	62.5	FGM	-	OpenFOAM	[23]
n-Dodecane	103	62.5	TFM [2]	Dynamic structure	Converge	[24]
n-Dodecane	54	125	CMC	$k-\ell$ two-equations	Star-CD	[25]
n-Dodecane	54	240	PaSR [3]	One-equation eddy	OpenFOAM	[26]
n-Dodecane/ methane	54, 96	160, 80, 62.5	WSR	Implicit LES	OpenFOAM	[8, 14, 15]
n-Dodecane	54	-	LEM	-	KIVA	[27]

[1] Compressible filtered mass density function (FMDF).

[2] Tabulated Flamelet Model (TFM).

[3] Partially stirred reactor (PaSR) model.

used a very fine spatial resolution to compensate the absence of the TCI effect. However, Varna *et al.* [28] pointed out that TCI is important for the spray flame under engine-like conditions, especially for the low temperature case with a long IDT. The IDT is typically prolonged by the ambient primary fuel [8, 14, 29], it is hence desirable to incorporate a TCI model in dual-fuel ignition simulations. The commonly used TCI models are the Conditional Moment-Closure (CMC) [25], the probability density function (PDF) model [18], the linear eddy model (LEM) [20, 27], and the Flamelet Generation Manifold (FGM) [23]. Table 1 shows a list of recent LES studies of the ECN spray combustion cases. A summary of the unsteady Reynolds-averaged Navier–Stokes (URANS) simulations is available in Ref. [30].

Set against these backgrounds, LES which is known to have better capability in predicting flow structure and mixing is carried out to study n-heptane/methanol dual-fuel combustion in a constant volume combustion chamber. In addition to this, an Eulerian stochastic field (ESF) transported probability density function (TPDF) model is employed to account for the SGS TCI effects. The baseline case uses the ECN Spray-H (n-heptane fueled) conditions. The associated experimental data is used for the validation of the current LES-TPDF model under both non-reacting spray and reacting spray conditions. A series of methanol-air equivalence ratios are selected to investigate the ignition process. The main purpose of this work is to elucidate the effects of ambient methanol concentration on the ignition process of an n-heptane spray under conditions relevant to RCCI engines.

2. Methodology

2.1. Eulerian-Lagrangian approach

In order to describe the two-phase flow in the spray combustion, the Lagrangian particle tracking approach is applied. In the LES framework, the gas phase is governed by spatially filtered Navier-Stokes equations, while the Lagrangian liquid phase is described and tracked using a large number of parcels. The interaction between the gas and liquid phases is considered via the source terms in the mass conservation, momentum, species and energy transport equations. Details of the LES spray model are referred to Ref. [31, 32]. A one-equation SGS kinetic energy model (k-equation model) is used to model the SGS viscosity. The ambient methanol-air mixture is assumed to be in a quiescent gas phase, following the previous LES [8, 14, 15] studies. The n-heptane fuel is injected as liquid droplets, with the initial droplet size following the Rosin-Rammler distribution. The mean diameter of droplets is set as half the injector nozzle diameter, $d_n/2$. The maximum size is set to the diameter of the injector nozzle, d_n, where $d_n = 0.1mm$. The evaporation rate is modelled using the Spalding formula [33]. The Ranz-Marshall correlation [34, 35] is used to model the heat transfer between the liquid and gas phases. The current numerical configurations are validated using experimental data from the ECN [13]. This will be discussed in Section 3.3.

A finite-rate chemistry is considered in the present study. Several n-heptane mechanisms [36–39] are evaluated for modeling of the ignition process of n-heptane/methanol-air mixture under a range of equivalence ratios, temperatures, and pressure conditions relevant to the present dual-fuel combustion cases. The n-heptane mechanism of Lu *et al.* (hereinafter denoted as Lu-68) with 68 species and 283 reactions [36] has shown the best trade-off between computational efficiency

and model accuracy in terms of the prediction of IDT. In addition, this mechanism has been applied in both ECN spray cases [16] and the direct numerical simulation (DNS) study of n-heptane/methanol dual-fuel combustion [40]. To speed up the integration of the chemical reaction rates, a chemistry coordinate mapping (CCM) method is employed. In the CCM approach, the integration of the stiff chemical reaction rates is performed in a low-dimensional chemical phase space, and the results are mapped back to the mesh points in the physical space. In the present study, the phase space coordinates include the mixture fraction, temperature, scalar dissipation rate, and the mass fraction of n-heptane. This approach can speed up the time-consuming integration of the chemical reaction rates by a factor of 10 [41]. However, the species transportation cannot be accelerated. Therefore, an overall 2 to 5 times reduction of the clock time is achieved [41, 42] . Details of the CCM method and its application to the simulation of spray combustion can be found in Refs. [32, 41–43].

The OpenFOAM code [44] is used in this study. The solver is based on the finite volume method. The second order backward Euler scheme is applied for the temporal integration and the second order normalised variable diagram (NVD) scheme named Gamma [45] is used for the convective fluxes discretization.

2.2. Eulerian stochastic field method

As aforementioned in the introduction, the TCI effects are important particularly in cases with long ignition delay times. To accommodate the TCI in spray combustion, a ESF-based TPDF approach is employed [46]. In this method, the one-point one-time joint PDF is expressed as an ensemble of a series of stochastic

fields, where the PDF is written as,

$$P\left(\psi;\mathbf{x},t\right)=\frac{1}{N_F}\sum_{n=1}^{N_F}\prod_{\alpha=1}^{N_s}\delta(\psi_\alpha-\xi_\alpha^n) \tag{1}$$

Here, δ represents the Dirac delta function, while N_F and N_s are the number of stochastic fields and the number of scalars, respectively. The scalars include the mass fractions of species and the enthalpy. ξ_α^n denotes the α-th scalar in the n-th stochastic field.

The ESF equation in its discrete form is given in Eq. (2), describing the evolution of each stochastic field,

$$\begin{aligned}\overline{\rho}d\xi_\alpha^n=&-\overline{\rho}\tilde{\mathbf{U}}\nabla\xi_\alpha^n dt+\nabla\left(\Gamma_t\nabla\xi_\alpha^n\right)dt+\overline{\rho}\sqrt{2\frac{\Gamma_t}{\overline{\rho}}}\nabla\xi_\alpha^n d\mathbf{W}^n\\&-\frac{\overline{\rho}C_\phi}{2\tau_{sgs}}(\xi_\alpha^n-\tilde{\phi}_\alpha)dt+\overline{\rho}\dot{\omega}_\alpha(\underline{\xi}^n)dt.\end{aligned} \tag{2}$$

Here, $d\mathbf{W}^n$ represents the increment of a vector Wiener process to take the random process into consideration, which is spatially uniform but varying in different fields. Γ_t denotes the total diffusion coefficient, accounting for both the laminar and SGS diffusion. In addition, $\tilde{\phi}_\alpha$ represents the mean scalar field, τ_{sgs} is the SGS mixing time scale, and $C_\phi=2$ is a model constant for micro-mixing. The same model constants as in Ref. [30] are used, where more details about these constants can be found. The number of stochastic fields is set to 12, following the suggestion of a previous study [47].

2.3. Case set-up

Table 2: Setup of the computational cases.

	Single-fuel		Dual-fuel	
	Case A	Case B	Case C	Case D
T [K]	1000	900	900	900
O_2 [vol. %]	0	0.21	0.21	0.21
ϕ_m [-]	0	0	0.1	0.3

Table 2 shows the four computational cases in this study. Cases A and B are the single-fuel cases, which have been studied in the ECN Spray-H experiments [13]. They are selected for validations of the current LES models under non-reacting (Case A) and reacting spray (Case B) conditions, respectively. The validation of the non-reacting spray is only performed at an ambient temperature of 1000 K due to the absence of experimental data at lower ambient temperatures. Effects of ambient methanol concentration on pilot fuel ignition characteristics are subsequently investigated in Cases B, C and D at the ambient temperature of 900 K. The ambient temperature of 900 K is selected since the associated interaction between methanol and n-heptane is stronger than that at higher ambient temperatures. The ignition delay of the methanol at 1000 K condition is comparable to that of n-heptane [40]. Methanol fueled dual-fuel engine at such a high temperature is less dependent on the ignition assistance of n-heptane. Case B serves as the model validation case and the baseline reference condition for the evaluation of the effects of the ambient mixture equivalence ratio on the dual-fuel combustion process. Cases C and D are the dual-fuel cases, with different methanol concentration in the ambient

mixture. In the dual-fuel configuration, the liquid n-heptane is used to mimic the pilot diesel fuel in the RCCI engines. The ambient methanol concentration is parameterized using equivalence ratios (ϕ_m), which is defined as the ratio of the actual methanol-"air" ratio to the stoichiometric methanol-"air" ratio. It is worth mentioning that the "air" is not the atmosphere air but resembles those of the ECN experiment to mimic the in-cylinder mixture of engines. The "air" density is set to 14.8 kg/m^3, while mole concentrations of O_2, N_2, CO_2 and H_2O are set to 21%, 69.33%, 6.11% and 3.56%, respectively [13]. The gaseous methanol is mixed with "air" to form a homogeneous and quiescent primary fuel-air mixture before the n-heptane injection, following the previous LES works [8, 14, 15, 48, 49]. According to the ideal gas equation of state, the pressure is calculated from the gas density, ambient temperature and the mixture average molar mass. Details of the ambient mixture initial conditions can be found in Table 3. As shown, ϕ_m of 0.1 and 0.3 are investigated in the current LES. The ϕ_m of 0.3 is chosen based on the engine conditions defined in Ref. [50]. It is an averaged global equivalence ratio under the medium-load condition of the diesel/methanol RCCI engine. On the other hand, the selection of ϕ_m of 0.1 is based on the experiment in Ref. [10]. It is found in Ref. [10] that under very lean condition, the associated low amount of ambient methanol concentration is sufficient to retard the ignition delay of the pilot fuel. In practice, the equivalence ratio distribution is not perfectly homogeneous in the engines [9]. There may exist local lean mixture even at the high-load engine conditions. It is important to know how the ignition and combustion processes evolve when the pilot fuel is injected into these very lean mixture.

Table 3: Initial conditions of the ambient mixture.

Case	Density	Pressure	Ambient methanol/air mass fraction composition				
	[kg/m^3]	[MPa]	CH_3OH	O_2	N_2	CO_2	H_2O
A	14.8	4.2906	0	0	0.8763	0.1001	0.0237
B	14.8	3.7577	0	0.2280	0.6590	0.0913	0.0218
C	14.8	3.7532	0.0150	0.2246[1]	0.6491	0.0899	0.0214
D	14.8	3.7445	0.0437	0.2180[1]	0.6302	0.0873	0.0208

[1] The ambient oxidizer gas in Cases C and D is a mixture of "air" and gaseous methanol. The addition of methanol reduces the oxygen mass fraction.

In all four cases, liquid n-heptane is delivered into a constant volume chamber at an injection pressure of 150 MPa. It undergoes break up, evaporation and mixing with ambient mixture. The chamber configuration is the same as that in the ECN Spray-H experiments, which is a cube with a side length of 108 mm. The injection duration of n-heptane is 6.6 ms with a total mass of 17.5 mg, the injection mass flow rate is calculated using an injection model described in Ref. [51]. A locally refined grid system is used, with the finest cell size of 250 μm. The maximum Courant–Friedrichs–Lewy number adopted in the simulation is 0.1, which gives a typical time step of the temporal integration of 50 ns. The present grid resolution is similar to the majority of the recent LES studies [16, 17, 19, 21, 26], cf. Table 1. In particular, the LES-ESF study performed by Gallot-Lavallée *et al.* using a mesh size of 500 μm showed a fairly good prediction of IDT and flame lift-off length (LOL) [18]. The LES studies of Kahila *et al.* [8] used a finer mesh (with a mesh size of 160, 80 and 62.5 μm) due to the absence of a TCI model. A mesh sensitive analysis (125, 250 and 500 μm grid) is performed on both non-reacting

and reacting spray to show the capability of the current grid resolution and time step in predicting the spray, ignition and flame stabilization. As will be shown later, the present grid and time step show an adequate resolution of the spray, evaporation and flame dynamics. The computational cost varies from case to case due to the difference in physical end times. Since the IDT varies in these cases, the physical end times in Cases B, C and D are 1.5, 2.5 and 3.0 ms, respectively. For the readers' reference, the clock time for Case B, which is performed to 1.5 ms in a 250 μm grid, are approximately 28 days with the use of 144 processors (approximately 100,000 CPU hours).

3. Results and discussion

3.1. The performance of the chemical mechanism

An evaluation of the methanol sub-mechanism in the current Lu-68 n-heptane mechanism is conducted to investigate the accuracy of this mechanism in the prediction of the ignition process in the ambient methanol/air mixture. Figure 1 shows the IDTs of stoichiometric and lean methanol/air mixture (equivalence ratio of 0.5) predicted by the Lu-68 mechanism and two detailed methanol mechanisms, as well as the corresponding high-pressure shock-tube measurements at National University of Ireland (NUI) Galway [52]. The initial pressure is chosen as 50 bar, which is similar in the current spray flame cases. The two detailed methanol mechanisms considered are the Aramco 2.0 mechanism [53] and the Konnov mechanism [54]. It is shown that the IDTs predicted using the Lu-68 mechanism are comparable to those calculated using the detailed mechanisms and the shock tube measurement.

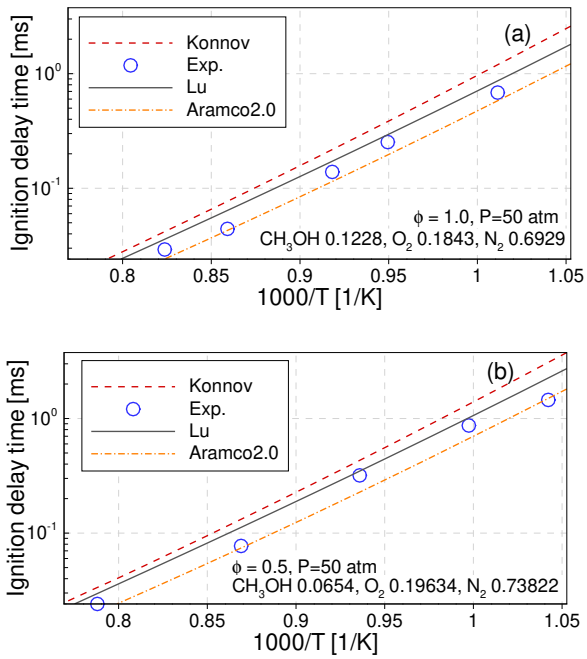

Figure 1: IDT predicted using different mechanisms for (a) stoichiometric and (b) lean methanol/air mixture with equivalence ratio of 0.5 at a pressure of 50 bar across different initial temperatures. The symbols represent the high-pressure shock-tube experimental data from National University of Ireland (NUI) Galway [52].

3.2. Mesh sensitivity analysis

Figure 2 shows the evolution of the liquid penetration length (LPL) and the vapor penetration length (VPL) calculated using three different mesh resolutions. The LPL is defined as the distance from the injector nozzle to the downstream position where the liquid fuel mass within this region accounts for 95% of the liquid mass in the domain. The VPL is defined as the maximum distance from the nozzle outlet to the location with the fuel mass fraction reaching 0.1% [13]. The horizontal axis represents the time after the start of injection (ASI), whereas the vertical axis shows the liquid and the vapor penetration lengths. As shown, the LES results using the finer mesh resolutions of 250 and 125 μm agree with each

other, while those using 500 µm diverge.

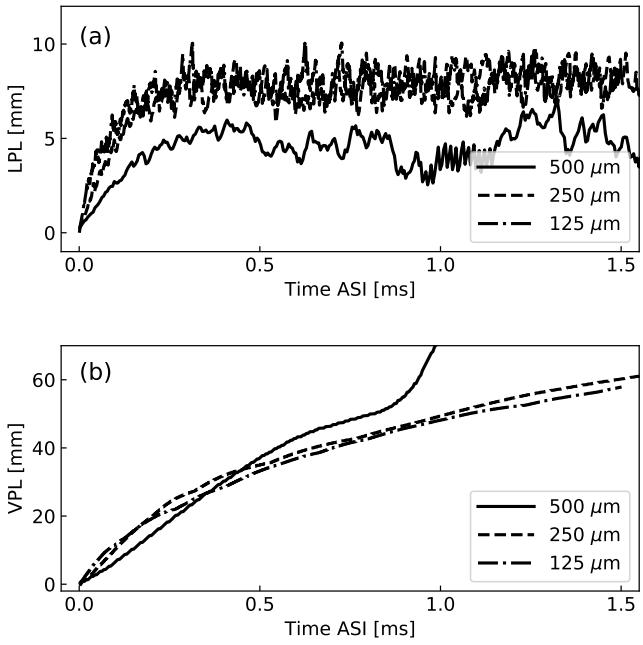

Figure 2: Temporal evolution of (a) the liquid penetration length (LPL), and (b) the vapor penetration length (VPL) predicted in LES with mesh resolutions of 125, 250 and 500 µm.

Figure 3 shows the evolution of the pressure rise and the flame LOL of the reacting spray using these three different mesh resolutions. The LOL is defined as the distance from the fuel nozzle to the farthest location where Favre-average OH mass fraction reaches 2% of its maximum in the domain after a quasi-steady flame is established. As seen in Figure 3a, the mean pressure rise profiles are found to be relatively insensitive to the mesh resolution. Figure 3b depicts that the LOL predicted using the 500 µm mesh is lower while those predicted using both the 250 µm and 125 µm resolutions agree with each other. Therefore, the 250 µm mesh, which provides reasonable accuracy in prediction of non-reacting

and reacting sprays at an affordable computational cost, is chosen for the following LES.

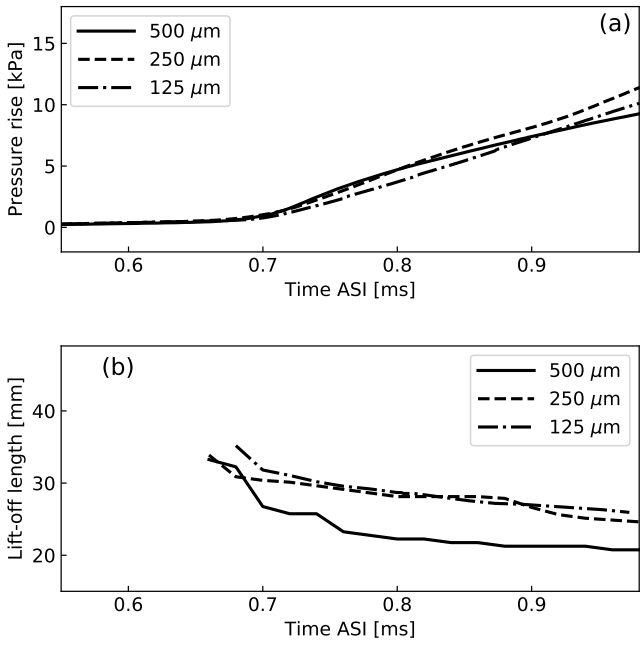

Figure 3: (a) The LES predicted pressure rise, and (b) the flame lift-off length (LOL) using mesh resolutions of 125, 250 and 500 μm.

3.3. Validation of the LES spray combustion model

Figure 4a shows the LPL and VPL in the non-reacting case (Case A) from the present LES and the corresponding ECN Spray-H experiments, under the 1000 K and oxygen-free condition. The experimental data were obtained using Schlieren imaging and Mie-scattering [13]. Figure 4b shows the spatial distribution of the mean mixture fraction in the LES and experiment. The error bar indicates the uncertainty of the experimental data obtained from the Rayleigh scattering [13]. The current LES model setup and grid resolution yield in good agreement with

the measurements.

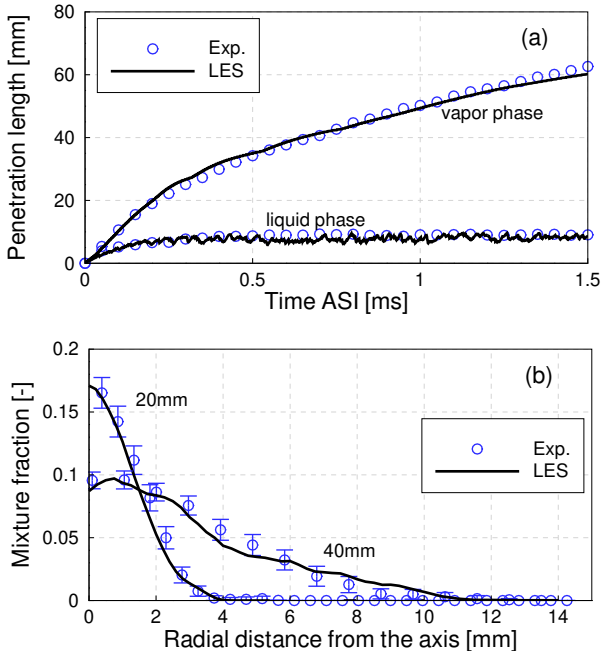

Figure 4: Comparisons of LES and experimental (a) liquid and vapor penetration lengths, and (b) mean mixture fraction at two axial positions (20 mm and 40 mm) downstream the nozzle in the non-reacting spray case. The mean mixture profiles in (b) are time averaged and ensemble averaged for the LES and experimental results, respectively.

The simulated IDT and LOL of the reacting spray case (Case B) are next validated using the experimental measurements. The IDT is defined based on the time at which the maximal time derivative of temperature is reached, following the ECN suggestion [13]. The IDT and LOL predicted in the current LES are 0.80 ms and 25 mm, respectively. These agree with the experimental IDT of 0.79 ms and LOL of 25.5 mm [13] reasonably well, where the relative differences remain below 2%. Moreover, the LES replicates the experimental pressure profile (shown in the next section). In summary, the present LES spray combustion model is capable of

simulating the spray vaporization and vapor mixing processes, the ignition timing and the flame stabilization. In the following, the LES model is applied to predict and analyze the spray combustion process for both the single- and dual-fuel cases.

3.4. Effects of ambient methanol on pressure rise and heat-release rate

Figure 5 shows the temporal evolution of pressure rise (the difference between the chamber pressure and its initial pressure) and net HRR, which is the heat release rate term integrated over the entire chamber, for Cases B, C, and D (with ambient methanol equivalence ratio varying from 0 to 0.3). Before the onset of ignition, the chamber pressure decreases due to the endothermic evaporation process during the n-heptane injection. This is followed by a pressure rise along side with a noticeable HRR, indicating the onset of ignition. Both the initial HRR and the pressure-rise rate are rather low; this stage of ignition is known as the first-stage ignition or the low temperature ignition. Thereafter, around 0.6 ms ASI, HRR increases rapidly to a substantially high value, along with a rapid increase of chamber pressure. The start of the high HRR indicates the onset of second-stage ignition, also known as the high temperature ignition stage. This two-stage ignition process is observed for the n-heptane fuel, while pure methanol ignition undergoes only the high temperature stage [12]. As shown in the inset of Fig. 5, where the first-stage HRR is displayed, the onset of first-stage ignition is retarded in the dual-fuel cases ($\phi_m = 0.1$ and $\phi_m = 0.3$). This is consistent with the observation in methane-based dual-fuel experiments [11] and LES [8] studies. Moreover, the higher methanol-air equivalence ratio in the ambient mixture, the longer retardation time of the first-stage ignition, and the lower the peak HRR from the first-stage ignition. Furthermore, the ambient methanol also retards the second-stage ignition, evident by the time difference between the second-stage

ignition and the first-stage ignition, which increases with the increase of ϕ_m in the ambient mixture.

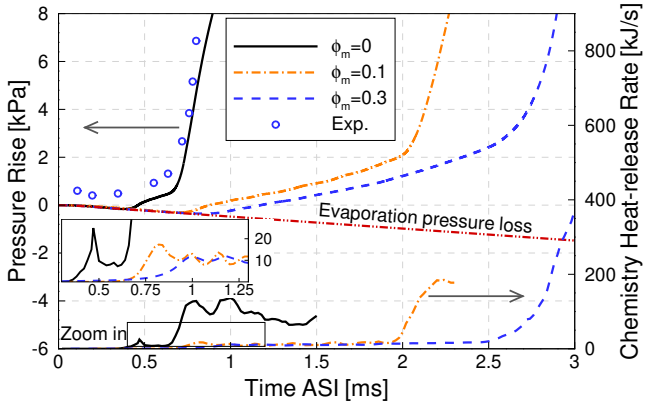

Figure 5: Effects of ambient methanol concentration on pressure rise and total heat-release rate for Cases B, C, and D. The experimental pressure rise is shown using symbols.

Figure 6 shows the evolution of the maximum chemistry HRR in the computational domain for Cases B, C and D. A semi-logarithmic coordinates is used to demonstrate the two-stage heat releases and the weak heat release before the first-stage ignition. The two-stage heat releases are clearly demonstrated by the two plateaus in the figure. It is found that the single-fuel case has the highest maximum chemistry HRR in the first-stage heat release, which is consistent with the observation in Fig. 5. On the contrary, the maximum chemistry HRR of the single-fuel case is the lowest in the second-stage heat release. It is also found that the dual-fuel Cases C ($\phi_m = 0.1$) and D ($\phi_m = 0.3$) have a higher heat release before 0.15 ms ASI, shown in the inset of Fig. 6.

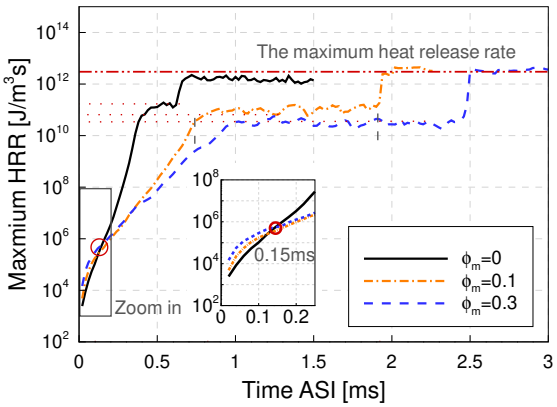

Figure 6: The maximum chemistry heat-release rate in the domain for the reacting Cases B, C, and D.

3.5. Effects of ambient methanol concentration on the ignition process

In order to track the ignition event, the most reactive local mixture is defined. The HRR of the local mixture (in each computational cell) is compared and the one with the highest HRR is defined as the most reactive local mixture. The spatial location of the most reactive local mixture changes with time. The most reactive local mixture is tracked in order to investigate how it evolves and where it is located. The temporal evolution of heptyl-peroxide (RO_2) and OH mass fractions in the most reactive local mixture is shown in Figure 7. To illustrate the wide range, mass fractions in vertical coordinates are shown in log-scale. RO_2 has been recommended by ECN [13] as the indicator of the first-stage ignition: the first-stage IDT is suggested to be at the time of RO_2 mass fraction reaching 20% of its maximum, denoted as τ_1 in Fig. 7a with the vertical dashed lines. On the other hand, OH is used as the indicator for the second-stage ignition , denoted as τ_2 in Fig. 7b. It is seen that the mass fractions of RO_2 and OH of the most reactive mixture increases (approximately) exponentially with time (ASI) until it reaches a

plateau shortly after τ_1, and the mass fraction of OH reaches a second plateau after τ_2. In the second-stage ignition, the maximum OH mass fraction is independent of ϕ_m, while during the transition period from the first-stage ignition to the second-stage ignition, OH mass fraction decreases with ϕ_m in the ambient mixture. The transition time from the onset of first-stage ignition to the second-stage ignition is 0.45 ms, 1.23 ms and 1.74 ms for Cases B, C, and D, respectively, showing an increasing retardation effect of methanol on the n-heptane ignition process with ϕ_m. Similar retardation effect was reported for n-dodecane/methane-air dual-fuel combustion [11].

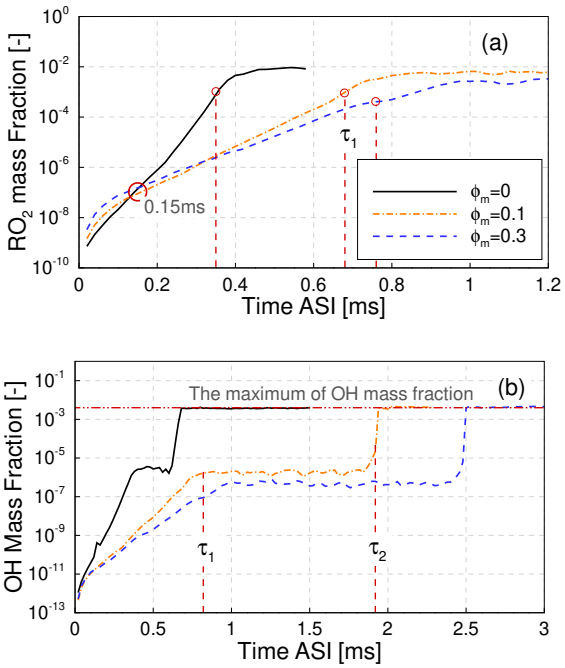

Figure 7: Temporal evolution of mass fraction of RO_2, Y_{RO_2} (a), and OH, Y_{OH} (b), in the most reactive local mixture for Cases B, C, and D (with ϕ_m varying from 0 to 0.3), respectively. The vertical dashed lines indicate the time of first-stage ignition (τ_1, a) and the first- and second-stage ignition (τ_1 and τ_2, b). The two plateaus in the OH profiles indicate the transition period from the onset of the first-stage ignition to the onset of the second-stage ignition, and the period after the onset of the second-stage ignition.

The maximal mass fraction of RO_2 in the most reactive mixture is higher initially (before 0.15 ms ASI) in the cases with higher methanol concentration in the ambient mixture. This indicates that the ambient methanol enhances the production of RO_2. However, shortly after 0.15 ms ASI, the suppression effect of methanol on RO_2 is evident. The underlying mechanism behind this will be investigated in Section 3.7.

3.6. *Effects of methanol on the structure of the spray flame*

In a three-dimensional n-heptane/methanol dual-fuel spray flame, during the liquid n-heptane injection, the oxidation reactions in the methanol-air mixture take place, but not to the critical point of auto-ignition. This period of time is referred to as the ignition induction time. This implies that in the present n-heptane/methanol dual-fuel combustion process, the effects of methanol chemistry on the n-heptane ignition is different at different spatial locations of the spray jet due to the discrepancy in the induction time.

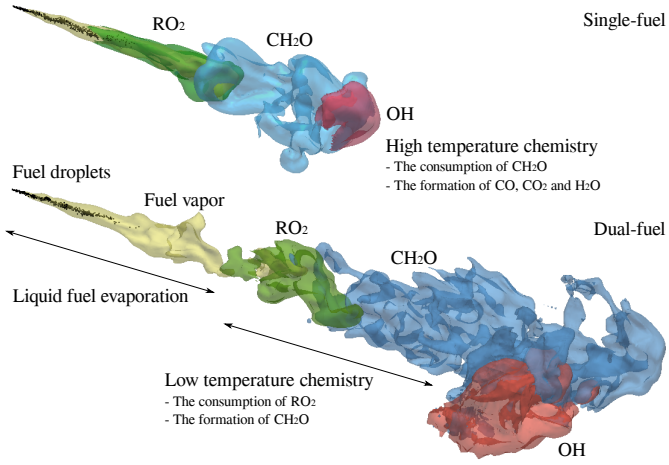

Figure 8: Three-dimensional flame structure at the instance of second-stage ignition for the single-fuel Case B (upper) and dual-fuel Case D (bottom). Black dots indicate the fuel droplets.

Figure 8 shows the three-dimensional flame structure of single-fuel (Case B) and dual-fuel combustion (Case D) at the instance of second-stage ignition. The n-heptane is delivered as liquid fuel. The liquid n-heptane droplets then break up and evaporate to fuel vapor in the immediate downstream of the fuel jet. The intermediate species, such as RO_2 and CH_2O, are produced in the low-temperature ignition region. The high-temperature ignition takes place further downstream of

the spray, where the intermediate species are oxidized to CO_2 and H_2O with the participation of radicals such as OH.

The fuel vapor is enveloped by the RO_2 in the single-fuel case, while the RO_2 region in the dual-fuel case is in the downstream of the fuel vapor region. The ambient methanol/air mixture retards the onset of the first-stage ignition, affects the cool flame structure, and postpones the onset of second-stage ignition kernel further downstream. The postponed high temperature ignition extends the mixing time before the start of high-temperature combustion, reducing the high-temperature and rich-fuel regions which are favorable for soot formation. This result is consistent with the soot reduction in dual-fuel engines reported in the literature [3, 55, 56].

To investigate the first-stage ignition kernel structure of the present spray flames in more detail, the spatial and temporal distributions of RO_2, HO_2, CH_2OH, and OH mass fractions before the onset of the first-stage ignition in a cross plane along the spray axis, are plotted in Fig. 9. The mass fractions are normalized by its maximal value in the domain for the given case at the given instance of times.

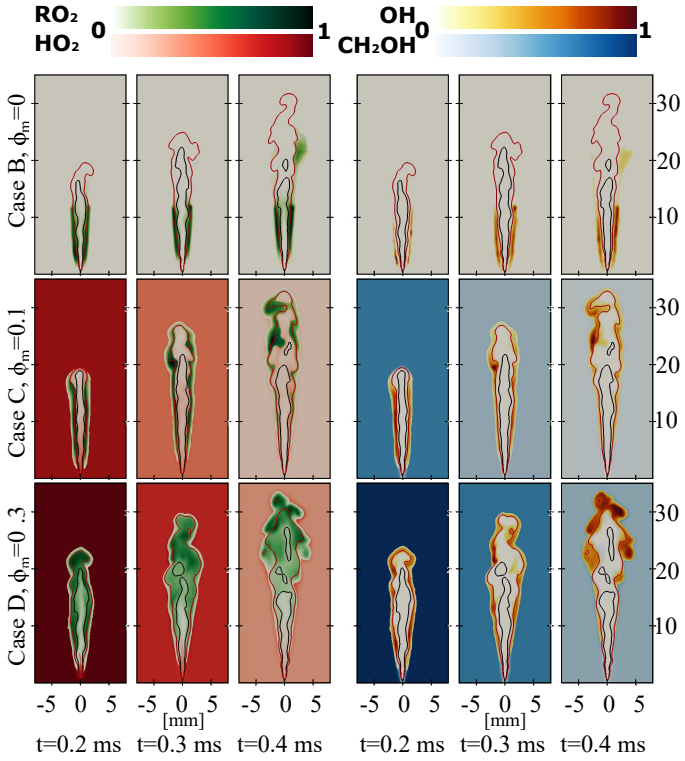

Figure 9: Distributions of RO_2 and HO_2 (left hand side), OH and CH_2OH (right hand side) prior to the onset of first-stage ignition in a cross section along the spray axis. The red line denotes the iso-line of stoichiometric mixture fraction, and the black line is the iso-line of temperature of 700 K.

For Case B ($\phi_m = 0$), the formation of RO_2 starts in the upstream region of the spray jet, around the iso-surface of the stoichiometric mixture fraction. As time goes on, the fuel vapor continues to penetrate downstream but most of the RO_2 still concentrates upstream, until a new reactive region appearing at 0.4 ms downstream around stoichiometric contour line. At this stage, $t \leq 0.4$ ms, the concentration of HO_2 is rather low. CH_2OH is negligible in Case B.

In contrast, the flame structure in the dual-fuel cases is significantly different. Due to the presence of methanol in the ambient gas, oxidation reactions take place

in the ambient mixture, giving rise to the formation of HO_2 and CH_2OH. This affects the formation of RO_2 and OH radicals. In Case C, with the methanol-air equivalence ratio of $\phi_m = 0.1$, the RO_2 is formed not only in the near nozzle region but also downstream, around the iso-surface of the stoichiometric mixture fraction. In Case D, with a higher methanol-air equivalence ratio of $\phi_m = 0.3$, the RO_2 fills up the entire fuel-rich region of the jet.

As a key species generated in the methanol oxidation reactions, HO_2 is essential for n-heptane ignition since it participates in the reaction forming heptyl radicals, $C_7H_{16} + HO_2 = C_7H_{15} + H_2O_2$, which leads further to the formation of RO_2. This explains the enhanced formation of RO_2 in the cool flame downstream region of spray jet, and the elevated mass fraction of RO_2 in the early first-stage ignition, i.e., $t < 0.15$ ms, Fig. 7a. However, as shown in Fig. 7b, the presence of methanol in the ambient gas has, in general, a suppression effect on the ignition of n-heptane, due to the non-linear interaction among the different elementary reactions involved. This will be next examined using the reaction pathways.

3.7. Analysis of the dual-fuel reaction pathways

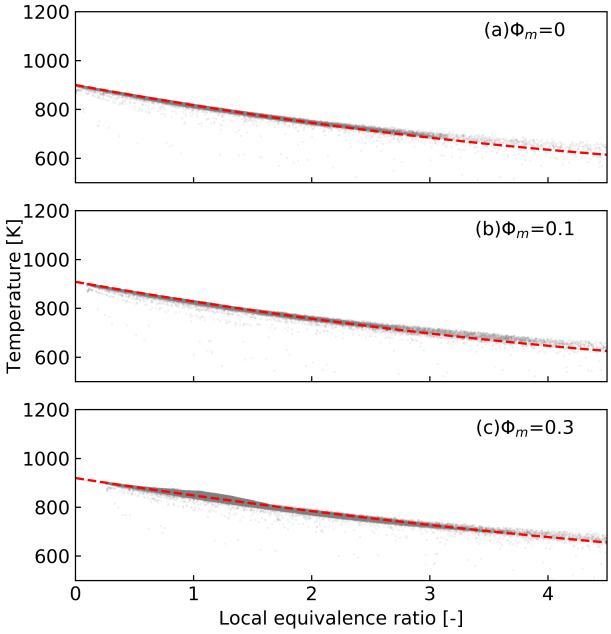

Figure 10: The scatter plot of all the LES cells in $\phi - T$ diagram before the first-stage ignition, and mixing lines for the case with ϕ_m of (a) 0, (b) 0.1 and (c) 0.3.

Figure 10 shows the $\phi - T$ diagram for the reacting Cases B, C and D before the first-stage ignition. The local equivalence ratio, ϕ, is defined as suggested in Ref. [57]. All of the computational cells are shown as gray dots. The dashed line is a fitting curve for the gray dots using the least squares method. As seen in Fig. 5, chemical heat release is absent before the first-stage ignition for both single- and dual-fuel cases. Therefore, no obvious temperature rise is found in Figure 10. Due to liquid n-heptane evaporation and mixing, the local temperature decreases with the increase of the local equivalence ratio. All of the LES cells collapse into a line, which is the mixing line for the n-heptane and methanol/air mixture.

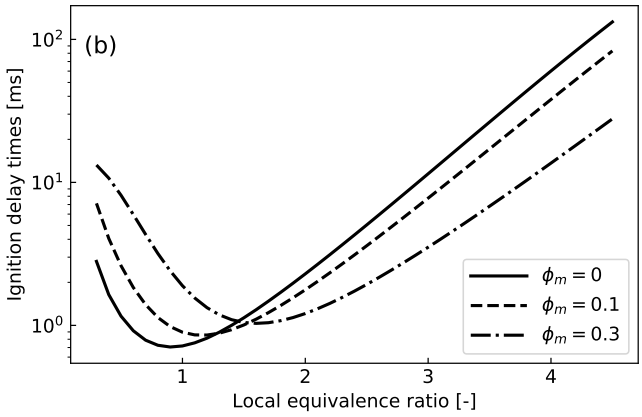

Figure 11: The ignition delay times of the n-heptane/methanol-air mixture in zero-dimensional homogeneous reactor simulations. The solid, dashed and dot-dashed lines denote initial methanol equivalence ratio ϕ_m of 0, 0.1 and 0.3, respectively.

Zero-dimensional homogeneous reactor simulations are conducted along the mixing line to explain the effects of methanol on the ignition of n-heptane. Figure 11 shows the high temperature IDTs of the n-heptane/methanol-air mixture at different local equivalence ratios. Each equivalence ratio represents a thermophysical state in the LES. The initial composition and temperature of the zero-dimensional simulations are extracted from the mixing line in Fig. 10. For all of the ϕ_m, IDT first decreases and then increases with the increase of the local equivalence ratio. The shortest IDT locates at near-stoichiometric mixture for single fuel cases ($\phi_m = 0$). It is shifted to the rich region in the $\phi_m = 0.1$ and $\phi_m = 0.3$ cases. In addition, it is found that the shortest IDT increases with the increase of the ϕ_m. This implies that a high methanol concentration delays the n-heptane high temperature ignition, which is consistent with the observation in the LES.

Table 4: The IDTs of the zero- and three-dimensional cases.

ϕ_m [-]	zero-dimensional		three-dimensional	
	τ_1	τ_2	τ_1	τ_2
0	0.22	0.61	0.35	0.80
0.1	0.23	1.18	0.68	1.91
0.3	0.30	1.59	0.76	2.50

Furthermore, three zero-dimensional cases are further investigated according to the composition of the stoichiometric mixture in the spray Cases B, C and D. The IDTs of the zero- and three-dimensional cases are shown in Table 4. The rates of reactions are compared to identify the relative importance of OH and HO_2 consumption rates in different reactions. A conversion ratio of species i in reaction j (β_{ij}) is defined as, $\beta_{ij} = I_{ij}/I_i$, where i represents either OH or HO_2. I_{ij} is the integration of the consumption rate of species i in reaction j, within the induction time before the onset of the second-stage ignition. I_i is the sum of I_{ij} over all reactions. The conversion ratios for OH and HO_2 in key reactions are listed in Table 5.

Table 5: Conversion ratios of OH and HO_2 in key reactions.

Key reactions \ ϕ_m [-]	0	0.1	0.3
$CH_3OH + OH = CH_2OH + H_2O$ (R1)	0	9.45%	32.28%
$CH_2O + OH = HCO + H_2O$ (R3)	40.01%	39.13%	38.02%
$C_7H_{16} + HO_2 = C_7H_{15} + H_2O_2$ (R4)	2.10%	2.64%	2.96%
$C_7H_{16} + OH = C_7H_{15} + H_2O$ (R5)	16.16%	11.71%	6.71%

The ambient methanol contributes to the consumption of OH through CH_3OH + OH = CH_2OH + H_2O reaction (denoted as R1). As seen in Table 5, the percentage of OH consumption in reaction R1 increases with the increase of the ambient methanol-air equivalence ratio, ϕ_m. About 32% of OH is consumed by CH_3OH in R1 in the $\phi_m = 0.3$ case. This reduces the OH accumulation rate, prolonging the first-stage ignition delay times, τ_1. Meanwhile, the intermediate product, CH_2OH, is formed in the ambient methanol-air mixture. The oxidation of CH_2OH, in reaction $CH_2OH + O_2 = CH_2O + HO_2$ (denoted as R2), generates HO_2. Even though HO_2 will be converted to H_2O_2 and supply OH through reaction $H_2O_2 + M = OH + OH + M$, this reaction has a high activation energy, thus, the formation of OH from methanol-air mixture is limited before the temperature increases up to 1000 K [12]. OH is therefore consumed by reacting with methanol via R1 (but cannot be replenished) in the low temperature ignition stage. As such, the maximum OH mass fraction in the dual-fuel spray cases is lower than that in the single-fuel case during the transition induction period, $\tau_1 < t < \tau_2$. Thereafter, the high temperature reaction condition is met, OH is consumed in a series of high temperature reactions. One of the important reactions is the oxidation of formaldehyde (CH_2O), $CH_2O + OH = HCO + H_2O$ (denoted as R3). The existence of CH_3OH has a rather minor effect on the OH consumption in R3, as shown in Table 5. This explains the nearly constant maximal value of OH mass fractions for different ambient methanol concentrations after the onset of second ignition, $t > \tau_2$, as illustrated earlier in Fig. 7b.

The formation of HO_2 from the ambient methanol in reaction R2 contributes to the consumption of C_7H_{16} through the reaction $C_7H_{16} + HO_2 = C_7H_{15} + H_2O_2$ (denoted as R4). This leads to the elevated production of RO_2 during the early

stages of the first-stage ignition, shown in Fig. 7a, and the change of the cool flame structure in Fig. 9. On the other hand, the reaction C_7H_{16} + OH = C_7H_{15} + H_2O (denoted as R5) slows down, with the OH conversion ratio decreasing from 16% ($\phi_m = 0$) to 7% ($\phi_m = 0.3$). The suppression of reaction R5 by the ambient methanol is the reason for the retardation of the first-stage ignition and the transition from τ_1 to τ_2, shown in Fig. 7.

4. Conclusion

LES with a TPDF model is performed to investigate the effects of the ambient methanol-air equivalence ratio (ϕ_m from 0 to 0.3) on the n-heptane spray combustion under RCCI engine-like conditions. The baseline case is chosen from ECN n-heptane spray experiments. The LES models are validated using the associated experimental data. A good agreement between the LES prediction and the ECN experiments, in terms of the liquid length, vapor penetration length, mixture fraction, ignition delay time and lift-off length, is achieved. The dual-fuel combustion results generated using the LES-TPDF model are analyzed to elucidate the effects of methanol chemistry on the ignition of the n-heptane spray. The following conclusions are drawn.

(1) The ambient methanol has a general effect of suppressing the ignition of n-heptane. Both the first-stage and second-stage ignitions of n-heptane are retarded by the ambient methanol. A longer transition time between the first- and second-stage ignitions, as well as a lower first local peak value of the heat release rate are observed when the ambient methanol concentration (i.e. ϕ_m) increases. The reason behind the suppression of ignition is that the concentration of radicals (e.g. OH) is reduced by reaction with ambient methanol, i.e., through elementary

reaction $CH_3OH + OH = CH_2OH + H_2O$. The associated OH consumption rate increases with the increase of ϕ_m.

(2) In the earlier induction period before the onset of first-stage ignition, the ambient methanol has an effect of enhancing the formation of heptyl-peroxide (RO_2) that has been considered as the indicator of the first-stage ignition. Chemical pathway analysis shows that HO_2 generated in the ambient methanol promotes the formation heptyl radicals, via $C_7H_{16} + HO_2 = C_7H_{15} + H_2O_2$, this subsequently enhancing the formation of RO_2. However, the consumption of OH through reaction $CH_3OH + OH = CH_2OH + H_2O$ suppresses the reaction $C_7H_{16} + OH = C_7H_{15} + H_2O$, which eventually retards the onset of both the first-stage and the second-stage ignition of n-heptane.

(3) Under the lean ambient mixture conditions studied in the present work, the ambient methanol affects the n-heptane spray flame structures in both the ignition stage and in the steady spray flame stage. In the single-fuel methanol-free case, the low temperature ignition and cool flame indicator, RO_2, is shown to distribute around the stoichiometric mixture in the proxmity of the fuel nozzle, with the cool flame enveloping the fuel rich region. In the dual-fuel cases, RO_2 is found in the entire fuel-rich region further downstream. The onset of second-stage ignition kernel is postponed at further downstream, this resulting a longer liftoff length in the methanol/n-heptane dual-fuel cases than that of single fuel n-heptane spray flame. The postponed ignition and the longer liftoff length extend the mixing time before the start of high-temperature combustion, this reducing the high-temperature and rich-fuel regions in the dual-fuel cases This explains the reduced soot emission in dual-fuel engines reported in the literature.

Acknowledgments

This work is sponsored by Swedish Research Council (VR), and Swedish Energy Agency through KC-CECOST. Shijie Xu and Shenghui Zhong are sponsored by China Scholarship Council. We thank Rui Li for the assistance on chemical analysis. The simulations are performed on resources provided by the Swedish National Infrastructure for Computing (SNIC) at HPC2N and PDC.

References

[1] Y. Li, M. Jia, Y. Liu, M. Xie, Numerical study on the combustion and emission characteristics of a methanol/diesel reactivity controlled compression ignition (RCCI) engine, Applied energy 106 (2013) 184–197.

[2] B. Ma, A. Yao, C. Yao, T. Wu, B. Wang, J. Gao, C. Chen, Exergy loss analysis on diesel methanol dual fuel engine under different operating parameters, Applied Energy 261 (2020) 114483.

[3] D. Splitter, R. Hanson, S. Kokjohn, R. D. Reitz, Reactivity controlled compression ignition (RCCI) heavy-duty engine operation at mid-and high-loads with conventional and alternative fuels, Tech. Rep., SAE Technical Paper, 2011.

[4] X. Kan, L. Wei, X. Li, H. Li, D. Zhou, W. Yang, C.-H. Wang, Effects of the three dual-fuel strategies on performance and emissions of a biodiesel engine, Applied Energy 262 (2020) 114542.

[5] D. Zhou, W. Yang, H. An, J. Li, Application of CFD-chemical kinetics ap-

proach in detecting RCCI engine knocking fuelled with biodiesel/methanol, Applied Energy 145 (2015) 255–264.

[6] J. Liu, F. Yang, H. Wang, M. Ouyang, S. Hao, Effects of pilot fuel quantity on the emissions characteristics of a CNG/diesel dual fuel engine with optimized pilot injection timing, Applied Energy 110 (2013) 201–206.

[7] K. Ryu, Effects of pilot injection timing on the combustion and emissions characteristics in a diesel engine using biodiesel–CNG dual fuel, Applied Energy 111 (2013) 721–730.

[8] H. Kahila, A. Wehrfritz, O. Kaario, V. Vuorinen, Large-eddy simulation of dual-fuel ignition: Diesel spray injection into a lean methane-air mixture, Combustion and Flame 199 (2019) 131–151.

[9] Z. Chen, C. Yao, A. Yao, Z. Dou, B. Wang, H. Wei, M. Liu, C. Chen, J. Shi, The impact of methanol injecting position on cylinder-to-cylinder variation in a diesel methanol dual fuel engine, Fuel 191 (2017) 150–163.

[10] Z. Yin, C. Yao, P. Geng, J. Hu, Visualization of combustion characteristic of diesel in premixed methanol–air mixture atmosphere of different ambient temperature in a constant volume chamber, Fuel 174 (2016) 242–250.

[11] A. Srna, M. Bolla, Y. M. Wright, K. Herrmann, R. Bombach, S. S. Pandurangi, K. Boulouchos, G. Bruneaux, Effect of methane on pilot-fuel autoignition in dual-fuel engines, Proceedings of the Combustion Institute 37 (4) (2019) 4741–4749.

[12] H. Xu, C. Yao, G. Xu, Chemical kinetic mechanism and a skeletal model for oxidation of n-heptane/methanol fuel blends, Fuel 93 (2012) 625–631.

[13] Engine combustion network, https://ecn.sandia.gov, Accessed Jan., 2020.

[14] H. Kahila, O. Kaario, Z. Ahmad, M. G. Masouleh, B. Tekgül, M. Larmi, V. Vuorinen, A large-eddy simulation study on the influence of diesel pilot spray quantity on methane-air flame initiation, Combustion and Flame 206 (2019) 506–521.

[15] B. Tekgül, H. Kahila, O. Kaario, V. Vuorinen, Large-eddy simulation of dual-fuel spray ignition at different ambient temperatures, Combustion and Flame 215 (2020) 51–65.

[16] S. Som, D. E. Longman, Z. Luo, M. Plomer, T. Lu, P. K. Senecal, E. Pomraning, Simulating flame lift-off characteristics of diesel and biodiesel fuels using detailed chemical-kinetic mechanisms and large eddy simulation turbulence model, Journal of Energy Resources Technology 134 (3) (2012) 032204.

[17] A. Irannejad, A. Banaeizadeh, F. Jaberi, Large eddy simulation of turbulent spray combustion, Combustion and Flame 162 (2) (2015) 431–450.

[18] S. Gallot-Lavallée, W. Jones, Large eddy simulation of spray auto-ignition under EGR conditions, Flow, Turbulence and Combustion 96 (2) (2016) 513–534.

[19] C.-W. Tsang, Y. Wang, C. Wang, A. Shelburn, L. Liang, K. Puduppakkam, A. Modak, C. Naik, E. Meeks, C. Rutland, Evaluation and Validation of Large-Eddy-Simulation (LES) for Gas Jet and Sprays, Tech. Rep., SAE Technical Paper, 2017.

[20] H. Wei, W. Zhao, J. Qi, Z. Liu, L. Zhou, Effect of injection timing on the ignition process of n-heptane spray flame in a methane/air environment, Fuel 245 (2019) 345–359.

[21] C. Gong, M. Jangi, X.-S. Bai, Large eddy simulation of n-dodecane spray combustion in a high pressure combustion vessel, Applied Energy 136 (2014) 373–381.

[22] Y. Pei, S. Som, E. Pomraning, P. K. Senecal, S. A. Skeen, J. Manin, L. M. Pickett, Large eddy simulation of a reacting spray flame with multiple realizations under compression ignition engine conditions, Combustion and Flame 162 (12) (2015) 4442–4455.

[23] A. Wehrfritz, O. Kaario, V. Vuorinen, B. Somers, Large eddy simulation of n-dodecane spray flames using flamelet generated manifolds, Combustion and Flame 167 (2016) 113–131.

[24] P. Kundu, M. M. Ameen, S. Som, Importance of turbulence-chemistry interactions at low temperature engine conditions, Combustion and Flame 183 (2017) 283–298.

[25] C. K. Blomberg, L. Zeugin, S. S. Pandurangi, M. Bolla, K. Boulouchos, Y. M. Wright, Modeling split injections of ECN "Spray A" using a conditional moment closure combustion model with RANS and LES, SAE International Journal of Engines 9 (4) (2016) 2107–2119.

[26] A. Hadadpour, M. Jangi, K. M. Pang, X. S. Bai, The role of a split injection strategy in the mixture formation and combustion of diesel spray: A large-

eddy simulation, Proceedings of the Combustion Institute 37 (4) (2019) 4709–4716.

[27] W. Zhao, H. Wei, M. Jia, Z. Lu, K. H. Luo, R. Chen, L. Zhou, Flame–spray interaction and combustion features in split-injection spray flames under diesel engine-like conditions, Combustion and Flame 210 (2019) 204–221.

[28] A. Varna, A. Wehrfritz, E. R. Hawkes, M. J. Cleary, T. Lucchini, G. D'Errico, S. Kook, Q. N. Chan, Application of a multiple mapping conditioning mixing model to ECN Spray A, Proceedings of the Combustion Institute 37 (3) (2019) 3263–3270.

[29] Q. Wang, C. Yao, Z. Dou, B. Wang, T. Wu, Effect of intake pre-heating and injection timing on combustion and emission characteristics of a methanol fumigated diesel engine at part load, Fuel 159 (2015) 796–802.

[30] K. M. Pang, M. Jangi, X.-S. Bai, J. Schramm, J. H. Walther, Modelling of diesel spray flames under engine-like conditions using an accelerated Eulerian Stochastic Field method, Combustion and Flame 193 (2018) 363–383.

[31] M. Jangi, R. Solsjo, B. Johansson, X.-S. Bai, On large eddy simulation of diesel spray for internal combustion engines, International Journal of Heat and Fluid Flow 53 (2015) 68–80.

[32] C. Gong, M. Jangi, X.-S. Bai, Large eddy simulation of n-dodecane spray combustion in a high pressure combustion vessel, Applied Energy 136 (2014) 373–381.

[33] D. B. Spalding, The combustion of liquid fuels, in: Symposium (international) on combustion, vol. 4, 847–864, 1953.

[34] W. E. Ranz, W. R. Marshall, Evaporation from drops, Part I, Chem. Eng. Prog 48 (3) (1952) 141–146.

[35] W. E. Ranz, W. R. Marshall, Evaporation from drops, Part II, Chem. Eng. Prog 48 (3) (1952) 173–180.

[36] T. Lu, C. K. Law, C. S. Yoo, J. H. Chen, Dynamic stiffness removal for direct numerical simulations, Combustion and Flame 156 (8) (2009) 1542–1551.

[37] R. Li, S. Li, F. Wang, X. Li, Sensitivity analysis based on intersection approach for mechanism reduction of cyclohexane, Combustion and Flame 166 (2016) 55–65.

[38] S. Liu, J. C. Hewson, J. H. Chen, H. Pitsch, Effects of strain rate on high-pressure nonpremixed n-heptane autoignition in counterflow, Combustion and flame 137 (3) (2004) 320–339.

[39] K. M. Pang, N. Karvounis, J. H. Walther, J. Schramm, Numerical investigation of soot formation and oxidation processes under large two-stroke marine diesel engine-like conditions using integrated CFD-chemical kinetics, Applied energy 169 (2016) 874–887.

[40] S. Hu, C. Gong, X.-S. Bai, Dual Fuel Combustion of N-heptane/methanol-air-EGR Mixtures, Energy Procedia 105 (2017) 4943–4948.

[41] M. Jangi, X. Zhao, D. C. Haworth, X.-S. Bai, Stabilization and liftoff length of a non-premixed methane/air jet flame discharging into a high-temperature

environment: An accelerated transported PDF method, Combustion and Flame 162 (2) (2015) 408–419.

[42] M. Jangi, X.-S. Bai, Multidimensional chemistry coordinate mapping approach for combustion modelling with finite-rate chemistry, Combustion Theory and Modelling 16 (6) (2012) 1109–1132.

[43] M. Jangi, R. Yu, X.-S. Bai, Development of chemistry coordinate mapping approach for turbulent partially premixed combustion, Flow, turbulence and combustion 90 (2) (2013) 285–299.

[44] The OpenFOAM Foundation, https://www.openfoam.gov, Accessed Jan., 2020.

[45] H. Jasak, H. G. Weller, A. D. Gosman, High resolution NVD differencing scheme for arbitrarily unstructured meshes, International Journal for Numerical Methods in Fluids 31 (2) (1999) 431–449, ISSN 0271-2091.

[46] L. Valiño, A field Monte Carlo formulation for calculating the probability density function of a single scalar in a turbulent flow, Flow, turbulence and combustion 60 (2) (1998) 157–172.

[47] M. Jangi, M. Altarawneh, B. Z. Dlugogorski, Large-eddy simulation of methanol pool fires using an accelerated stochastic fields method, Combustion and Flame 173 (2016) 89–98.

[48] S. Xu, S. Zhong, K. M. Pang, S. Yu, M. Jangi, X.-s. Bai, Effects of ambient methanol on pollutants formation in dual-fuel spray combustion at varying ambient temperatures: A large-eddy simulation, Applied Energy 279 (2020) 115774.

[49] Y. Zhang, S. Xu, S. Zhong, X.-S. Bai, H. Wang, M. Yao, Large eddy simulation of spray combustion using flamelet generated manifolds combined with artificial neural networks, Energy and AI (2020) 100021.

[50] A. B. Dempsey, N. R. Walker, R. Reitz, Effect of piston bowl geometry on dual fuel reactivity controlled compression ignition (RCCI) in a light-duty engine operated with gasoline/diesel and methanol/diesel, SAE International Journal of Engines 6 (1) (2013) 78–100.

[51] L. Xu, X.-S. Bai, M. Jia, Y. Qian, X. Qiao, X. Lu, Experimental and modeling study of liquid fuel injection and combustion in diesel engines with a common rail injection system, Applied Energy 230 (2018) 287–304.

[52] U. Burke, W. K. Metcalfe, S. M. Burke, K. A. Heufer, P. Dagaut, H. J. Curran, A detailed chemical kinetic modeling, ignition delay time and jet-stirred reactor study of methanol oxidation, Combustion and Flame 165 (2016) 125–136.

[53] National University of Ireland Galway, http://c3.nuigalway.ie/combustionchemistrycentre/mechanismdownloads, Accessed Jan., 2020.

[54] M. Christensen, E. Nilsson, A. Konnov, A systematically updated detailed kinetic model for CH2O and CH3OH combustion, Energy & Fuels 30 (8) (2016) 6709–6726.

[55] Q. Tang, H. Liu, X. Ran, M. Li, M. Yao, Effects of direct-injection fuel types and proportion on late-injection reactivity controlled compression ignition, Combustion and Flame 211 (2020) 445–455.

[56] Q. Tang, X. Liu, H. Liu, H. Wang, M. Yao, Investigation on the dual-fuel active-thermal atmosphere combustion strategy based on optical diagnostics and numerical simulations, Fuel 276 (2020) 118023.

[57] L. Xu, X.-S. Bai, C. Li, P. Tunestål, M. Tunér, X. Lu, Combustion characteristics of gasoline DICI engine in the transition from HCCI to PPC: Experiment and numerical analysis, Energy 185 (2019) 922–937.

LES/TPDF investigation of the effects of ambient methanol concentration on pilot fuel ignition characteristics and reaction front structures

Shijie Xu[a,*], Kar Mun Pang[b], Yaopeng Li[a,c], Ahmad Hadadpour[a], Senbin Yu[a], Shenghui Zhong[a,d], Mehdi Jangi[e], Xue-song Bai[a]

[a]*Department of Energy Sciences, Lund University, 22100 Lund, Sweden*
[b]*MAN Energy Solutions, Teglholmsgade 41, 2450 Copenhagen SV, Denmark*
[c]*Key Laboratory of Ocean Energy Utilization and Energy Conservation of Ministry of Education, Dalian University of Technology, 116024 Dalian, P.R. China*
[d]*State Key Laboratory of Engines, Tianjin University, 135 Yaguan Rd, 300350 Tianjin, P.R. China*
[e]*School of Mechanical Engineering, University of Birmingham, Edgbaston, Birmingham B15 2TT, UK*

Abstract

Large-eddy simulations with a transported probability density function model coupled with a finite-rate chemistry is applied to study the ignition process of an n-heptane spray in a constant volume chamber with a premixed methanol-air atmosphere under conditions relevant to reactivity controlled compression ignition (RCCI) engines. ~~A non-reacting spray and three~~ Three reacting spray cases with initial methanol-air equivalence ratio (ϕ_m) ranging from 0 to 0.3 are investigated ~~under initial temperatures~~ at an initial temperature of 900 K~~and 1000 K~~. The case setup is based on the Engine Combustion Network Spray-H configuration, where n-heptane fuel is used. The effects of the ambient methanol-air equivalence ratio on the ignition characteristics and the reaction front structures in n-heptane/methanol RCCI combustion are studied in detail. It is found that the ambient methanol affects

*Corresponding author.
E-mail address: shijie.xu@energy.lth.se

the low temperature chemistry of n-heptane, which results in a change of spatial distribution of key species such as heptyl-peroxide, and therefore the cool flame structure. With the presence of methanol in the ambient ~~gas~~ mixture cool flame is found in the entire fuel-rich region of the n-heptane jet, ~~whereas without methanol~~ while when methanol is absent in the ambient mixture, the cool flame is established only around the stoichiometric mixture close to the n-heptane injector nozzle. In general, both low- and high-temperature ignition stages of n-heptane ignition are retarded by the methanol chemistry. ~~A negative correlation between~~ An increase in ϕ_m ~~and the value of the first stage~~ leads to a decrease of the peak heat release rate ~~is observed.~~ of the n-heptane first-stage ignition. The chemistry of methanol inhibits the n-heptane ignition by decreasing the overall hydroxyl radicals (OH) formation rate and reducing the OH concentration during the transition period from the ~~first stage~~ first-stage ignition to the ~~second stage~~ second-stage ignition. As a result, the transition time between the two ignition stages is prolonged. Under the present lean methanol/air ambient mixture conditions, the impact of methanol on n-heptane ignition has a tendency of reducing the ~~high temperature~~ high-temperature, fuel-rich region, which is in favor of soot reduction.

Keywords: Dual-fuel combustion, Auto-ignition, Engine Combustion Network, Large eddy simulation, Eulerian stochastic field

---

1. Introduction

Methanol is a promising alternative fuel to fossil fuels. ~~Compared~~ As compared with natural gas and hydrogen, methanol is easier to store, transport, distribute, and use since methanol is ~~liquid~~ in liquid form at room temperature. Methanol can be produced from a wealth of sources, such as coal, natural gas, biomass and

municipal waste. One ~~challenge~~ of the main challenges in utilizing methanol in conventional compression-ignition (CI) engines is the difficulty in igniting the fuel due to its high latent heat of evaporation and long ignition-delay time (IDT). This issue becomes more severe in the condition of a cold start or at low engine loads [1, 2]. As a result, novel combustion strategies, e.g., dual-fuel combustion, are developed to improve the ignition process in methanol fueled CI engines. The engines using dual-fuel combustion strategies are known as dual-fuel engines. One of the dual-fuel ~~combustion strategies~~ engines is the reactivity controlled compression ignition (RCCI) ~~concept. In an~~ engine. In the RCCI engine, a low-reactivity fuel (primary fuel) is ~~injected~~ delivered into the cylinder during the intake stroke to form a premixed fuel-air mixture. The mixture is then ignited by injecting a high-reactivity fuel (pilot fuel) during the compression stroke. Due to the lean premixed combustion in RCCI, high-temperature and rich-fuel regions can be avoided in the cylinder, leading to reduced soot and NOx emissions [3–6]. An engineering challenge in the dual-fuel engine is the control of ignition time and heat release rate (HRR) [7]. Unlike the ignition of a conventional diesel engine, the auto-ignition mechanism in a dual-fuel engine is not well understood [8]. In practice, the equivalence ratio distribution of the primary fuel/air mixture may not be perfectly homogenous in the dual-fuel engines [9]. When the pilot fuel is introduced, the associated ignition characteristics vary due to the local condition [9]. This further complicates the auto-ignition mechanism in dual-fuel engines.

Several experimental and numerical studies were carried out to improve the understandings of pilot fuel ignition in the ambient primary fuel/air mixture. Yin *et al.* [10] performed experiments on diesel/methanol dual-fuel combustion in a constant volume combustion chamber under a range of ambient tempera-

tures (840–960 K) with methanol-air equivalence ratio (ϕ_m) of 0.1. The results showed that when the temperature is below ~~920K~~920 K, the IDT of diesel in the methanol-air atmosphere is longer than that in the pure air atmosphere. However, ~~no~~ detailed analysis of the ignition phenomenon, ~~including~~ such as complex two-stage ignitions, was ~~available~~ not provided, due to the lack of intermediate species in the measurements. Srna *et al.* [11] reported optical diagnosis experiments of n-dodecane spray combustion in a methane-air atmosphere in a rapid compression-expansion machine (RCEM). It was found that the ambient methane could affect the onset of the ~~first stage~~ first-stage ignition (the cool flame) but the temporal separation of the ~~first stage ignition and second stage~~ first-stage ignition and the second-stage ignition was shown to be independent of the methane concentration in the ambient methane-air mixture. Xu *et al.* [12] studied the reaction paths of the n-heptane/methanol blends. The results showed that radical pool was a bridge connecting methanol and n-heptane in oxidation, where the methanol concentration was important. Kahila *et al.* [8] conducted a large eddy simulation (LES) of an n-dodecane/methane-air dual-fuel combustion in the Engine Combustion Network (ECN) [13] constant volume configuration. It was found that the low-temperature reactions of the pilot fuel (n-dodecane) provided intermediate species and heat, which played an important role in the primary fuel (methane) oxidation. In turn, both the first and the second ignition stages of the pilot fuel were retarded in the methane-air atmosphere, mainly due to the consumption of OH in the ambient methane oxidation. ~~To the best of the authors' knowledge, detailed numerical simulations and analyses~~ The same group also investigated different aspects of n-dodencane/methane dual-fuel combustion using their LES models [8, 14, 15]. Yet, LES on methanol based dual-fuel combustion ~~are yet to~~

~~be carried out. This has motivated~~ have been rare. This motivates the present study which aims to investigate the effects of ambient methanol concentration on pilot fuel ignition.

~~The recent LES study~~ It may also be worth mentioning that the recent LES studies [8, 14, 15] of dual-fuel combustion ~~[8, 14, 15] have~~ used a well-stired reactor (WSR) assumption, in which turbulence-chemistry interaction (TCI) in the sub-grid scale (SGS) has been neglected. They used a very fine spatial resolution to compensate the ~~neglected~~ absence of the TCI effect. However, Varna *et al.* [28] pointed out that TCI is important for the spray flame ~~in~~ under engine-like conditions, especially for the low temperature case with a long IDT. ~~Since the~~ The IDT is typically ~~longer in dual-fuel combustion~~prolonged by the ambient primary fuel [8, 14, 29], it is hence desirable to incorporate a TCI model in dual-fuel ignition simulations. The commonly used TCI models are the Conditional Moment-Closure (CMC) [25], the probability density function (PDF) model [18], the linear eddy model (LEM) [20, 27], and the Flamelet Generation Manifold (FGM) [23]. Table 1 shows a list of recent LES studies of the ECN spray combustion cases. A summary of the unsteady Reynolds-averaged Navier–Stokes (URANS) simulations is available in Ref. [30].

Set against these backgrounds, LES which is known to have better capability in predicting flow structure and mixing ~~,~~ is carried out to study n-heptane/methanol dual-fuel combustion in a constant volume combustion chamber. In addition to this, an Eulerian stochastic field (ESF) transported probability density function (TPDF) model is employed to account for the SGS TCI effects. The baseline case uses the ECN Spray-H (n-heptane fueled) conditions. The associated experimental data is used for the validation of the current LES-TPDF model under both non-

Table 1: Recent LES studies of ECN spray flames.

Fuel	Species number	Mesh size [~~mm~~ μm]	Combustion model	Turbulence model	Code	Ref.
n-Heptane	42, 68	250	WSR	Smagorinsky	Converge	[16]
n-Heptane	44	200	FMDF [1]	-	In-house	[17]
n-Heptane	22	500	ESF	Dynamic Smagorinsky	In-house	[18]
n-Heptane	140	250, 125, 62.5	WSR	Smagorinsky, dynamic structure	ANSYS	[19]
n-Heptane/ methane	44	-	LEM	-	KIVA	[20]
n-Dodecane	103	250	WSR	One-equation eddy	OpenFOAM	[21]
n-Dodecane	103	62.5	WSR	Dynamic structure	Converge	[22]
n-Dodecane	257, 103	62.5	FGM	-	OpenFOAM	[23]
n-Dodecane	103	62.5	TFM [2]	Dynamic structure	Converge	[24]
n-Dodecane	54	125	CMC	$k-\ell$ two-equations	Star-CD	[25]
n-Dodecane	54	240	PaSR [3]	One-equation eddy	OpenFOAM	[26]
n-Dodecane/ methane	54, 96	160, 80, 62.5	WSR	Implicit LES	OpenFOAM	[8, 14, 15]
n-Dodecane	54	-	LEM	-	KIVA	[27]

[1] Compressible filtered mass density function (FMDF).

[2] Tabulated Flamelet Model (TFM).

[3] Partially stirred reactor (PaSR) model.

reacting spray and reacting spray conditions. A series of methanol-air equivalence ratios are selected to investigate the ignition process. The main purpose of this work is to elucidate the effects of ambient methanol concentration on the ignition process of an n-heptane spray under conditions relevant to RCCI engines.

2. Methodology

2.1. Eulerian-Lagrangian approach

In order to describe the two-phase flow in the spray combustion, the Lagrangian particle tracking approach is applied. In the LES framework, the gas phase is governed by spatially filtered Navier-Stokes equations, while the Lagrangian liquid phase is described and tracked using a large number of parcels. The interaction between the gas and liquid phases is considered via the source terms in the mass conservation, momentum, species and energy transport equations. Details of the LES spray model are referred to Ref. [31, 32]. A one-equation SGS kinetic energy model (k-equation model) is used to model the SGS viscosity. The ambient methanol-air mixture is assumed to be in a quiescent gas phase, following the previous LES [8, 14, 15] studies. The n-heptane fuel is injected as liquid droplets, with the initial droplet size following the Rosin-Rammler distribution. The mean diameter of droplets is set as half the injector nozzle diameter, $d_n/2$. The maximum size is set to the diameter of the injector nozzle, d_n, where $d_n = 0.1mm$. The evaporation rate is modelled using the Spalding formula [33]. The Ranz-Marshall correlation [34, 35] is used to model the heat transfer between the liquid and gas phases. The current numerical configurations ~~will be validated against experimental data as~~ are validated using experimental data from the ECN [13]. This will be discussed in Section 3.3.

A finite-rate chemistry is considered in the present study. Several n-heptane mechanisms [36–39] are evaluated for modeling of the ignition process of n-heptane/methanol-air mixture under a range of equivalence ratios, temperatures, and pressure conditions relevant to the present dual-fuel combustion cases. The n-heptane mechanism of Lu *et al.* (hereinafter denoted as Lu-68) with 68 species and 283 reactions [36] has shown the best trade-off between computational efficiency and model accuracy in terms of the prediction of IDT. In addition, this mechanism has been applied in both ECN spray cases [16] and the direct numerical simulation (DNS) study of n-heptane/methanol dual-fuel combustion [40]. To speed up the integration of the chemical reaction rates, a chemistry coordinate mapping (CCM) method is employed. In the CCM approach, the integration of the stiff chemical reaction rates is performed in a low-dimensional chemical phase space, and the results are mapped back to the mesh points in the physical space. In the present study, the phase space coordinates include the mixture fraction, temperature, scalar dissipation rate, and the mass fraction of n-heptane. This approach can speed up the time-consuming integration of the chemical reaction rates by a factor of 10 [41]. However, the species transportation cannot be accelerated. Therefore, an overall 2 to 5 times reduction of the clock time is achieved [41, 42] . Details of the CCM method and its application to the simulation of spray combustion can be found in Refs. ~~[32, 41]~~[32, 41–43].

The OpenFOAM code [44] is used in this study. The solver is based on the finite volume method~~, with a~~ . The second order backward Euler scheme ~~for~~ is applied for the temporal integration and the second order normalised variable diagram (NVD) scheme named Gamma [45] ~~for~~ is used for the convective fluxes discretization.

2.2. *Eulerian stochastic field method*

As aforementioned in the introduction, the TCI effects are important particularly in cases with long ignition delay times. To accommodate the TCI in spray combustion, a ESF-based TPDF approach is employed ~~based on the ESF method~~ [46]. In this method, the one-point one-time joint PDF is expressed as an ensemble of a series of stochastic fields, where the PDF is written as,

$$P\left(\psi;\mathbf{x},t\right)=\frac{1}{N_F}\sum_{n=1}^{N_F}\prod_{\alpha=1}^{N_s}\delta(\psi_\alpha-\xi_\alpha^n) \tag{1}$$

Here, δ represents the Dirac delta function, while N_F and N_s are the number of stochastic fields and the number of scalars, respectively. The scalars include the mass fractions of species and the enthalpy. ξ_α^n denotes the α-th scalar in the n-th stochastic field.

The ESF equation in its discrete form is given in Eq. (2), describing the evolution of each stochastic field,

$$\begin{aligned}\overline{\rho}d\xi_\alpha^n=&-\overline{\rho}\tilde{\mathbf{U}}\nabla\xi_\alpha^n dt+\nabla\left(\Gamma_t\nabla\xi_\alpha^n\right)dt+\overline{\rho}\sqrt{2\frac{\Gamma_t}{\overline{\rho}}}\nabla\xi_\alpha^n d\mathbf{W}^n\\&-\frac{\overline{\rho}C_\phi}{2\tau_{sgs}}(\xi_\alpha^n-\tilde{\phi}_\alpha)dt+\overline{\rho}\dot{\omega}_\alpha(\underline{\xi}^n)dt.\end{aligned} \tag{2}$$

Here, $d\mathbf{W}^n$ represents the increment of a vector Wiener process to take the random process into consideration, which is spatially uniform but varying in different fields. Γ_t denotes the total diffusion coefficient, accounting for both the laminar and SGS diffusion. In addition, $\tilde{\phi}_\alpha$ represents the mean scalar field, τ_{sgs} is the SGS mixing time scale, and $C_\phi=2$ is a model constant for micro-mixing. The same model constants as in Ref. [30] are used, where more details about these constants can be found. The number of stochastic fields is set to 12, following the suggestion of a previous study [47].

2.3. Case set-up

Table 2: Setup of the computational cases.

	Single-fuel		Dual-fuel	
	Case A	Case B	Case C	Case D
T [K]	1000	900	900	900
O_2 [vol. %]	0	0.21	0.21	0.21
ϕ_m [-]	0	0	0.1	0.3

Table 2 shows the four computational cases in this study. Cases A and B are the single-fuel cases, which have been studied in the ECN Spray-H experiments [13]. They are selected for validations of the current LES models under non-reacting (Case A) and reacting spray (Case B) conditions, respectively. ~~In addition,~~ The validation of the non-reacting spray is only performed at an ambient temperature of 1000 K due to the absence of experimental data at lower ambient temperatures. Effects of ambient methanol concentration on pilot fuel ignition characteristics are subsequently investigated in Cases B, C and D at the ambient temperature of 900 K. The ambient temperature of 900 K is selected since the associated interaction between methanol and n-heptane is stronger than that at higher ambient temperatures. The ignition delay of the methanol at 1000 K condition is comparable to that of n-heptane [40]. Methanol fueled dual-fuel engine at such a high temperature is less dependent on the ignition assistance of n-heptane. Case B serves as ~~a~~ the model validation case and the baseline reference condition for the evaluation of the effects of the ambient mixture equivalence ratio on the dual-fuel combustion process. Cases C and D are the dual-fuel cases, with

different methanol concentration in the ambient mixture. In the dual-fuel configuration, the liquid n-heptane is used to mimic the pilot diesel fuel in the RCCI engines. The ambient methanol ~~cocentration~~ concentration is parameterized using equivalence ratios (ϕ_m) , which is defined as the ratio of the actual methanol-"air" ratio to the stoichiometric methanol-"air" ratio. It is worth mentioning that the "air" is not the atmosphere air ~~. For the sake of validation, it is set as ECN experiments with a gas density of~~ but resembles those of the ECN experiment to mimic the in-cylinder mixture of engines. The "air" density is set to 14.8 kg/m^3~~and a mole concentration~~ , while mole concentrations of O_2~~21%~~, N_2~~69.33%~~, CO_2 ~~6.11%,~~ and H_2O are set to 21%, 69.33%, 6.11% and 3.56%~~[13].~~ , respectively [13]. The gaseous methanol is mixed with "air" to form a homogeneous and quiescent primary fuel-air mixture before the n-heptane injection, following the previous LES works [8, 14, 15, 48, 49]. According to the ideal gas equation of state, the pressure is calculated from the gas density, ambient temperature and the mixture average molar mass. Details of the ambient mixture initial conditions can be found in Table 3. As shown, ϕ_m of 0.1 and 0.3 are investigated in the current LES. The ϕ_m of 0.3 is chosen based on the engine conditions defined in Ref. [50]. It is an averaged global equivalence ratio under the medium-load condition of the diesel/methanol RCCI engine. On the other hand, the selection of ϕ_m of 0.1 is based on the experiment in Ref. [10]. It is found in Ref. [10] that under very lean condition, the associated low amount of ambient methanol concentration is sufficient to retard the ignition delay of the pilot fuel. In practice, the equivalence ratio distribution is not perfectly homogeneous in the engines [9]. There may exist local lean mixture even at the high-load engine conditions. It is important to know how the ignition and combustion processes evolve when the pilot fuel is injected

into these very lean mixture.

Table 3: Initial conditions of the ambient mixture.

Case	Density [kg/m^3]	Pressure [MPa]	Ambient methanol/air mass fraction composition				
			CH_3OH	O_2	N_2	CO_2	H_2O
A	14.8	4.2906	0	0	0.8763	0.1001	0.0237
B	14.8	3.7577	0	0.2280	0.6590	0.0913	0.0218
C	14.8	3.7532	0.0150	0.2246[1]	0.6491	0.0899	0.0214
D	14.8	3.7445	0.0437	0.2180[1]	0.6302	0.0873	0.0208

[1] The ambient oxidizer gas in Cases ~~B,~~ C and D is a mixture of ~~air and CO_2 and H_2O (with the same composition as that specified in Case B)~~"air" and gaseous methanol. The addition of methanol reduces the oxygen mass fraction.

In all four cases, liquid n-heptane is ~~injected~~ delivered into a constant volume chamber at an injection pressure of 150 MPa. It undergoes break up, evaporation and mixing with ambient mixture. The chamber configuration is the same as that in the ECN Spray-H experiments, which is a cube with a side length of 108 ~~*mm*~~mm. The injection duration of n-heptane is 6.6 ~~*ms*~~ ms with a total mass of 17.5 ~~*mg*~~mg, the injection mass flow rate is calculated using an injection model described in Ref. [51]. A locally refined grid system is used, with the finest cell size of ~~0.25 *mm*~~250 μm. The maximum Courant–Friedrichs–Lewy number adopted in the simulation is 0.1, which gives a typical time step of the temporal integration of 50 ~~*ns*~~ns. The present grid resolution is similar to ~~most LES studies reported recently~~ the majority of the recent LES studies [16, 17, 19, 21, 26], cf. Table 1. In particular, the ~~LES study of~~ LES-ESF study performed by Gallot-Lavallée *et al.* ~~based on a coarse mesh (with a mesh size of 0.5 *mm*, which is coarser than the~~

present 0.25 *mm* mesh) with the presently used ESF-TPDF model using a mesh size of 500 µm showed a fairly good prediction of IDT and flame lift-off length (LOL) [18]. The LES studies of Kahila *et al.* [8] used a finer mesh (with a mesh size of 0.16, 0.08 and 0.0625 *mm*) but without 160, 80 and 62.5 µm) due to the absence of a TCI model[8]. In terms of the computation cost, it varied with the simulation time . The simulation timesin Case A mesh sensitive analysis (125, 250 and 500 µm grid) is performed on both non-reacting and reacting spray to show the capability of the current grid resolution and time step in predicting the spray, ignition and flame stabilization. As will be shown later, the present grid and time step show an adequate resolution of the spray, evaporation and flame dynamics. The computational cost varies from case to case due to the difference in physical end times. Since the IDT varies in these cases, the physical end times in Cases B, C and D were are 1.5, 2.5 and 3.0 *ms*ms, respectively. It took 100, 000 CPU hours For the readers' reference, the clock time for Case Bto run up to , which is performed to 1.5 *ms* with ms in a 250 µm grid, are approximately 28 days with the use of 144 processors in parallel(approximately 100,000 CPU hours).

3. Results and discussion

3.1. The performance of the chemical mechanism

An evaluation of the methanol sub-mechanism in the current Lu-68 n-heptane mechanism is conducted to investigate the accuracy of this mechanism in the prediction of the ignition process in the ambient methanol/air mixture. Figure 1 shows the IDT IDTs of stoichiometric and lean methanol/air mixture (equivalence ratio of 0.5) predicted by the Lu-68 mechanism and two detailed methanol mechanisms, as well as the corresponding high-pressure shock-tube experiments measurements

at National University of Ireland (NUI) Galway [52]. The initial pressure is chosen as 50 bar, which is similar ~~to current spray flames~~in the current spray flame cases. The two detailed methanol mechanisms considered are the Aramco 2.0 mechanism [53] and the Konnov mechanism [54]. It is shown that the IDTs predicted using the Lu-68 mechanism are comparable to those calculated using the detailed mechanisms and the shock tube ~~data~~measurement.

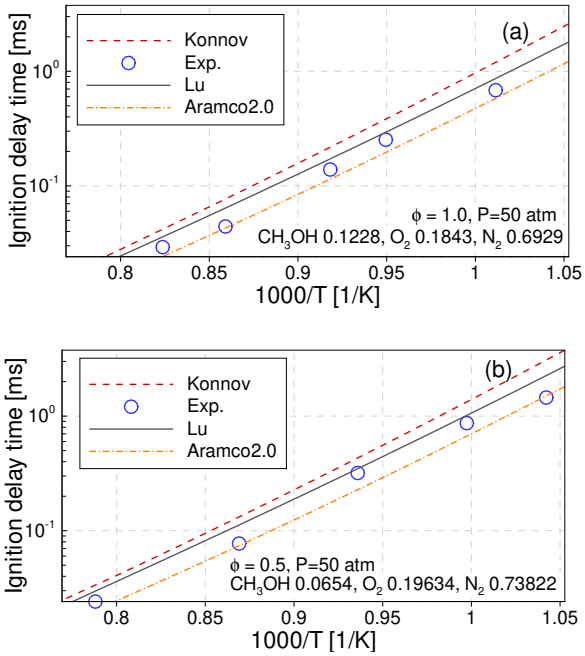

Figure 1: IDT predicted using different ~~mechanism~~ mechanisms for (a) stoichiometric and (b) lean methanol/air mixture with equivalence ratio of 0.5 at ~~different initial temperatures and~~ a pressure of 50 bar across different initial temperatures. The symbols represent the ~~the~~ high-pressure shock-tube experimental data from National University of Ireland (NUI) Galway [52].

3.2. Mesh sensitivity analysis

Figure 2 shows the evolution of the liquid penetration length (LPL) and the vapor penetration length (VPL) calculated using three different mesh resolutions. The LPL is defined as the distance from the injector nozzle to the downstream

position where the liquid fuel mass within this region accounts for 95% of the liquid mass in the domain. The VPL is defined as the maximum distance from the nozzle outlet to the location with the fuel mass fraction reaching 0.1% [13]. The horizontal axis represents the time after the start of injection (ASI), whereas the vertical axis shows the liquid and the vapor penetration lengths. As shown, the LES results using the finer mesh resolutions of 250 and 125 µm agree with each other, while those using 500 µm diverge.

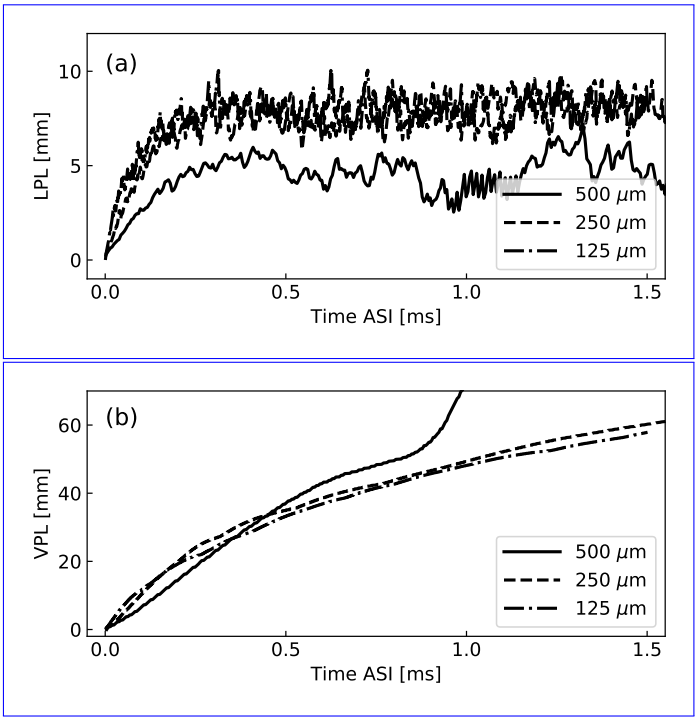

Figure 2: Temporal evolution of (a) the liquid penetration length (LPL), and (b) the vapor penetration length (VPL) predicted in LES with mesh resolutions of 125, 250 and 500 µm.

Figure 3 shows the evolution of the pressure rise and the flame LOL of the reacting spray using these three different mesh resolutions. The LOL is defined as the distance from the fuel nozzle to the farthest location where Favre-average

OH mass fraction reaches 2% of its maximum in the domain after a quasi-steady flame is established. As seen in Figure 3a, the mean pressure rise profiles are found to be relatively insensitive to the mesh resolution. Figure 3b depicts that the LOL predicted using the 500 µm mesh is lower while those predicted using both the 250 µm and 125 µm resolutions agree with each other. Therefore, the 250 µm mesh, which provides reasonable accuracy in prediction of non-reacting and reacting sprays at an affordable computational cost, is chosen for the following LES.

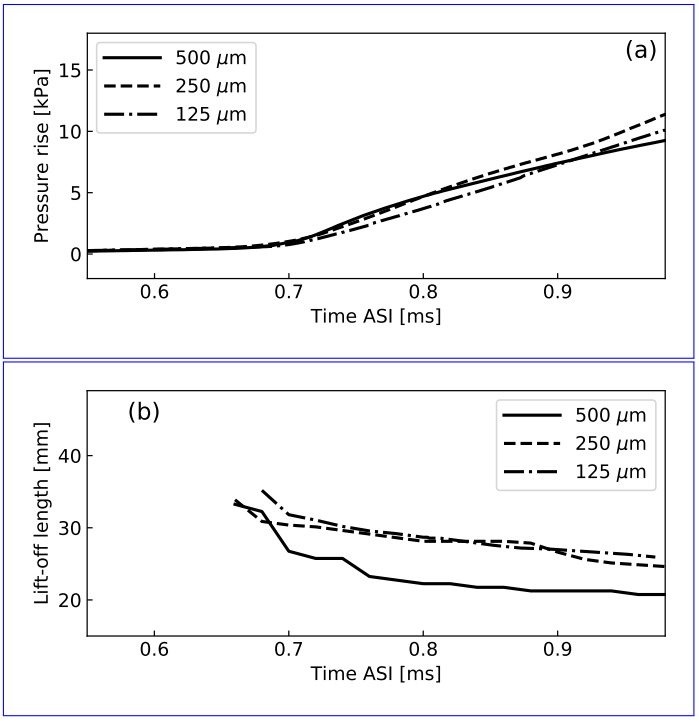

Figure 3: (a) The LES predicted pressure rise, and (b) the flame lift-off length (LOL) using mesh resolutions of 125, 250 and 500 µm.

3.3. Validation of the LES spray combustion model

Figure 4a shows the LPL and VPL in the non-reacting case (Case A) from the present LES and the corresponding ECN Spray-H experiments, under the 1000 K and oxygen-free condition. The experimental data were obtained using Schlieren imaging and Mie-scattering [13]. Figure 4b shows the spatial distribution of the mean mixture fraction ~~from LES and experiments~~in the LES and experiment. The error bar indicates the uncertainty ~~in~~ of the experimental data obtained from the Rayleigh scattering [13]. The current LES model setup and grid resolution yield in good agreement with the measurements.

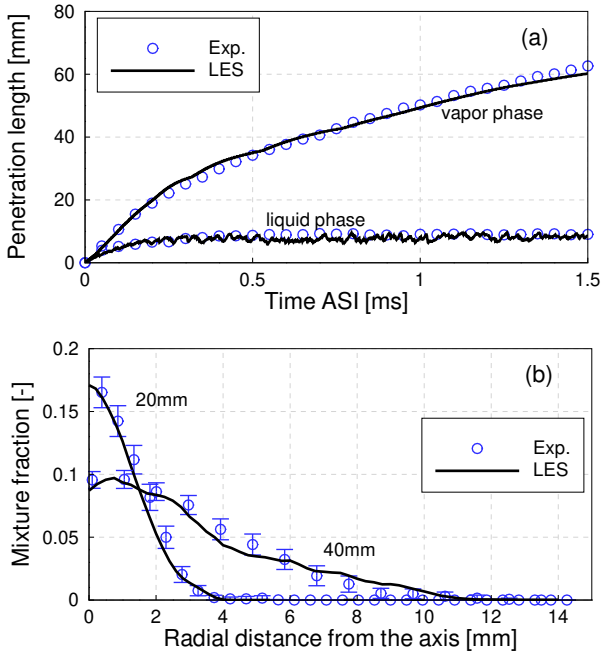

Figure 4: Comparisons of LES and experimental (a) liquid and vapor penetration lengths, and (b) mean mixture fraction at two axial positions (20 mm and 40 mm) downstream the nozzle in the non-reacting spray case. The mean mixture profiles in (b) are time averaged and ensemble averaged for the LES and experimental results, respectively.

~~For~~ The simulated IDT and LOL of the reacting spray case (~~case B) , the IDT and lift-off length (LOL) from LES and experiments are compared~~Case B) are next validated using the experimental measurements. The IDT ~~from LES~~ is defined based on the time at which the maximal time derivative of temperature is reached, following the ECN suggestion [13]. The IDT and LOL predicted in the current LES are 0.80 ~~*ms*~~ ms and 25 ~~*mm*~~mm, respectively. These agree with the experimental IDT of 0.79 ~~*ms*~~ ms and LOL of 25.5 ~~*mm*~~ mm [13] reasonably well, where the relative differences remain below 2%. Moreover, the LES replicates the experimental pressure profile (shown in the next section). In summary, the present LES spray combustion model is capable of simulating the spray vaporization and vapor mixing processes, the ignition timing and the flame stabilization. In the following, the LES model is applied to predict and analyze the spray combustion process for both the single- and dual-fuel cases.

3.4. Effects of ambient methanol on pressure rise and heat-release rate

Figure 5 shows the temporal evolution of pressure rise (the difference between the chamber pressure and its initial pressure) and net HRR, which is the heat release rate term integrated over the entire chamber, for ~~cases~~ Cases B, C, and D (with ambient methanol equivalence ratio varying from 0 to 0.3). Before the onset of ignition, the chamber pressure decreases due to the endothermic evaporation process during the n-heptane injection. ~~After a short while, a pressure rise is observed, along with~~ This is followed by a pressure rise along side with a noticeable HRR, indicating the onset of ignition. Both the initial HRR and the pressure-rise rate are rather low; this stage of ignition is known as the ~~first stage ignition or~~ first-stage ignition or the low temperature ignition. Thereafter, around 0.6 ms ASI, HRR increases rapidly to a substantially high value, along with a rapid increase of

chamber pressure. The start of the high HRR indicates the onset of ~~second stage~~ second-stage ignition, also known as the high temperature ignition stage. This two-stage ignition process is observed for the n-heptane fuel, while pure methanol ignition undergoes only the high temperature stage [12]. As shown in the inset of Fig. 5, where the ~~first stage~~ first-stage HRR is displayed, the onset of ~~first stage~~ first-stage ignition is retarded in the dual-fuel cases ($\phi_m = 0.1$ and $\phi_m = 0.3$). This is consistent with the observation in methane-based dual-fuel experiments [11] and LES [8] studies. Moreover, the higher methanol-air equivalence ratio in the ambient mixture, the longer retardation time of the ~~first stage~~ first-stage ignition, and the lower the peak HRR from the ~~first stage~~ first-stage ignition. Furthermore, the ambient methanol also retards the ~~second stage~~ second-stage ignition, evident by the time difference between the ~~second stage~~ second-stage ignition and the ~~first stage~~ first-stage ignition, which increases with the increase of ϕ_m in the ambient mixture.

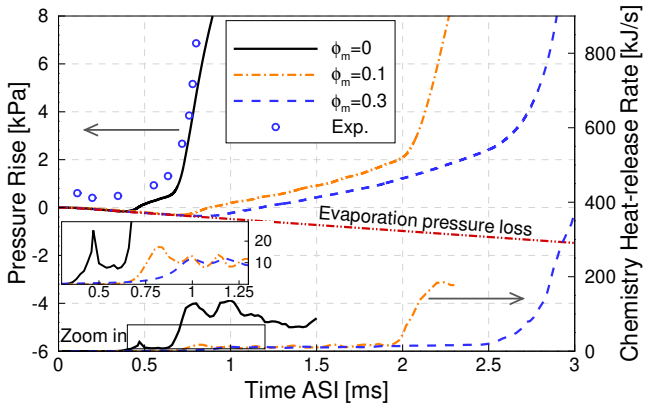

Figure 5: ~~Effect~~ Effects of ambient methanol concentration on pressure rise and total heat-release rate for ~~cases~~ Cases B, C, and D. The experimental pressure rise is shown using symbols.

Figure 6 shows the evolution of the maximum chemistry HRR in the computational domain for Cases B, C and D. A semi-logarithmic coordinates is used to demonstrate the two-stage heat releases and the weak heat release before the first-stage ignition. The two-stage heat releases are clearly demonstrated by the two plateaus in the figure. It is found that the single-fuel case has the highest maximum chemistry HRR in the first-stage heat release, which is consistent with the observation in Fig. 5. On the contrary, the maximum chemistry HRR of the single-fuel case is the lowest in the second-stage heat release. It is also found that the dual-fuel Cases C ($\phi_m = 0.1$) and D ($\phi_m = 0.3$) have a higher heat release before 0.15 ms ASI, shown in the inset of Fig. 6.

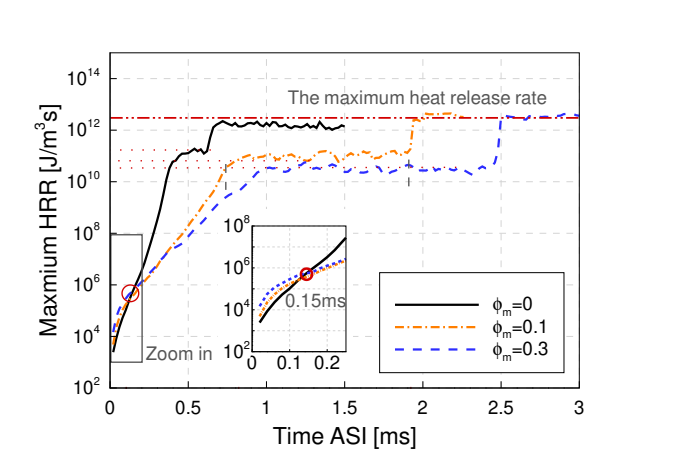

Figure 6: The maximum chemistry heat-release rate in the domain for the reacting Cases B, C, and D.

3.5. Effects of ambient methanol concentration on the ignition process

In order to track the ignition event, the most reactive local mixture is defined. The HRR of the local mixture (in each computational cell) is compared and the one with the highest HRR is defined as the most reactive local mixture. The

spatial location of the most reactive local mixture changes with time. The most reactive local mixture is tracked in order to investigate how it evolves and where it is located. The temporal evolution of heptyl-peroxide (RO_2) and OH mass fractions in the most reactive local mixture is shown in Figure 7. To illustrate the wide range, mass fractions in vertical coordinates are shown in log-scale. RO_2 has been recommended by ECN [13] as the ~~marker of the first stage~~ indicator of the first-stage ignition: the ~~first stage~~ first-stage IDT is suggested to be at the time of RO_2 mass fraction reaching 20% of its maximum, denoted as τ_1 in Fig. 7a with the vertical dashed lines. On the other hand, OH is used as the indicator for the ~~second stage~~ second-stage ignition , denoted as τ_2 in Fig. 7b. It is seen that the mass fractions of RO_2 and OH of the most reactive mixture increases (approximately) exponentially with time (ASI) until it reaches a plateau shortly after τ_1, and the mass fraction of OH reaches a second plateau after τ_2. In the ~~second stage~~ second-stage ignition, the maximum OH mass fraction is independent of ϕ_m, while during the transition period from the ~~first stage~~ first-stage ignition to the ~~second stage ignition, it~~ second-stage ignition, OH mass fraction decreases with ϕ_m in the ambient mixture. The transition time from the onset of ~~first stage~~ first-stage ignition to the second-stage ignition is 0.45 ms, 1.23 ms and 1.74 ms for Cases B, C, and D, respectively, showing an increasing retardation effect of methanol on the n-heptane ignition process with ϕ_m. Similar retardation effect ~~has been~~ was reported for n-dodecane/methane-air dual-fuel combustion [11].

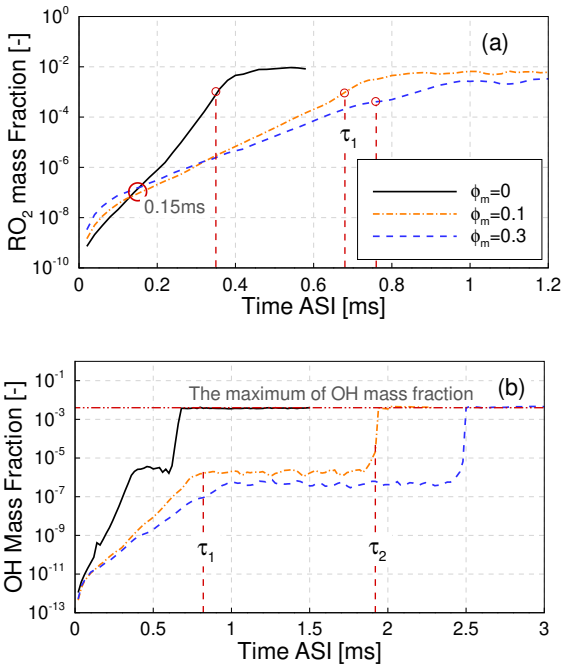

Figure 7: Temporal evolution of mass fraction of RO_2, Y_{RO_2} (a), and OH, Y_{OH} (b), in the most reactive local mixture for ~~cases~~ Cases B, C, and D (with ϕ_m varying from 0 to 0.3), respectively. The vertical dashed lines indicate the time of ~~first stage~~ first-stage ignition (τ_1, a) and the ~~first~~ first- and ~~second stage~~ second-stage ignition (τ_1 and τ_2, b). The two plateaus in the OH profiles indicate the transition period from the onset of the ~~first stage~~ first-stage ignition to the onset of the ~~second stage~~ second-stage ignition, and the period after the onset of the ~~second stage~~ second-stage ignition.

The maximal mass fraction of RO_2 in the most reactive mixture is higher initially (before 0.15 ms ASI) in the cases with higher methanol concentration in the ambient mixture. This indicates that the ambient methanol enhances the production of RO_2. However, shortly after 0.15 ms ASI, the suppression effect of methanol on RO_2 is evident. The underlying mechanism behind this ~~is~~ will be investigated in Section 3.7.

3.6. *Effects of methanol on the structure of the spray flame*

In a three-dimensional n-heptane/methanol dual-fuel spray flame, during the liquid n-heptane injection, the ~~ignition~~ oxidation reactions in the methanol-air mixture take place, but not to the critical point of auto-ignition. This period of time is referred to as the ignition induction time. This implies that in the present n-heptane/methanol dual-fuel combustion process, the effects of methanol chemistry on the n-heptane ignition is different at different spatial locations of the spray jet due to the discrepancy in the induction time.

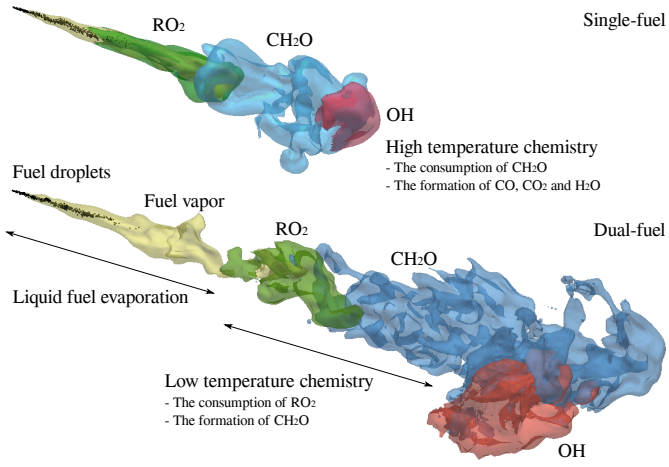

Figure 8: Three-dimensional flame structure at the instance of ~~second stage~~ second-stage ignition for the single-fuel Case B (upper) and dual-fuel Case D (bottom). Black dots indicate the fuel droplets.

Figure 8 shows the three-dimensional flame structure of single-fuel (Case B) and dual-fuel combustion (Case D) at the instance of ~~second stage~~ second-stage ignition. The ~~liquid~~ n-heptane is ~~injected and evaporated~~ delivered as liquid fuel. The liquid n-heptane droplets then break up and evaporate to fuel vapor in the immediate downstream of the fuel jet. The intermediate species, such as RO_2 and

CH_2O, are produced in the low-temperature ignition region. The high-temperature ignition takes place ~~in downstream regions~~ further downstream of the spray, where the intermediate species are oxidized to CO_2 and H_2O with the participation of radicals such as OH.

The fuel vapor is enveloped by the RO_2 in the single-fuel case, while the RO_2 region in the dual-fuel case is in the downstream of the fuel vapor region. The ambient methanol/air mixture retards the onset of the ~~first stage~~ first-stage ignition, affects the cool flame structure, and postpones the onset of ~~second stage ignition kernel at~~ second-stage ignition kernel further downstream. The postponed high temperature ignition extends the mixing time before the start of high-temperature combustion, ~~which reduces~~ reducing the high-temperature and rich-fuel regions ~~forming soot~~ which are favorable for soot formation. This result is consistent with the soot reduction in dual-fuel engines reported in the literature [3, 55, 56].

To investigate the ~~first stage~~ first-stage ignition kernel structure of the present spray flames in more detail, the spatial and temporal distributions of RO_2, HO_2, CH_2OH, and OH mass fractions before the onset of the ~~first stage~~ first-stage ignition in a cross plane along the spray axis, are plotted in Fig. 9. The mass fractions are normalized by its maximal value in the domain for the given case at the given instance of times.

For Case B ($\phi_m = 0$), the formation of RO_2 starts in the upstream region of the spray jet, around the iso-surface of the stoichiometric mixture fraction. As time goes on, the fuel vapor continues to penetrate downstream but most of the RO_2 still concentrates upstream, until a new reactive region appearing at 0.4 ms ~~in the~~ downstream around stoichiometric contour line. At this stage, $t \leq 0.4$ ms, the concentration of HO_2 is rather low. CH_2OH is negligible in Case B.

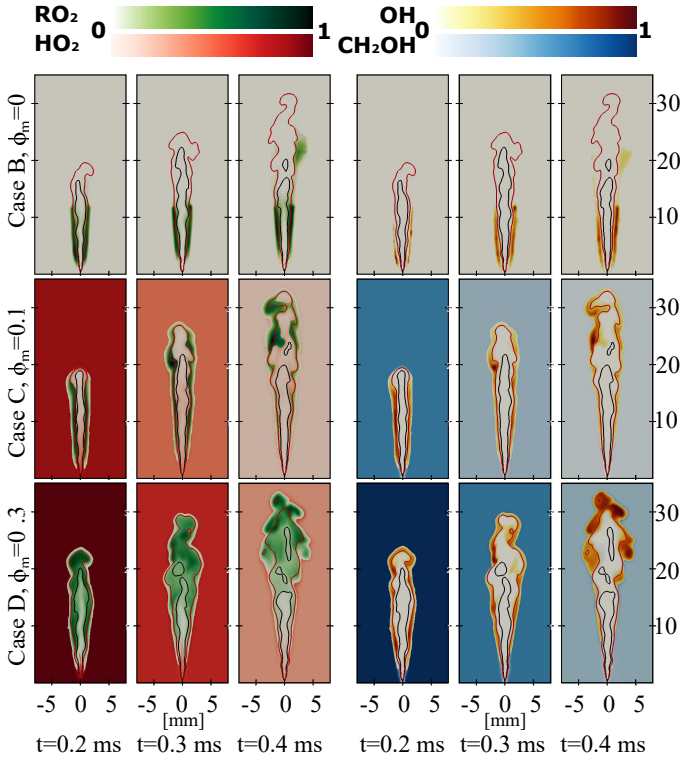

Figure 9: Distributions of RO_2 and HO_2 (left hand side), OH and CH_2OH (right hand side) prior to the onset of ~~first stage~~ first-stage ignition in a cross section along the spray axis. The red line denotes the iso-line of stoichiometric mixture fraction, and the black line is the iso-line of temperature of 700 K.

In contrast, the flame structure in the dual-fuel cases is significantly different. Due to the presence of methanol in the ambient gas, ~~ignition~~ oxidation reactions take place in the ambient mixture, giving rise to the formation of HO_2 and CH_2OH~~,~~ ~~among other species~~. This affects the formation of RO_2 and OH radicals. In Case C, with the methanol-air equivalence ratio of $\phi_m = 0.1$, the RO_2 is formed not only in the near nozzle region but also downstream, around the iso-surface of the stoichiometric mixture fraction. In Case D, with a higher methanol-air equivalence ratio of $\phi_m = 0.3$, the RO_2 fills up the entire fuel-rich region of the jet.

As a key species generated in the methanol ~~ignition~~ oxidation reactions, HO_2 is essential for n-heptane ignition since it participates in the reaction forming heptyl radicals, C_7H_{16} + $HO_2 = C_7H_{15}$ + H_2O_2, which leads further to the formation of RO_2. This explains the enhanced formation of RO_2 in the cool flame downstream region of spray jet, and the elevated mass fraction of RO_2 in the early ~~first stage~~ first-stage ignition, i.e., $t < 0.15$ ms, Fig. 7a. However, as shown in Fig. 7b, the presence of methanol in the ambient gas has, in general, a suppression effect on the ignition of n-heptane, due to the non-linear interaction among the different elementary reactions involved. This will be next examined using the reaction pathways.

3.7. Analysis of the dual-fuel reaction pathways

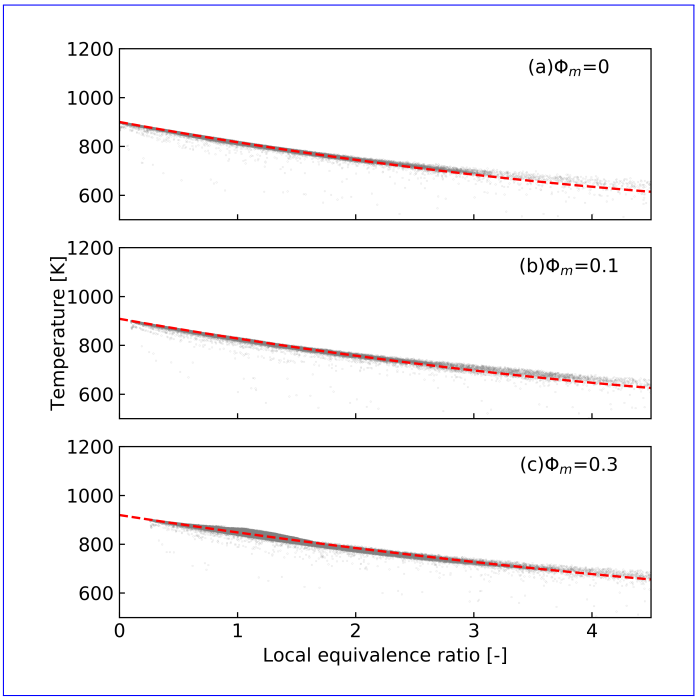

Figure 10: The scatter plot of all the LES cells in $\phi - T$ diagram before the first-stage ignition, and mixing lines for the case with ϕ_m of (a) 0, (b) 0.1 and (c) 0.3.

Figure 10 shows the $\phi - T$ diagram for the reacting Cases B, C and D before the first-stage ignition. The local equivalence ratio, ϕ, is defined as suggested in Ref. [57]. All of the computational cells are shown as gray dots. The dashed line is a fitting curve for the gray dots using the least squares method. As seen in Fig. 5, chemical heat release is absent before the first-stage ignition for both single- and dual-fuel cases. Therefore, no obvious temperature rise is found in Figure 10. Due to liquid n-heptane evaporation and mixing, the local temperature decreases with the increase of the local equivalence ratio. All of the LES cells collapse into a line, which is the mixing line for the n-heptane and methanol/air mixture.

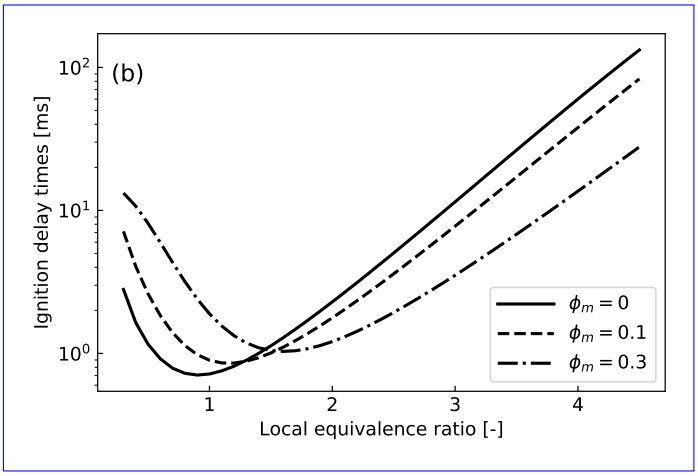

Figure 11: The ignition delay times of the n-heptane/methanol-air mixture in zero-dimensional homogeneous reactor simulations. The solid, dashed and dot-dashed lines denote initial methanol equivalence ratio ϕ_m of 0, 0.1 and 0.3, respectively.

Zero-dimensional homogeneous reactor simulations are conducted ~~to identify the reaction path and~~ along the mixing line to explain the effects of methanol on the ignition of n-heptane. Figure 11 shows the high temperature IDTs of the n-heptane/methanol-air mixture at different local equivalence ratios. Each equivalence ratio represents a thermophysical state in the LES. The initial composition and temperature of the zero-dimensional simulations are extracted from the mixing line in Fig. 10. For all of the ϕ_m, IDT first decreases and then increases with the increase of the local equivalence ratio. The shortest IDT locates at near-stoichiometric mixture for single fuel cases ($\phi_m = 0$). It is shifted to the rich region in the $\phi_m = 0.1$ and $\phi_m = 0.3$ cases. In addition, it is found that the shortest IDT increases with the increase of the ϕ_m. This implies that a high methanol concentration delays the n-heptane high temperature ignition, which is consistent with the observation in the LES.

Table 4: The IDTs of the zero- and three-dimensional cases.

ϕ_m [-]	zero-dimensional		three-dimensional	
	τ_1	τ_2	τ_1	τ_2
0	0.22	0.61	0.35	0.80
0.1	0.23	1.18	0.68	1.91
0.3	0.30	1.59	0.76	2.50

Furthermore, three zero-dimensional cases are further investigated according to the composition of the stoichiometric mixture in the spray ~~cases~~ Cases B, C and D. The IDTs of the zero- and three-dimensional cases are shown in Table 4.The rates of reactions are compared to identify the relative importance of OH and HO_2 consumption rates in different reactions. A conversion ratio of species i in reaction j (β_{ij}) is defined as, $\beta_{ij} = I_{ij}/I_i$, where i represents either OH or HO_2. I_{ij} is the integration of the consumption rate of species i in reaction j, within the induction time before the onset of the ~~second stage~~ second-stage ignition. I_i is the sum of I_{ij} over all reactions. The conversion ratios for OH and HO_2 in key reactions are listed in Table 5.

Table 5: Conversion ratios of OH and HO_2 in key reactions.

Key reactions \ ϕ_m [-]	0	0.1	0.3
$CH_3OH + OH = CH_2OH + H_2O$ (R1)	0	9.45%	32.28%
$CH_2O + OH = HCO + H_2O$ (R3)	40.01%	39.13%	38.02%
$C_7H_{16} + HO_2 = C_7H_{15} + H_2O_2$ (R4)	2.10%	2.64%	2.96%
$C_7H_{16} + OH = C_7H_{15} + H_2O$ (R5)	16.16%	11.71%	6.71%

The ambient methanol contributes to the consumption of OH through CH_3OH + OH = CH_2OH + H_2O reaction (denoted as R1). As seen in Table 5, the percentage of OH consumption in reaction R1 increases with the increase of the ambient methanol-air equivalence ratio, ϕ_m. About 32% of OH is consumed by CH_3OH in R1 in the $\phi_m = 0.3$ case. This reduces the OH accumulation rate, prolonging the ~~first stage~~ first-stage ignition delay times, τ_1. Meanwhile, the intermediate product, CH_2OH, is formed in the ambient methanol-air mixture. The oxidation of CH_2OH, in reaction $CH_2OH + O_2 = CH_2O + HO_2$ (denoted as R2), generates HO_2. Even though HO_2 will be converted to H_2O_2 and supply OH through reaction $H_2O_2 + M = OH + OH + M$, this reaction has a high activation energy, thus, the formation of OH from methanol-air mixture is limited before the temperature increases up to 1000 K [12]. OH is therefore consumed by reacting with methanol via R1 (but cannot be replenished) in the low temperature ignition stage. As such, the maximum OH mass fraction in the dual-fuel spray cases is lower than that in the single-fuel case during the transition induction period, $\tau_1 < t < \tau_2$. Thereafter, the high temperature reaction condition is met, OH is consumed in a series of high temperature reactions. One of the important reactions is the oxidation of formaldehyde (CH_2O), $CH_2O + OH = HCO + H_2O$ (denoted as R3). The existence of CH_3OH has a rather minor effect on the OH consumption in R3, as shown in Table 5. This explains the nearly constant maximal value of OH mass fractions for different ambient methanol concentrations after the onset of second ignition, $t > \tau_2$, as illustrated earlier in Fig. 7b.

The formation of HO_2 from the ambient methanol in reaction R2 contributes to the consumption of C_7H_{16} through the reaction $C_7H_{16} + HO_2 = C_7H_{15} + H_2O_2$ (denoted as R4). This leads to the elevated production of RO_2 during the early

stages of the ~~first stage~~ first-stage ignition, shown in Fig. 7a, and the change of the cool flame structure in Fig. 9. On the other hand, the reaction C_7H_{16} + OH = C_7H_{15} + H_2O (denoted as R5) ~~is slowed~~ slows down, with the OH conversion ratio decreasing from 16% ($\phi_m = 0$) to 7% ($\phi_m = 0.3$). The suppression of reaction R5 by the ambient methanol is the reason for the retardation of the ~~first stage~~ first-stage ignition and the transition from τ_1 to τ_2, shown in Fig. 7.

4. Conclusion

LES with a ~~transported probability density function (TPDF)~~ TPDF model is performed to investigate the effects of the ambient methanol-air equivalence ratio (ϕ_m from 0 to 0.3) on the n-heptane spray combustion under ~~reactivity controlled compression ignition (RCCI)~~ RCCI engine-like conditions. The baseline case is chosen from ECN n-heptane spray experiments. The LES models are validated ~~against experiments~~using the associated experimental data. A good agreement between the LES prediction and the ECN experiments, in terms of the liquid length, vapor penetration length, mixture fraction, ignition delay time and lift-off length, is achieved. The dual-fuel combustion results generated using the LES-TPDF model are analyzed to elucidate the effects of methanol chemistry on the ignition of the n-heptane spray. The following conclusions are drawn.

(1) ~~Ambient~~ The ambient methanol has a general effect of suppressing the ignition of n-heptane. Both the first-stage and second-stage ignitions of n-heptane are retarded by the ambient methanol. A longer transition time between the ~~two ignition stages and~~ first- and second-stage ignitions, as well as a lower first local peak value of the heat release rate are observed when ~~increasing~~ the ambient methanol concentration (i.e. ϕ_m) increases. The reason behind the suppression of

ignition is that the concentration of radicals (e.g. OH) is reduced by reaction with ambient methanol, ~~e.g.~~ i.e., through elementary reaction $CH_3OH + OH = CH_2OH + H_2O$. The associated OH consumption rate increases with the increase of ϕ_m.

(2) In the earlier induction period before the onset of first-stage ignition, the ambient methanol has an effect of enhancing the formation of heptyl-peroxide (RO_2) that has been considered as the ~~marker~~ indicator of the first-stage ignition. Chemical pathway analysis shows that HO_2 generated in the ambient methanol promotes the formation heptyl radicals, via $C_7H_{16} + HO_2 = C_7H_{15} + H_2O_2$, this subsequently enhancing the formation of RO_2. However, the consumption of OH through reaction $CH_3OH + OH = CH_2OH + H_2O$ suppresses the reaction $C_7H_{16} + OH = C_7H_{15} + H_2O$, which ~~retards eventually~~ eventually retards the onset of both the first-stage and the second-stage ignition of n-heptane.

(3) Under the lean ambient mixture conditions studied in the present work, the ambient methanol affects the n-heptane spray flame structures in both the ignition stage and in the steady spray flame stage. In the single-fuel methanol-free case, the low temperature ignition and cool flame ~~marker~~indicator, RO_2, is shown to distribute around the stoichiometric mixture in the proxmity of the fuel nozzle, with the cool flame enveloping the fuel rich region. In the dual-fuel cases, RO_2 is found in the entire fuel-rich region ~~farther~~ further downstream. The onset of the second-stage ignition kernel is postponed at further downstream, this resulting a longer liftoff length in the methanol/n-heptane dual-fuel cases than that of single fuel n-heptane spray flame. The postponed ignition and the longer liftoff length extend the mixing time before the start of high-temperature combustion, this reducing the high-temperature and rich-fuel regions in the dual-fuel cases ~~,~~ ~~which~~ This explains the reduced soot emission in dual-fuel engines reported in the

literature.

Acknowledgments

This work is sponsored by Swedish Research Council (VR), and Swedish Energy Agency through KC-CECOST. Shijie Xu and Shenghui Zhong are sponsored by China Scholarship Council. We thank Rui Li for the assistance on chemical analysis. The simulations are performed on resources provided by the Swedish National Infrastructure for Computing (SNIC) at HPC2N and PDC.

References

[1] Y. Li, M. Jia, Y. Liu, M. Xie, Numerical study on the combustion and emission characteristics of a methanol/diesel reactivity controlled compression ignition (RCCI) engine, Applied energy 106 (2013) 184–197.

[2] B. Ma, A. Yao, C. Yao, T. Wu, B. Wang, J. Gao, C. Chen, Exergy loss analysis on diesel methanol dual fuel engine under different operating parameters, Applied Energy 261 (2020) 114483.

[3] D. Splitter, R. Hanson, S. Kokjohn, R. D. Reitz, Reactivity controlled compression ignition (RCCI) heavy-duty engine operation at mid-and high-loads with conventional and alternative fuels, Tech. Rep., SAE Technical Paper, 2011.

[4] X. Kan, L. Wei, X. Li, H. Li, D. Zhou, W. Yang, C.-H. Wang, Effects of the three dual-fuel strategies on performance and emissions of a biodiesel engine, Applied Energy 262 (2020) 114542.

[5] D. Zhou, W. Yang, H. An, J. Li, Application of CFD-chemical kinetics approach in detecting RCCI engine knocking fuelled with biodiesel/methanol, Applied Energy 145 (2015) 255–264.

[6] J. Liu, F. Yang, H. Wang, M. Ouyang, S. Hao, Effects of pilot fuel quantity on the emissions characteristics of a CNG/diesel dual fuel engine with optimized pilot injection timing, Applied Energy 110 (2013) 201–206.

[7] K. Ryu, Effects of pilot injection timing on the combustion and emissions characteristics in a diesel engine using biodiesel–CNG dual fuel, Applied Energy 111 (2013) 721–730.

[8] H. Kahila, A. Wehrfritz, O. Kaario, V. Vuorinen, Large-eddy simulation of dual-fuel ignition: Diesel spray injection into a lean methane-air mixture, Combustion and Flame 199 (2019) 131–151.

[9] Z. Chen, C. Yao, A. Yao, Z. Dou, B. Wang, H. Wei, M. Liu, C. Chen, J. Shi, The impact of methanol injecting position on cylinder-to-cylinder variation in a diesel methanol dual fuel engine, Fuel 191 (2017) 150–163.

[10] Z. Yin, C. Yao, P. Geng, J. Hu, Visualization of combustion characteristic of diesel in premixed methanol–air mixture atmosphere of different ambient temperature in a constant volume chamber, Fuel 174 (2016) 242–250.

[11] A. Srna, M. Bolla, Y. M. Wright, K. Herrmann, R. Bombach, S. S. Pandurangi, K. Boulouchos, G. Bruneaux, Effect of methane on pilot-fuel autoignition in dual-fuel engines, Proceedings of the Combustion Institute 37 (4) (2019) 4741–4749.

[12] H. Xu, C. Yao, G. Xu, Chemical kinetic mechanism and a skeletal model for oxidation of n-heptane/methanol fuel blends, Fuel 93 (2012) 625–631.

[13] Engine combustion network, https://ecn.sandia.gov, Accessed Jan., 2020.

[14] H. Kahila, O. Kaario, Z. Ahmad, M. G. Masouleh, B. Tekgül, M. Larmi, V. Vuorinen, A large-eddy simulation study on the influence of diesel pilot spray quantity on methane-air flame initiation, Combustion and Flame 206 (2019) 506–521.

[15] B. Tekgül, H. Kahila, O. Kaario, V. Vuorinen, Large-eddy simulation of dual-fuel spray ignition at different ambient temperatures, Combustion and Flame 215 (2020) 51–65.

[16] S. Som, D. E. Longman, Z. Luo, M. Plomer, T. Lu, P. K. Senecal, E. Pomraning, Simulating flame lift-off characteristics of diesel and biodiesel fuels using detailed chemical-kinetic mechanisms and large eddy simulation turbulence model, Journal of Energy Resources Technology 134 (3) (2012) 032204.

[17] A. Irannejad, A. Banaeizadeh, F. Jaberi, Large eddy simulation of turbulent spray combustion, Combustion and Flame 162 (2) (2015) 431–450.

[18] S. Gallot-Lavallée, W. Jones, Large eddy simulation of spray auto-ignition under EGR conditions, Flow, Turbulence and Combustion 96 (2) (2016) 513–534.

[19] C.-W. Tsang, Y. Wang, C. Wang, A. Shelburn, L. Liang, K. Puduppakkam, A. Modak, C. Naik, E. Meeks, C. Rutland, Evaluation and Validation of

Large-Eddy-Simulation (LES) for Gas Jet and Sprays, Tech. Rep., SAE Technical Paper, 2017.

[20] H. Wei, W. Zhao, J. Qi, Z. Liu, L. Zhou, Effect of injection timing on the ignition process of n-heptane spray flame in a methane/air environment, Fuel 245 (2019) 345–359.

[21] C. Gong, M. Jangi, X.-S. Bai, Large eddy simulation of n-dodecane spray combustion in a high pressure combustion vessel, Applied Energy 136 (2014) 373–381.

[22] Y. Pei, S. Som, E. Pomraning, P. K. Senecal, S. A. Skeen, J. Manin, L. M. Pickett, Large eddy simulation of a reacting spray flame with multiple realizations under compression ignition engine conditions, Combustion and Flame 162 (12) (2015) 4442–4455.

[23] A. Wehrfritz, O. Kaario, V. Vuorinen, B. Somers, Large eddy simulation of n-dodecane spray flames using flamelet generated manifolds, Combustion and Flame 167 (2016) 113–131.

[24] P. Kundu, M. M. Ameen, S. Som, Importance of turbulence-chemistry interactions at low temperature engine conditions, Combustion and Flame 183 (2017) 283–298.

[25] C. K. Blomberg, L. Zeugin, S. S. Pandurangi, M. Bolla, K. Boulouchos, Y. M. Wright, Modeling split injections of ECN "Spray A" using a conditional moment closure combustion model with RANS and LES, SAE International Journal of Engines 9 (4) (2016) 2107–2119.

[26] A. Hadadpour, M. Jangi, K. M. Pang, X. S. Bai, The role of a split injection strategy in the mixture formation and combustion of diesel spray: A large-eddy simulation, Proceedings of the Combustion Institute 37 (4) (2019) 4709–4716.

[27] W. Zhao, H. Wei, M. Jia, Z. Lu, K. H. Luo, R. Chen, L. Zhou, Flame–spray interaction and combustion features in split-injection spray flames under diesel engine-like conditions, Combustion and Flame 210 (2019) 204–221.

[28] A. Varna, A. Wehrfritz, E. R. Hawkes, M. J. Cleary, T. Lucchini, G. D'Errico, S. Kook, Q. N. Chan, Application of a multiple mapping conditioning mixing model to ECN Spray A, Proceedings of the Combustion Institute 37 (3) (2019) 3263–3270.

[29] Q. Wang, C. Yao, Z. Dou, B. Wang, T. Wu, Effect of intake pre-heating and injection timing on combustion and emission characteristics of a methanol fumigated diesel engine at part load, Fuel 159 (2015) 796–802.

[30] K. M. Pang, M. Jangi, X.-S. Bai, J. Schramm, J. H. Walther, Modelling of diesel spray flames under engine-like conditions using an accelerated Eulerian Stochastic Field method, Combustion and Flame 193 (2018) 363–383.

[31] M. Jangi, R. Solsjo, B. Johansson, X.-S. Bai, On large eddy simulation of diesel spray for internal combustion engines, International Journal of Heat and Fluid Flow 53 (2015) 68–80.

[32] C. Gong, M. Jangi, X.-S. Bai, Large eddy simulation of n-dodecane spray

combustion in a high pressure combustion vessel, Applied Energy 136 (2014) 373–381.

[33] D. B. Spalding, The combustion of liquid fuels, in: Symposium (international) on combustion, vol. 4, 847–864, 1953.

[34] W. E. Ranz, W. R. Marshall, Evaporation from drops, Part I, Chem. Eng. Prog 48 (3) (1952) 141–146.

[35] W. E. Ranz, W. R. Marshall, Evaporation from drops, Part II, Chem. Eng. Prog 48 (3) (1952) 173–180.

[36] T. Lu, C. K. Law, C. S. Yoo, J. H. Chen, Dynamic stiffness removal for direct numerical simulations, Combustion and Flame 156 (8) (2009) 1542–1551.

[37] R. Li, S. Li, F. Wang, X. Li, Sensitivity analysis based on intersection approach for mechanism reduction of cyclohexane, Combustion and Flame 166 (2016) 55–65.

[38] S. Liu, J. C. Hewson, J. H. Chen, H. Pitsch, Effects of strain rate on high-pressure nonpremixed n-heptane autoignition in counterflow, Combustion and flame 137 (3) (2004) 320–339.

[39] K. M. Pang, N. Karvounis, J. H. Walther, J. Schramm, Numerical investigation of soot formation and oxidation processes under large two-stroke marine diesel engine-like conditions using integrated CFD-chemical kinetics, Applied energy 169 (2016) 874–887.

[40] S. Hu, C. Gong, X.-S. Bai, Dual Fuel Combustion of N-heptane/methanol-air-EGR Mixtures, Energy Procedia 105 (2017) 4943–4948.

[41] M. Jangi, X. Zhao, D. C. Haworth, X.-S. Bai, Stabilization and liftoff length of a non-premixed methane/air jet flame discharging into a high-temperature environment: An accelerated transported PDF method, Combustion and Flame 162 (2) (2015) 408–419.

[42] M. Jangi, X.-S. Bai, Multidimensional chemistry coordinate mapping approach for combustion modelling with finite-rate chemistry, Combustion Theory and Modelling 16 (6) (2012) 1109–1132.

[43] M. Jangi, R. Yu, X.-S. Bai, Development of chemistry coordinate mapping approach for turbulent partially premixed combustion, Flow, turbulence and combustion 90 (2) (2013) 285–299.

[44] The OpenFOAM Foundation, https://www.openfoam.gov, Accessed Jan., 2020.

[45] H. Jasak, H. G. Weller, A. D. Gosman, High resolution NVD differencing scheme for arbitrarily unstructured meshes, International Journal for Numerical Methods in Fluids 31 (2) (1999) 431–449, ISSN 0271-2091.

[46] L. Valiño, A field Monte Carlo formulation for calculating the probability density function of a single scalar in a turbulent flow, Flow, turbulence and combustion 60 (2) (1998) 157–172.

[47] M. Jangi, M. Altarawneh, B. Z. Dlugogorski, Large-eddy simulation of methanol pool fires using an accelerated stochastic fields method, Combustion and Flame 173 (2016) 89–98.

[48] S. Xu, S. Zhong, K. M. Pang, S. Yu, M. Jangi, X.-s. Bai, Effects of ambient methanol on pollutants formation in dual-fuel spray combustion at varying

ambient temperatures: A large-eddy simulation, Applied Energy 279 (2020) 115774.

[49] Y. Zhang, S. Xu, S. Zhong, X.-S. Bai, H. Wang, M. Yao, Large eddy simulation of spray combustion using flamelet generated manifolds combined with artificial neural networks, Energy and AI (2020) 100021.

[50] A. B. Dempsey, N. R. Walker, R. Reitz, Effect of piston bowl geometry on dual fuel reactivity controlled compression ignition (RCCI) in a light-duty engine operated with gasoline/diesel and methanol/diesel, SAE International Journal of Engines 6 (1) (2013) 78–100.

[51] L. Xu, X.-S. Bai, M. Jia, Y. Qian, X. Qiao, X. Lu, Experimental and modeling study of liquid fuel injection and combustion in diesel engines with a common rail injection system, Applied Energy 230 (2018) 287–304.

[52] U. Burke, W. K. Metcalfe, S. M. Burke, K. A. Heufer, P. Dagaut, H. J. Curran, A detailed chemical kinetic modeling, ignition delay time and jet-stirred reactor study of methanol oxidation, Combustion and Flame 165 (2016) 125–136.

[53] National University of Ireland Galway, http://c3.nuigalway.ie/combustionchemistrycentre/mechanismdownloads, Accessed Jan., 2020.

[54] M. Christensen, E. Nilsson, A. Konnov, A systematically updated detailed kinetic model for CH2O and CH3OH combustion, Energy & Fuels 30 (8) (2016) 6709–6726.

[55] Q. Tang, H. Liu, X. Ran, M. Li, M. Yao, Effects of direct-injection fuel types and proportion on late-injection reactivity controlled compression ignition, Combustion and Flame 211 (2020) 445–455.

[56] Q. Tang, X. Liu, H. Liu, H. Wang, M. Yao, Investigation on the dual-fuel active-thermal atmosphere combustion strategy based on optical diagnostics and numerical simulations, Fuel 276 (2020) 118023.

[57] L. Xu, X.-S. Bai, C. Li, P. Tunestål, M. Tunér, X. Lu, Combustion characteristics of gasoline DICI engine in the transition from HCCI to PPC: Experiment and numerical analysis, Energy 185 (2019) 922–937.

Text File

Bib File

Figures

*Declaration of Interest Statement

Declaration of interests

☒ The authors declare that they have no known competing financial interests or personal relationships that could have appeared to influence the work reported in this paper.

☐The authors declare the following financial interests/personal relationships which may be considered as potential competing interests:

Credit Author Statement

Shijie Xu: Conceptualization, Investigation, Writing- Original draft preparation

Kar Mun Pang: Investigation, Writing - Review & Editing

Yaopeng Li: Conceptualization, Writing - Review & Editing

Ahmad Hadadpour: Validation, Software

Senbin Yu: Writing - Review & Editing

Shenghui Zhong: Software, Investigation, Validation

Mehdi Jangi: Methodology

Xue-Song Bai: Supervision, Project administration, Funding acquisition, Writing - Review & Editing